

# A 2dF Spectroscopic Study of Globular Clusters in NGC 5128: Probing the Formation History of the Nearest Giant Elliptical

Michael A. Beasley<sup>1</sup>, Terry Bridges<sup>2</sup>, Eric Peng<sup>3</sup>, William E. Harris<sup>4</sup>,  
Gretchen L.H. Harris<sup>5</sup>, Duncan A. Forbes<sup>6</sup> and Glen Mackie<sup>6</sup>

<sup>\*</sup>, <sup>†</sup>, <sup>‡</sup>, <sup>§</sup>, <sup>¶</sup>, <sup>||</sup>, <sup>\*\*</sup>

<sup>1</sup>*Instituto de Astrofísica de Canarias, Via Lactea, E-38200 La Laguna, Tenerife, Spain*

<sup>2</sup>*Department of Physics, Queen's University, Kingston, ON K7L 3N6, Canada*

<sup>3</sup>*Herzberg Institute of Astrophysics, National Research Council of Canada, 5071 West Saanich Road, Victoria, BC V9E 2E7, Canada*

<sup>4</sup>*Department of Physics and Astronomy, McMaster University, Hamilton, ON L8S 4M1*

<sup>5</sup>*Department of Physics and Astronomy, University of Waterloo, Waterloo, ON N2L 3G1, Canada*

<sup>6</sup>*Centre for Astrophysics and Supercomputing, Swinburne University of Technology, Hawthorn, VIC 3122, Australia*

17 December 2018

## ABSTRACT

We have performed a spectroscopic study of globular clusters (GCs) in the nearest giant elliptical NGC 5128 using the 2dF facility at the Anglo-Australian telescope. We obtained integrated optical spectra for a total of 254 GCs, 79 of which are newly confirmed on the basis of their radial velocities and spectra. In addition, we obtained an integrated spectrum of the galaxy starlight along the southern major axis. We derive an empirical metallicity distribution function (MDF) for 207 GCs ( $\sim 14\%$  of the estimated total GC system) based upon Milky Way GCs. This MDF is multimodal at high statistical significance with peaks at  $[Z/H] \sim -1.3$  and  $-0.5$ . A comparison between the GC MDF and that of the stellar halo at 20 kpc ( $\sim 4R_e$ ) reveals close coincidence at the metal-rich ends of the distributions. However, an inner 8 kpc stellar MDF shows a clear excess of metal-rich stars when compared to the GCs. We compare a higher S/N subsample (147 GCs) with two stellar population models which include non-solar abundance ratio corrections. The vast majority of our sample ( $\sim 90\%$ ) appears old, with ages similar to the Milky Way GC system. There is evidence for a population of intermediate-age ( $\sim 4 - 8$  Gy) GCs ( $\leq 15\%$  of the sample) which are on average more metal-rich than the old GCs. We also identify at least one younger cluster ( $\sim 1 - 2$  Gy) in the central regions of the galaxy. Our observations are consistent with a picture where NGC 5128 has undergone at least two mergers and/or interactions involving star formation and limited GC formation since  $z = 1$ , however the effect of non-canonical hot stellar populations on the integrated spectra of GCs remains an outstanding uncertainty in our GC age estimates.

## Key words:

galaxies: individual: NGC 5128; galaxies: star clusters

## 1 INTRODUCTION

One of the principal tenets of extragalactic GC research is that “GCs trace the major episodes of star formation in their host galaxies”. Supporting evidence for this view includes the fact that the mean colours (a surrogate for metallicities at old ages) of blue and red GC subpopulations in galaxies are correlated with the host galaxy luminosity (e.g., Forbes, Brodie & Grillmair 1997; Larsen *et al.* 2001; Strader, Brodie & Forbes 2004; Peng *et al.* 2006; Brodie & Strader 2006).

<sup>\*</sup> email:beasley@iac.es

<sup>†</sup> tjb@astro.queensu.ca

<sup>‡</sup> Eric.Peng@nrc-cnrc.gc.ca

<sup>§</sup> glharris@astro.uwaterloo.ca

<sup>¶</sup> harris@physics.mcmaster.ca

<sup>||</sup> dforbes@astro.swin.edu.au

<sup>\*\*</sup> gmackie@astro.swin.edu.au

Further evidence that GCs may be used as proxies for star formation in galaxies comes from recent spectroscopic observations of the GC systems of early-type galaxies (Es). Strader *et al.* (2005) find little evidence of young GCs from a small sample of massive Es, in agreement with previous studies using either spectroscopy (Cohen, Blakeslee & Rhysov 1998; Beasley *et al.* 2000) or the measured luminosity function with the assumption of a universal mass function for all GCs (Puzia *et al.* 1999; Jordán *et al.* 2002). By contrast, Puzia *et al.* (2005) find evidence to suggest that up to 30% of GCs in less massive Es may have formed later than  $z = 1$ . Whether these younger GCs formed in dissipational mergers or by some other means is presently unclear. The finding of young GCs in lower-mass ellipticals has found some support in results from IR photometry (Hempel *et al.* 2007), which in conjunction with optical colours promises to break the age-metallicity degeneracy (e.g., Mould & Aaronson 1980). However, this technique is proving somewhat controversial (Larsen *et al.* 2005; Kundu *et al.* 2005), and the reliability of this approach needs to be fully tested both observationally and theoretically (e.g., Salaris & Cassisi 2007; Lee *et al.* 2006).

Notwithstanding ongoing argument about the use of IR photometry in age estimations, spectroscopy is still the method of choice for deriving ages and metallicities, and indeed is the only way to estimate abundance ratios and obtain kinematic information. The current picture from the spectroscopic studies is, qualitatively at least, in agreement with the “downsizing” phenomenon. Massive ellipticals are old, passively evolving systems while their less massive counterparts continue to merge and make stars and GCs at later epochs. Unfortunately, spectroscopic sample sizes of GC systems remain small. Most of the nearest massive Es are at Virgo distances which restricts samples to the brightest few percent of clusters on 8-m class telescopes. This not only places statistical limitations on the interpretation of data, but also raises the question of whether the most massive globular clusters are representative of the system at all (e.g., Harris *et al.* 2006a).

An obvious target with which to begin to remedy this problem of sample sizes is NGC 5128, the nearest giant elliptical galaxy. At a distance of  $\sim 4$  Mpc, over half of the GC system is amenable to spectroscopic observations (with the brightest third or so accessible to 4-m class telescopes). Moreover, NGC 5128 shows extensive evidence for one or more recent interactions, including shells (Malin 1978), a central, highly inclined gas and dust disk (e.g., Dufour *et al.* 1979), and a stream of young stars in its halo (Peng *et al.* 2002). Indeed, in view of all this recent activity in the galaxy, if the association between the GCs and field stars in ellipticals is to be understood, then NGC 5128 is an excellent place to start.

Peng, Ford & Freeman (2004) (hereafter PFF04) were the first to look in any detail at the spectroscopic ages and metallicities of GCs in NGC 5128, building on previous work by van den Bergh, Hesser & Harris (1981), Hesser, Harris & Harris (1986), Sharples (1988) and Held *et al.* (2002). Based upon spectra of 23 GCs with sufficient S/N, PFF04 found that the NGC 5128 GCs displayed a wide range of metallicities, and that the metal-rich GCs ( $[\text{Fe}/\text{H}] > -1$ ) had a spread in ages, with a mean age of  $\sim 5$  Gy. Based in part on the results for the GCs, PFF04 suggested that the NGC

5128 galaxy which we see today was assembled through the dissipational merger of two unequal-mass disks at  $z < 1$ . Bekki & Peng (2006) have modelled the same merger process to explain the kinematics and spatial distribution of its planetary nebula population.

In this paper we present the first results of an ongoing spectroscopic survey of the GC system of the nearby E/S0 NGC 5128, examining the ages, metallicities and abundance ratios of GC system in statistically significant numbers. The plan of this paper is as follows: In Section 2 we describe our candidate GC sample, observations and data reduction. In Section 3 we derive metallicity, age and abundance ratio estimates for the GCs and discuss properties of the NGC 5128 GC system. In Section 4, we present a summary of our results and a discussion. A detailed analysis of the kinematics of the GC system is presented in Woodley *et al.* (2007), and a discussion of the colour-metallicity relations will be forthcoming (Peng *et al.* 2007 in preparation).

Throughout the following, we adopt a distance of 3.8 Mpc to NGC 5128 (Rejkuba 2004). At this distance,  $1'' \sim 20$  pc.

## 2 THE DATA

The principal goals of our spectroscopic survey were twofold; to obtain optical spectra of GC candidates in NGC 5128 in order to increase the number of known *bona fide* GCs, and to obtain spectra for previously known, and newly identified clusters of sufficient quality for a metallicity, age and kinematic analysis of the GC system. We describe our observational approach in this section.

### 2.1 Observations and Data Reduction

The wide angular extent of the NGC 5128 GC system on the sky and the large number of candidate GCs in our sample required high multiplex over a wide-field. These requirements made the 2-degree field (2dF) instrument on the Anglo-Australian Telescope a logical choice. The 2dF permits up to 400 spectra to be obtained simultaneously over a  $2^\circ.1$  diameter field of view (see Lewis *et al.* 2002). The fibres are fed to two spectrographs with 200 fibres per spectrograph. Each fibre has a  $\sim 2$  arcsec diameter, matching well the NGC 5128 GCs which are unresolved at the median seeing of Siding Spring ( $\sim 1.3$  arcsec). Our observational set-up is given in Table 1. We observed previously known GCs taken from Peng *et al.* (2004b), as well as new GC candidates. These candidates were selected from the UBVRI photometry presented in Peng *et al.* (2004b, see their section 4 for a detailed description of the selection), and augmented with the wide-field Washington system photometry of Harris *et al.* (2004) to yield a master list of  $\sim 1000$  candidates to  $V \sim 20.5$ . We identified GC candidates from both sets of photometry using a combination of colour and morphological cuts that selected objects appearing slightly extended and having the colours of GCs. We also matched our catalogues with the X-ray point source detections of Kraft *et al.* (2001) and assigned a high priority to any optical counterparts since low-mass X-ray binaries are known to be associated with GCs (Clark 1975).

Spectra for GC candidates were obtained between the

nights of May 6 and May 11 in 2003. Two and a half nights were lost to bad weather and the remaining nights were clear. To maximise efficiency, our observing strategy was to first observe three “shallow” (3 hr) fields which encompassed all cluster candidates with no spectroscopic confirmation. These data were reduced on-the-fly at the telescope using the 2dF pipeline software 2DFDR (Taylor *et al.* 1996; Bailey *et al.* 2002). Radial velocities were measured using 2DFGRS, which implements a cross-correlation approach against empirical template spectra (Colless *et al.* 2001). Selecting by velocity (Section 2.2), an essentially clean sample of GCs was then constructed with which we made two plate configurations for deeper (8 hr) spectroscopy. Some 40 fibres were allocated to sample the sky uniformly across the field for sky subtraction. A further 10 fibres were positioned  $1' - 10'$  ( $\sim 1.2 - 12$  kpc) south of the galaxy centre along the major axis to sample the integrated galaxy light, but at the same time avoiding the prominent dust/gas lane in the galaxy.

The 10 galaxy fibre allocations were crucial for accurate removal of the galaxy background from the GC spectra, and for synthesizing an integrated spectrum of the galaxy for subsequent analysis. The flux-weighted combined galaxy spectrum corresponded to a position of approximately 2.3 arcmin south along the major axis. Adopting a V-band effective radius of 5.0 arcmin for NGC 5128 (Dufour *et al.* 1979), this corresponds to approximately an  $r_e/2$  aperture. In addition, spectra common between spectrographs 1 and 2 (from different plate configurations) were obtained for 11 previously identified GCs spanning a range of magnitudes. This allowed us to estimate the internal uncertainties of our radial velocity and linestrength measurements.

The sky and galaxy fibre allocations were used to remove the contribution from the sky and galaxy background from our GC observations. Beyond approximately 10 arcmin, the flux contribution from the spheroid was minimal, and an averaged sky spectrum created from the combined sky fibres was subtracted from the spectra of GCs beyond this radius. For GCs projected interior to this radius, the galaxy spectrum obtained along the major axis was scaled to the position of each GC (by fitting a smooth curve through a plot of the mean flux down each galaxy fibre versus radius) and subtracted from each GC (similarly, see Woodley, Harris & Harris 2005 and PFF04).

## 2.2 Radial Velocities

Preliminary radial velocities for all candidate GCs were obtained with 2DFDR as outlined in Section 2.1. We found no systematic differences in velocities of common objects between the spectrographs, however, during the observations, differences in the velocity zeropoints of order  $\sim 30$  km s $^{-1}$  were observed between standard stars with different plate configurations. Therefore, post-observing, GC velocities were re-determined with FXCOR in IRAF<sup>1</sup> using 12 F-K stellar templates which doubled as Lick standard stars. The velocity zeropoints of these templates were checked by

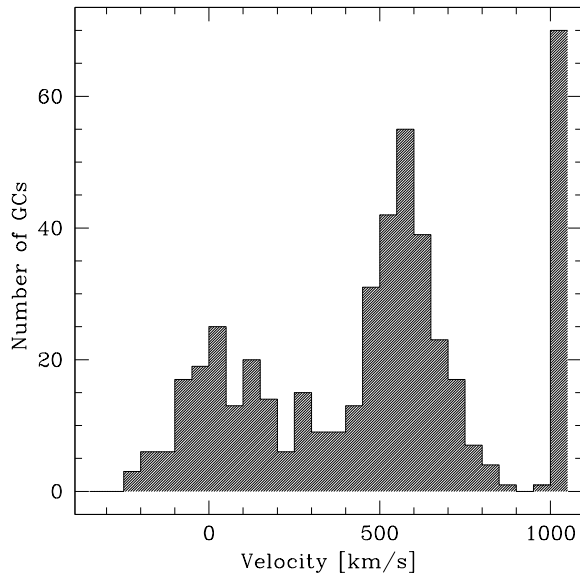


**Figure 1.** Histogram of 454 GC candidates for which velocities could be measured. The GC system of NGC 5128 is clearly visible with a mean velocity of  $\sim 550$  km s $^{-1}$ . The distribution of objects with a mean velocity of  $\sim 50$  km s $^{-1}$  are foreground Galactic stars. The pile-up at 1200 km s $^{-1}$  are background galaxies and is artificial.

cross-correlating them with synthetic spectra (Vazdekis *et al.* 2007, in preparation). Velocities were considered secure if they had a clearly defined cross-correlation peak, and a Tonry & Davis (1979)  $r$  value  $> 3$ . The velocity from the best-matching template was then adopted as the final velocity.

We noted during the analysis stage that there existed resolution variations in these data of up to  $\sim 20\%$  as a function of 2dF plate position. We verified that no systematic uncertainties were introduced in our measured radial velocities by smoothing all the spectra to a common resolution and re-measuring velocities. The only effect of the varying resolution was to increase our velocity uncertainties as a function of 2dF plate position. It should be noted though, that for index measurements the spectra were smoothed to a common resolution (Section 2.3) significantly lower than the instrumental resolution of our setup.

The velocity distribution of all the candidate clusters is shown in Figure 1. As can be seen, the velocity distribution of NGC 5128 GCs is well separated from background galaxies and reasonably well separated from Milky Way foreground stars. Following Peng *et al.* (2004b), and informed by Fig 1, we classify as GCs all candidates in the velocity interval of 250–1000 km s $^{-1}$ . At the lower bound, 250 km s $^{-1}$  misses very few GCs. For the field stars in the NGC 5128 planetary nebula (PN) sample of Peng, Ford, & Freeman (2004c), which is free from contamination, only 1% of PN velocities are below this cutoff. However, Fig 1 does suggest that some uncertainty in star/GC identification remains for cluster candidates with  $V \sim 250 - 350$  km s $^{-1}$ . Indeed, one of these objects could be clearly identified as a foreground star on the basis of its spectrum (object AAT304867 has  $V = 305 \pm 55$  km s $^{-1}$ , but exhibits strong molecular bands

<sup>1</sup> IRAF is distributed by the National Optical Astronomy Observatories, which are operated by the Association of Universities for Research in Astronomy, Inc., under cooperative agreement with the National Science Foundation.

in its spectrum characteristic of an M-type star). Another (AAT114993) has been identified as a star on the basis of *HST*/ACS imaging (Harris *et al.* 2006b) despite its having  $V=352 \pm 136 \text{ km s}^{-1}$  (though note the large velocity uncertainty).

In an attempt to quantify the level of contamination from foreground stars in this velocity range we ran KMM (Ashman, Bird & Zepf 1994) on the combined velocity distribution of stars and GCs assuming two homoscedastic populations<sup>2</sup>. KMM gave estimated means of 53 and 564  $\text{km s}^{-1}$  for the stars and GCs respectively, with a 50% posterior probability that an object belongs to either subpopulation (based purely on its radial velocity) occurring at a velocity of 290  $\text{km s}^{-1}$ . At 350  $\text{km s}^{-1}$  KMM predicts that the posterior probability that an object is in fact a GC is  $\sim 90\%$ . This probability falls to  $\sim 20\%$  at 250  $\text{km s}^{-1}$ . There are 25 GC candidates in the velocity range 250–350  $\text{km s}^{-1}$ , and based on KMM we estimate that approximately half of these may be foreground stars. We note that this potential contamination from foreground stars represents  $< 5\%$  of our GC sample.

In Fig 2 we compare our velocities with those from the study of Peng *et al.* (2004b), observed with a combination of 2dF and Hydra on the CTIO 4-m. We find good agreement between the two samples, but note a systematic offset in the sense of  $us\text{-Peng } et al. = +35 \text{ km s}^{-1}$ , with a dispersion of  $66 \pm 5 \text{ km s}^{-1}$ . The dispersion is consistent with our mean velocity uncertainty ( $59 \pm 4 \text{ km s}^{-1}$ ), though the source of the offset is unclear. We have re-checked the zeropoints of our template stars and heliocentric corrections and find no obvious systematic error. We separated our velocities by the spectral type of the best matching templates (F G & K types; Fig 2) and find the largest discrepancy for F-type GCs ( $us\text{-Peng } et al. = +74 \text{ km s}^{-1}$ , with a dispersion of  $77 \text{ km s}^{-1}$ ). The G & K templates give offsets of 30 and 23  $\text{km s}^{-1}$  respectively, with identical dispersions of 60  $\text{km s}^{-1}$ . Since the NGC 5128 GC system clearly spans a range of spectral types, it is possible that use of a single template for cross-correlation in Peng *et al.* (M31 GC 225-280) may have led to systematic variations in velocity as a function of spectral type.

Of 454 unique spectra for which we could derive reliable velocities, we classify 70 as galaxies, 130 as foreground stars and 254 as GCs belonging to NGC 5128. Of these 254 GCs, 79 had no previous velocity measurements. In Table 2 we list the velocities and co-ordinates of all GCs observed. The newly identified GCs are designated “AAT#” in Table 2, previously known GCs retain their previous designations (see PFF04). For completeness, we list the GC candidates which turned out to be stars or galaxies in Tables 3 and 4. We show a selection of the 2dF spectra in Figure 3.

### 2.3 Lick Indices

In order to compare our spectra to single stellar population models (SSPs), we calibrated them to the Lick system (Trager *et al.* 1998) using 12 Lick standard observed with the same 2dF configuration (Section 2.2). The standard

<sup>2</sup> Assuming two heteroscedastic populations in KMM made little difference

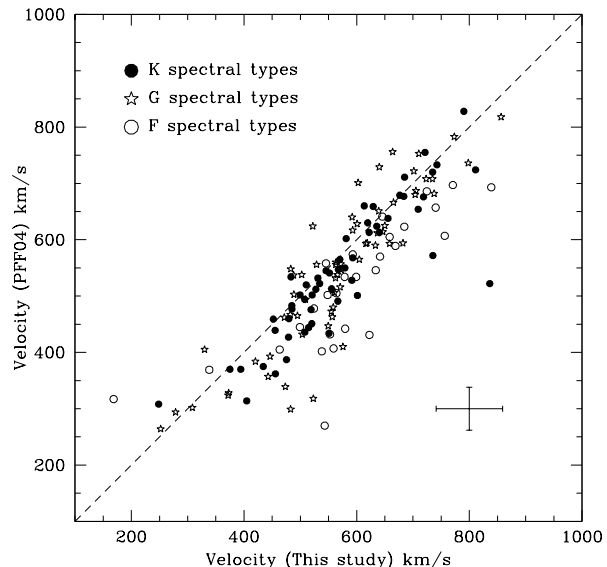


**Figure 2.** Comparison of 148 velocities in common between this study and PFF04. The dashed line is the 1-to-1 relation. Symbols correspond to the spectral type of the best cross-correlation template.

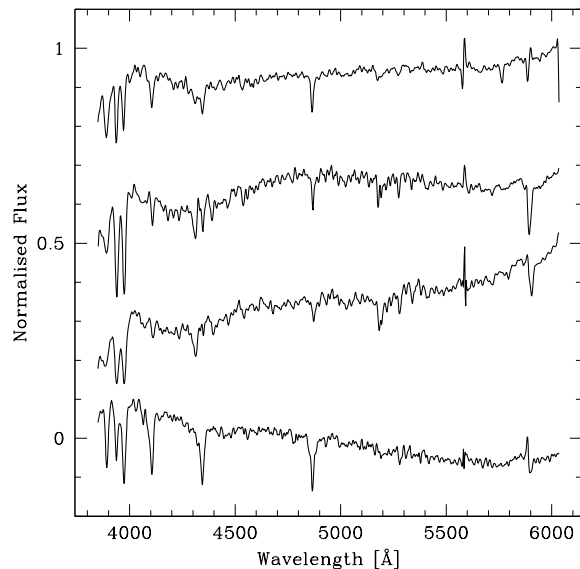


**Figure 3.** Example 2dF spectra of NGC 5128 GCs with median S/N ( $40\text{--}60 \text{ \AA}^{-1}$ ). From top to bottom GCs are AAT109711 (metal-poor, old), HGHH-21 (intermediate metallicity, old), K102 (metal-rich, old) and HGHH-279 (intermediate metallicity, young). Spectra are shown at the Lick/IDS resolution ( $\sim 8\text{--}11 \text{ \AA}$ ).

stars and the NGC 5128 GC spectra were smoothed with a wavelength-dependent Gaussian to the resolutions given in Worthey & Ottaviani (1997). The Lick index definitions of Worthey & Ottaviani (1997) and Trager *et al.* (1998) were measured for all spectra, and additive offsets from the Lick standards applied to the GC data. These offsets were obtained by comparing our Lick index measurements of the

standard stars to the Lick/IDS measurements<sup>3</sup>. Straight additive offsets (obtained using a weighted least-squares fit) were applied since there was little evidence of non-linearity in the index comparisons as a function of metallicity. The total uncertainty in our index measurements was calculated as the quadrature addition of the Poisson uncertainty, the repeat measurements uncertainty and the correction to Lick uncertainty. For most indices, the correction to the Lick system was by far the dominant uncertainty. Our Lick index measurements are listed in Table 5 and index uncertainties are given in Table 6.

### 3 ANALYSIS

#### 3.1 An empirical metallicity scale

Before turning to SSPs to derive population parameters, we wished to derive a purely empirical, model-independent metallicity scale for our data in order to rank the NGC 5128 GCs by their metal abundance. There is currently no metallicity scale which has been universally adopted in extragalactic GC research, but those which are used, derived either from integrated colours or spectroscopy, are invariably tied to either theoretical isochrones or Milky Way GC metallicities. We have chosen the latter route, and as a calibration set use Lick index data available for Milky Way GCs. We used GC data for 41 individual GCs taken from Schiavon *et al.* (2005) whose Lick indices were measured and calibrated to the Lick system by Mendel, Proctor & Forbes (2007), and 12 (Lick calibrated) GCs from Puzia *et al.* (2002b). The Schiavon *et al.* (2005) and Puzia *et al.* (2002b) samples have 11 GCs in common, giving a combined dataset of 53 spectra for 42 GCs. Since all the GC indices have been calibrated onto the Lick system, they are directly comparable to our data.

To derive empirical metallicities, we obtained correlations between the Lick index strengths and the Harris (1996, Feb 2003 version) catalogue metallicities of the Milky Way GCs (see e.g., Perret *et al.* 2002; Puzia *et al.* 2002b). The majority of these relations appear non-linear and we therefore characterised the relations with second-order polynomial fits, giving a metallicity estimate for each index measurement. These relations are shown in Figure 4 and the polynomial coefficients and the rms of the fits are listed in Table 7. All the indices, with the exceptions of Fe5015 and NaD, show clear correlations with metallicity. The Fe5015 index is seemingly affected by poor sky subtraction (Schiavon *et al.* 2005), whereas NaD is possibly affected by interstellar absorption. Of the remaining 21 available Lick indices we have chosen to use six indices: Fe4383, Mg<sub>2</sub>, Mg<sub>b</sub>, Fe5270, Fe5335 and Fe5406. These indices all have high correlation coefficients (Table 7), low residuals about the fit, and have relatively small uncertainties in the NGC 5128 data. We avoided the CN and G4300 indices due the unknown role of mixing in the GCs and also the Balmer lines which are affected by age variations. We also avoided the Mg<sub>1</sub> and Ca4455 indices which show signs of significant flattening at the lowest metallicities.

The individual index measurements were then combined

employing a Tukey biweighting scheme (giving outliers less weight, although we note that weighted and unweighted averages yielded very similar results). Uncertainties were derived robustly using the median absolute deviation scaled to asymptotically approach a normal standard deviation (allowing the calculation of a standard error on the mean). Between our final metallicity estimates for the Milky Way GCs and the Harris (1996) values we found a scatter of 0.12 dex. We then proceeded to use the above approach to assign metallicities to the NGC 5128 clusters based upon their Lick indices. Experiments suggested that a S/N<sup>4</sup> of 20 provided robust results, and we therefore took this as a (fairly conservative) minimum S/N for this exercise, leaving 207 GCs in the sample.

This empirical metallicity scale is tied to the Milky Way GC metallicities listed in the Harris (1996) catalogue which comprise a mixture of Zinn & West (1974) spectrophotometric metallicities and high resolution spectroscopic estimates. However, the high-dispersion spectroscopic measurements in the literature are now numerous enough that for most Milky Way clusters (including all the luminous, classic ones that we use below, for example, for Lick index standardization) these are the measurements that dominate the catalog metallicities. What exactly this metallicity scale measures ([Fe/H], [Z/H] or something else) is a matter of debate (e.g., Thomas, Maraston & Bender 2003; Mendel *et al.* 2007). Here we simply regard it as the “Galactic GC metallicity scale”. To reflect this ambiguous nature, we refer to our empirical metallicities as simply [M/H], which are directly comparable to any other metallicities based upon those in the Harris catalogue. Furthermore, in the following sections we use the following notation: we refer to the Harris (1996) catalogue metallicities as [Fe/H], [Z/H] refers to our SSP-derived metallicities,  $[\alpha/\text{Fe}]$  signifies any literature estimates of the  $\alpha$ -element over iron ratio, and [E/Fe] is our SSP-derived ratio of “enhanced” ( $\alpha$ ) elements over iron.

The empirical metallicities and uncertainties for the NGC 5128 GCs are listed in Table 2, and their resulting spectroscopic “metallicity distribution function” (MDF) is shown in Fig. 5. Assuming a total population of 1500 GCs in NGC 5128 (Harris *et al.* 2006b), this represents  $\sim 14\%$  of the GC system. To show the influence of our choice of binning on the precise form of the distribution we show the MDF using three different bin widths of 0.17 dex, 0.15 dex and 0.13 dex. We also overplot nonparametric kernel density estimates using the same kernel bandwidths as the histogram bin widths<sup>5</sup>. Irrespective of the exact choice of binning or density kernel, the NGC 5128 GC MDF looks non-Gaussian. We tested for the presence of metallicity subpopulations in the sample using KMM and the bayesian code Nmix (Richardson & Green 1997; see discussion in Strader *et al.* 2006). Using KMM in the 2-group, homoscedastic case, a bimodal distribution is preferred to a single gaussian with a  $p$ -value of 0. Nmix also finds that a (heteroscedastic) bimodal distribution is more probable than a unimodal one

<sup>4</sup> Signal-to-noise (S/N) values in this study are defined per Angstrom, and are the median value of the entire spectrum.

<sup>5</sup> For these data 0.17, 0.14 and 0.13 dex correspond approximately to Silverman’s (1986) “rule of thumb”, the Sheather & Jones (1991) method for bandwidth estimation and the median uncertainty in the empirical metallicities respectively.

<sup>3</sup> <http://astro.wsu.edu/worthey/html/system.html>

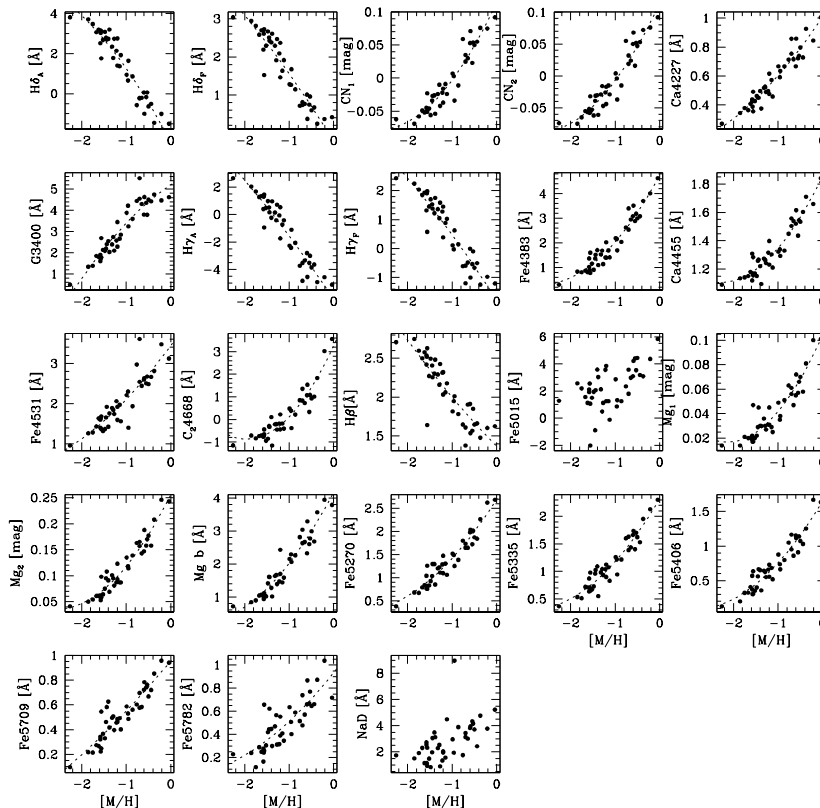


**Figure 4.** The behaviour of the Lick indices measured in the Schiavon *et al.* (2005) sample as a function of the metallicities listed in the Harris catalogue. Dashed lines are our least-squares polynomial fits to these data. No fits were attempted for the Fe5015 and NaD indices.

(45% and < 1% probabilities respectively). therefore, the GC system of NGC 5128 is convincingly multimodal in *spectroscopic* metallicity, reflecting the existence of at least two metallicity subpopulations (Strader *et al.* 2007, Kundu & zepf 2007) rather than a single population (Yoon *et al.* 2006).

It is also apparent that the empirical MDF of the NGC 5128 GCs is on average more metal-rich than that of the Milky Way GCs. A straight mean of the Milky Way GC metallicities gives  $[M/H] = -1.3$  whereas the corresponding value for the NGC 5128 GCs is  $[M/H] = -0.87$ . This result seems to be driven by two factors. Firstly, there is a larger fraction of metal-rich (hereafter red) GCs in the NGC 5128 sample than in the Milky Way sample. Secondly, both the metal-poor (hereafter blue) GCs and red GCs in NGC 5128 are on average more metal-rich than the corresponding populations in the Milky Way. In the bimodal case outlined above, KMM (Nmix) finds peaks at  $[M/H] = -1.34$  and  $-0.52$  ( $-1.30, -0.50$ ) for the NGC 5128 GCs, whereas the corresponding values for the Milky Way GCs are  $[M/H] = -1.62$  and  $-0.61$  ( $-1.62, -0.63$ ). The blue GCs in NGC 5128 are  $\sim 0.3$  dex more metal-rich than the blue GCs in the Milky Way. The red GCs in NGC 5128 are also, on average, slightly more metal-rich than the average of the Milky Way GCs ( $\sim 0.1$  dex).

These differences in the average *spectroscopic* metallic-

ities of the blue and red GC subpopulations between the two galaxies are broadly consistent with the positive correlation between galaxy luminosity and mean GC metallicity found photometrically (Larsen *et al.* 2001; Strader *et al.* 2004; Peng *et al.* 2006). In detail, the blue peak of the NGC 5128 GCs lies close to the upper envelope of the relation (Peng *et al.* 2006; Brodie & Strader 2006) – i.e. more metal-rich than the mean relation – whereas the red peak lies close to the lower envelope of the red relation (i.e. more metal-poor than the mean relation). Since the peaks in the MDF lie slightly off the galaxy colour-magnitude relations in such a fashion, no correction in the integrated magnitude of the galaxy can bring better agreement. However, both population peaks in our data lie within the scatter of the photometric relations.

We also note that the MDF the NGC 5128 GCs is *narrower* than that of the Milky Way GCs. The full-width half-maxima of the two distributions are 1.3 and 1.6 dex respectively. This seems to be largely driven by the blue peak in the NGC 5128 MDF which, being more metal-rich on average than the Milky Way blue peak, has been pushed into the red peak of the MDF.

Inspection of the NGC 5128 MDFs in Figure 5 suggests that there may be further metallicity substructure in the GC system. By eye, peaks in the MDF are apparent at

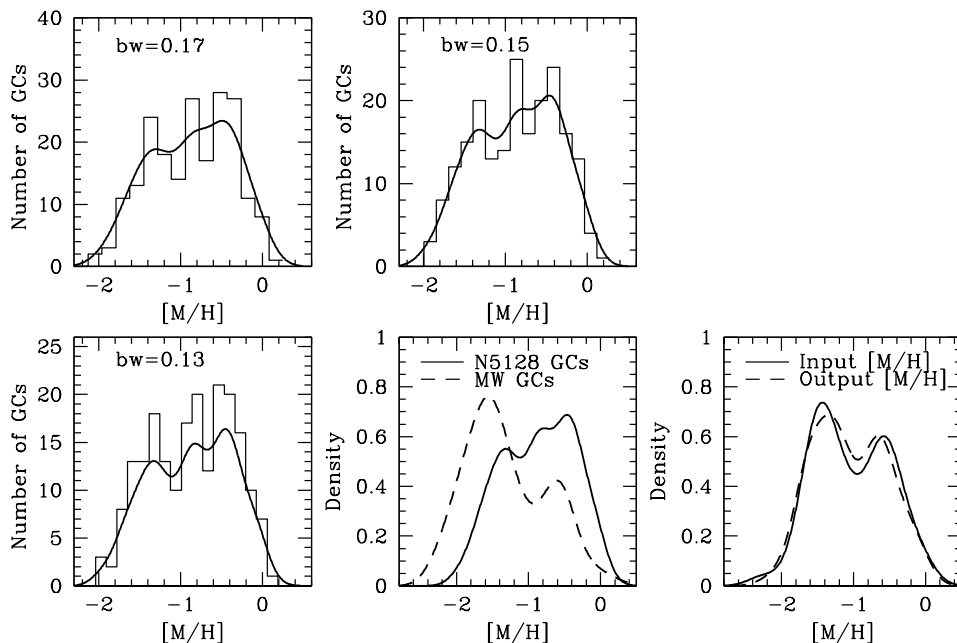


**Figure 5.** Metallicity distribution for 207 GCs ( $S/N > 20$ ) in NGC 5128 derived from an empirical relation based on Milky Way GCs (see text). *Top left panel:* histogram and Gaussian density kernel estimates with bin/kernel bandwidth 0.17 dex, *top centre panel:* 0.15 dex bin/kernel bandwidth, *bottom left panel:* 0.13 bin/kernel bandwidth (mean uncertainty in metallicities). *Bottom centre panel:* comparison between metallicity distributions of NGC 5128 GCs (solid line) and 148 Milky Way GCs (dashed line) taken from the Harris (1996) catalogue where the density kernel bandwidths are 0.15 and 0.19 for the NGC 5128 and the Milky Way GCs respectively. *Bottom right panel:* Comparison of the input Milky Way GC metallicities from the Harris catalogue with those recovered using the empirical metallicity calibration.

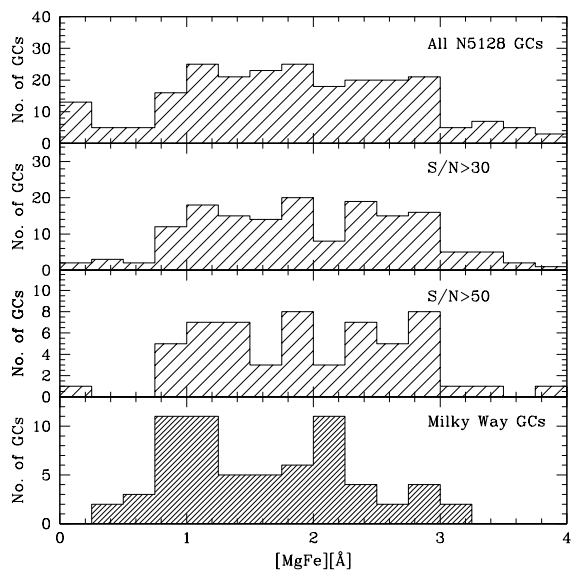


**Figure 6.** Distribution of  $[MgFe]$  of the NGC 5128 GCs for different  $S/N$  limits in the spectra. The lower panel shows the distribution for Milky Way GCs which is clearly bimodal. These NGC 5128 data exhibit a broad, perhaps trimodal distribution.

$[M/H] \sim -1.3, -0.4$  and also perhaps at  $[M/H] \sim -0.8$ . Results for KMM in the trimodal case were inconclusive, but  $N_{mix}$  found peaks at  $-1.43, -0.87$  and  $-0.38$  with a 54%

likelihood that there are three or more peaks in the distribution (recall likelihoods of 1% and 45% were found for the unimodal and bimodal cases respectively.) A test to check on the reality of this “trimodality” is to see if this is evident in the raw Lick indices. In Figure 6 we show histograms of the  $[MgFe]$  index of the NGC 5128 GCs compared to the Milky Way sample used for the metallicity calibration. We show  $[MgFe]$  because this index has higher  $S/N$  than most individual indices (being a combination of three indices) and it is thought to be relatively insensitive to  $\alpha$ -abundance variations (Thomas *et al.* 2003). The distribution of indices for all 254 GCs is broad and relatively flat. As the lower limit of the  $S/N$  of the spectra is increased, three peaks become increasingly evident. We note that similar behaviour is seen in other Lick indices with sufficient  $S/N$ , such as the  $Mg_2$  feature. By contrast, the Milky Way sample (42 unique GCs) is clearly bimodal in  $[MgFe]$ . These results are suggestive that there may be intrinsic substructure in the metal-rich peak of the N5128 MDF.

The radial distribution of the GC metallicities is shown in Figure 7. The entire system shows a mild decrease in  $[M/H]$  with increasing radius as emphasized by the sliding-mean values. A linear fit to the GC data finds a gradient of  $-0.019$  dex/arcmin ( $\sim -0.017$  dex/kpc) with a large dispersion of  $\sim 0.5$  dex (see also Woodley *et al.* 2005). We find no significant gradients in either the blue or red GC subpopulations. This being the case, the metallicity gradient seen for the whole sample must be largely driven by an increasing fraction of blue/red GCs with radius (e.g., Perrett *et al.* 2002; Harris *et al.* 2006b).

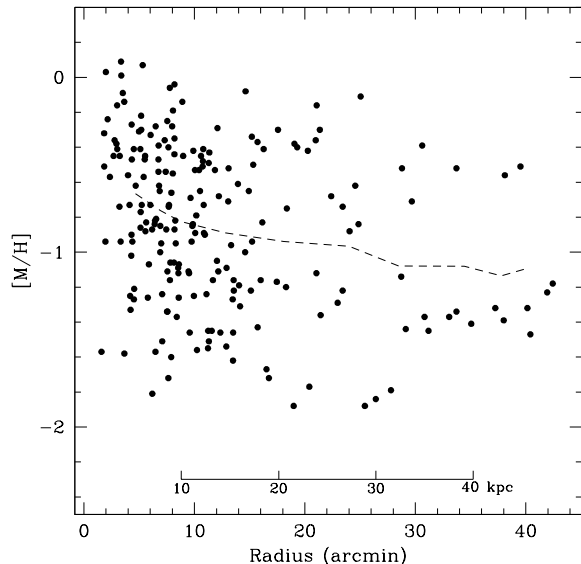


**Figure 7.** Radial distribution of spectroscopic metallicities for 207 GCs in NGC 5128. The dashed line is a sliding mean using a width of 5 arcmin.

One concern in using the Milky Way GCs as metallicity calibrators for extragalactic GC systems is the small number of Milky Way GCs with high metallicities. In the combined Schiavon+Puzia samples, only 5 unique GCs (10 spectra) have  $[\text{Fe}/\text{H}] \geq -0.5$ , with perhaps only NGC 6528 at solar metallicity. In order to give the reader an idea of the uncertainties in our metallicity calibration, we show in the bottom-right panel Fig. 5 a comparison of the metallicities of the input Milky Way GC calibrators with those recovered using our calibration on these same data. The plot shows that the extremes of the metallicity distribution are quite well constrained, although there is some small variation in the peak locations. KMM locates peak metallicities of  $-1.42$  and  $-0.57$  in the input sample, and finds peaks of  $-1.44$  and  $-0.54$  in the recovered metallicities. The mean metallicity of the sample does not change. Therefore, within the metallicity range of the Milky Way GC calibrators, the empirical metallicity scale is fairly well constrained. For metallicities above solar this is no longer the case. However, as shown in Figure 6, very few NGC 5128 GC have metallic indices stronger than the most metal-rich Milky Way GCs, and therefore the exact behaviour of the empirical calibration beyond solar metallicity is not of great concern.

### 3.1.1 Comparison between GCs and field stars

The existence of star-by-star photometry of the giants in NGC 5128 allows us to compare directly the MDF of the field stars with that of its GCs. Photometric MDFs have been constructed at projected radii of 8 kpc (Harris & Harris 2002), 20 kpc (Harris & Harris 2000) and at 38 kpc (Rejkuba *et al.* 2005) all determined from  $(V - I)$  photometry of the halo red-giant branch (RGB) stars with the cameras on board *HST*. An obvious problem here is choosing at what radius the GCs should be compared with the field stars. In the absence of a compelling scientific criterium, we have cho-

sen to compare our data with both the “middle field” at 20 kpc ( $\sim 4R_e$ ) from Harris & Harris (2000) and the “inner field” of Harris & Harris (2002) at 8 kpc ( $\sim 1.5R_e$ ). Note that although both these field star MDFs are photometric and the GC MDF is spectroscopic, all are calibrated to the metallicity scale of the Milky Way GCs in the Harris catalogue and are therefore readily comparable. We also note that our sample of GCs may be somewhat radially biased in the sense that the metal-rich GCs may be overrepresented. The KMM tests in performed in Section ?? find a blue GC fraction of 41% and a red GC fraction of 59%. From a sample of 300 NGC 5128 GCs (of which 100 are from this present study) Woodley *et al.* (2005) find that some 54% are blue and 46% are red. However, the true blue:red fraction will have to await a complete photometric catalogue.

The comparison of the MDFs is shown in Figure 8. In the figure, the normalised density distribution of the GCs has been scaled by a factor of 1.7 to illustrate the close coincidence of the metal-rich end of the GC MDF with that of the 20 kpc field (at  $[\text{M}/\text{H}] \sim -0.45$ ). In comparison, the average metallicity of the 8 kpc field star MDF is some 0.2 dex more metal rich than the GCs. Some  $\sim 16\%$  of the RGB stars in the 8 kpc field are more metal-rich than solar. This is probably only a lower limit since incompleteness effects due to problems in dealing with the reddest RGB stars mean that the most metal-rich stars in the MDF are probably underrepresented (Harris & Harris 2002). In addition, considering that the inner stellar field is at a galactocentric radius of  $\sim 1.5R_e$ , we might expect even more metal-rich stars in the central regions of the galaxy than are seen in the 8 kpc MDF. In contrast, few of the GCs in our sample are convincingly super-solar in metallicity; the most metal-rich GCs in NGC 5128 have comparable metal-line strengths to the most metal-rich Milky Way GCs in the Schiavon *et al.* (2005) and Puzia *et al.* (2002) samples (NGC 6528 and NGC 6553). So, although our GC sample is by no means complete in the inner regions of NGC 5128, it presently appears that a significant fraction of the galaxy stars were able to obtain levels of heavy-element enrichment substantially higher than any of its GCs.

The other principal feature in the comparison of the MDFs is, as discussed by Harris & Harris (2000; 2002), that the number ratio of GC to stars varies considerably with metallicity. No more than 10% of the stellar MDF is more metal-poor than  $[\text{M}/\text{H}] \sim -1$ , whereas 40% of the GCs are more metal-poor than  $[\text{M}/\text{H}] \sim -1$ . This implies that the ratio of efficiencies of metal-poor GCs to metal-poor stars is significantly higher than the corresponding metal-rich ratio, and/or the dynamical destruction efficiency of metal-poor GCs is considerably lower than that of their metal-rich counterparts. From the  $r_e/2$  integrated spectrum of the galaxy itself, we derive a mean metallicity of  $[\text{M}/\text{H}] = -0.40 \pm 0.12$ , in agreement with the metallicities found by Harris & Harris (2002).

In constructing the NGC 5128 GC MDF with an empirical metallicity calibration tied to Milky Way GCs, we have made the implicit assumptions that the NGC 5128 GCs have ages and abundance ratios comparable to the Milky Way GCs. These assumptions are tested in the following section where we estimate ages, metallicities and abundance ratios for a higher S/N subset of GCs using SSP models.



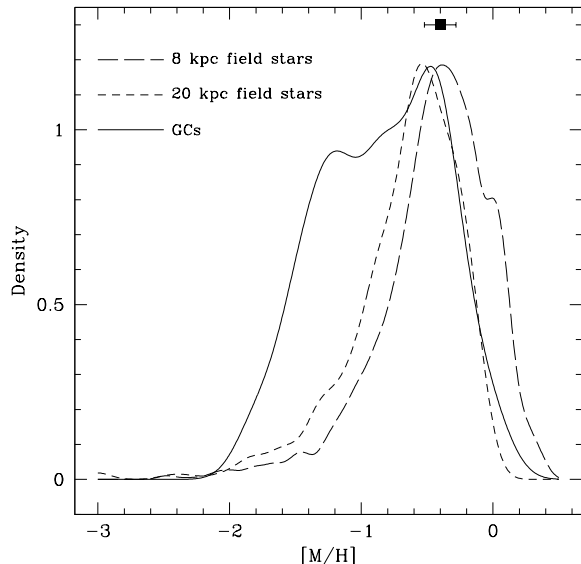


**Figure 8.** Comparison of the metallicity distribution functions of NGC 5128 halo field stars at 8 kpc (Harris & Harris 2002) and 20 kpc (Harris & Harris 2000) with the spectroscopic MDF of the NGC 5128 GCs. The normalised density distribution of the GCs has been scaled by  $\times 1.5$  to illustrate the similarities between the metal-rich ends of the distributions. The solid square represents the metallicity derived from the  $r_e/2$  integrated spectrum of NGC 5128 using our empirical metallicity calibration.

### 3.2 Stellar Population Models

Estimating ages, metallicities and abundance ratios from the integrated spectra of GCs requires the use of single-burst stellar population models (SSPs). However, as becomes readily apparent from the extensive literature on the subject, such parameter estimates remain model dependent.

Motivated by the studies of Proctor, Forbes & Beasley (2004) and Mendel *et al.* (2007), who compared SSP-derived ages, metallicities and abundance ratios with literature estimates for Milky Way GCs, we used two different sets of SSPs. We used the Lee & Worthey (2005) models (henceforth LW05 models) and the Thomas *et al.* (2003) models, augmented with the higher order Balmer-line calculations of Thomas, Maraston & Korn (2004) (henceforth collectively referred to as TMK04 models). Mendel *et al.* (2007) showed that the LW05 models, when corrected for non-solar abundance ratios (NSARs) using the fractional sensitivities of H02, and the TMK04 models are able to reproduce the ages, metallicities and  $[\alpha/\text{Fe}]$  ratios for Milky Way GCs with  $[\text{Fe}/\text{H}] \leq -0.5$  quite well. The LW05 models were particularly successful at recovering the  $[\alpha/\text{Fe}]$  patterns of Milky Way GCs found from high resolution spectroscopic estimates (e.g., Pritzl *et al.* 2005). At metallicities approaching the solar value, Mendel *et al.* (2007) found some evidence that the LW05 models underestimate the ages of MW GCs. In the case of the TMK04 SSPs, Mendel *et al.* (2007) showed that these models predict an age-metallicity relation for Milky Way GCs in the opposite sense to those found by CMD determinations (De Angeli *et al.* 2005). However, the TMK04 models seem better able to recover the ages of the most

metal-rich ( $[\text{Fe}/\text{H}] > -0.5$ ) Milky Way GCs. We note that neither of these models has been well tested in the intermediate and young age regime.

A detailed discussion of the LW05 models is given in LW05, and the correction of these models for NSARs is discussed in Mendel *et al.* (2007). Similarly, details of the TMK04 models are given in TMK04 and Thomas *et al.* (2003). For our purposes, the LW05 have been corrected for NSARs using the fractional sensitivities of H02, and have also been interpolated in age, metallicity and  $[\text{E}/\text{Fe}]$  to give finer grids spacings. The TMK04 SSPs are used as published, but have also been interpolated in age, metallicity and  $[\text{E}/\text{Fe}]$ . TMK04 provide two sets of models which assume different amounts of mass loss on the horizontal branch. Here we use the “blue horizontal branch” models, but note that this choice of model has no significant impact on our conclusions.

#### 3.2.1 Qualitative impressions

In Figure 9 we show the NGC 5128 and Milky Way samples compared to the LW05 and TMK04 models at  $[\text{E}/\text{Fe}] = 0$ . In the case of the NGC 5128 data, only clusters with median  $S/N \geq 50$  are shown in order to compare more directly with the higher  $S/N$  ( $\gg 50$ ) Milky Way data. From the figure we see that the NGC 5128 and Milky Way GCs span a comparable range of metallicities and in general follow the old-age lines of the models. Notwithstanding the larger scatter in these NGC 5128 data, at  $[\text{MgFe}] \sim 2 - 3$  a number of the NGC 5128 GCs exhibit an enhancement in their Balmer lines compared to the Milky Way sample. The locii of GCs with  $[\text{MgFe}] < 1.5$  coincide quite well in Figure 9 suggesting that there are no gross offsets between the two GC samples (with the possible exception of  $\text{H}\gamma_A$ ). This being the case, stronger Balmer indices in some NGC 5128 GCs when compared to the Milky Way sample (at a given  $[\text{MgFe}]$ ) would conventionally be interpreted as some of the NGC 5128 clusters having younger ages than those in the Milky Way sample. The position of the spheroid of NGC 5128 indicates a luminosity-weighted near-solar metallicity and a younger age than the Milky Way GCs and the majority of the NGC 5128 GCs.

Figure 10 shows Mg/Fe diagnostic model grids compared to the two datasets. In both the  $\text{Mgb} - \langle \text{Fe} \rangle$  and  $\text{Mg}_2 - \text{Fe}5406$  planes, the locii of the NGC 5128 GCs are shifted to the left of the Milky Way GCs (shifted to lower Mg and/or higher Fe). These plots suggest that the NGC 5128 GCs generally have lower Mg/Fe ratios than the Milky Way GCs at a given metallicity, and that the NGC 5128 spheroid has lower Mg/Fe ratios than its GCs. In the right-hand panels of Figure 10 we compare the  $\text{CN}_2$  measurements of the GCs at a fixed  $[\text{MgFe}]$ . The two GC systems show very similar CN values for a given  $[\text{MgFe}]$ , and both systems seem strongly enhanced in CN with respect to the model grids and the spheroid light of NGC 5128. This CN enhancement is becoming a seemingly typical characteristic of GC systems (e.g., Cenarro *et al.* 2007). We note that these NGC 5128 data show a significant spread in  $\text{CN}_2$  when compared to the Milky Way GCs.

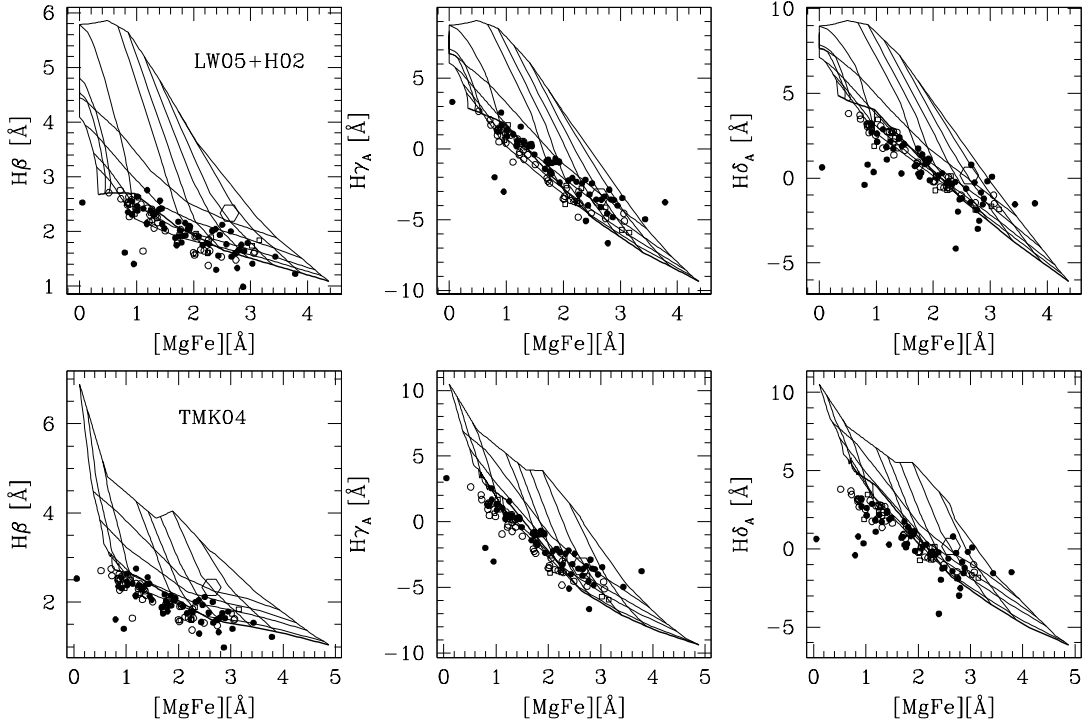


**Figure 9.** NGC 5128 and Milky Way GCs compared to SSP grids of LW05 (top panels) and TMK04 (lower panels) at  $[E/Fe]=0$ . Solid circles represent NGC 5128 GCs ( $S/N \geq 50$ ), open circles are MW GCs from Schiavon *et al.* (2005), squares are from Puzia *et al.* (2002). The large open hexagon shows the line strengths of the NGC 5128 spheroid ( $r_e/2$  aperture along the major axis). The LW05 SSPs shown cover the parameter space ( $[Z/H]=-2.5, -2.2, -2, -1.5, -0.75, -0.5, -0.25, 0, 0.25, 0.5$ ; ages=1,3,5,8,10,12 Gy) and TMK04 ( $[Z/H]=-2.25, -2.2, -2, -1.5, -0.75, -0.5, -0.25, 0, 0.2, 0.5, 0.67$ ; ages=1,3,5,8,10,15 Gy).

### 3.2.2 Multivariate model fits

To estimate the SSP model parameters which best describe these data, we employed the robust multi-index  $\chi^2$  fitting approach detailed in Proctor *et al.* (2004). This method has been used with success to estimate ages, metallicities and abundance ratios for both galaxies and extragalactic GCs, giving consistent results with single index-index determinations, but is more robust when confronted with problems such as varying S/N and background emission (e.g., Proctor *et al.* 2004; Pierce *et al.* 2006). Measured Lick index data are compared to the same indices measured from a SSP grid where  $[Z/H]$ , age and  $[E/Fe]$  are allowed to vary. For each grid point a  $\chi^2$  statistic is calculated. Any indices which are highly deviant from the fit are removed and  $\chi^2$  recalculated (in our case, we ran three iterations with a 5-3-5 $\sigma$  clipping pattern). The entire grid is then searched until  $\chi^2$  is minimized (see Proctor *et al.* 2004 for a detailed description). Uncertainties on the three parameters were determined by randomly perturbing the individual indices by their uncertainties and recalculating the fits.

In the case of the Milky Way data, the following indices were excluded from the entire fitting process:  $CN_1$ ,  $CN_2$  and  $Ca4227$  (due to very strong C and/or N enhancement in the spectra),  $Fe4531$  and  $Fe5015$  (problematic sky-subtraction in the Schiavon *et al.* 2005 data) and  $NaD$  (problems with

interstellar absorption). For the NGC 5128 data, indices excluded were  $CN_1$ ,  $CN_2$  and  $Ca4227$ ,  $NaD$ ,  $TiO_1$  and  $TiO_2$ . The two  $TiO$  indices did not fall into the wavelength range of these data. We also excluded  $H\gamma_A$  since there is some evidence of a systematic offset in this index compared to the Milky Way sample (e.g., see Figure 9).

Since the NGC 5128 spectra have a range of median S/N (10–114  $\text{\AA}^{-1}$ ) we tested the robustness of the fitting process as a function of the median S/N of the spectra. To this end we took the Schiavon *et al.* (2005) spectrum of NGC 104 (47 Tuc) and systematically degraded the S/N of the spectrum from 200–10  $\text{\AA}^{-1}$  by adding Poisson noise. For each S/N interval 100 degraded spectra were created with a random seed used in each case. The  $\chi^2$  fitting technique was then applied to the Lick indices measured from these spectra to see how well we could recover the initial best solutions. The results of this exercise are shown in Figure 11 using the LW05 models (similar results are obtained for the TMK04 models). Our simulations suggest that the  $\chi^2$  approach recovers the initial parameters down to median S/N  $\sim 20 - 30$ . At lower S/N we see that the fitting results become increasingly unreliable. In the example in Figure 11 it is noticeable that as the metallicity is overestimated, the age becomes increasingly underestimated which is a consequence of age–metallicity degeneracy. We also note that similar experiments on several other metal-rich GCs gener-

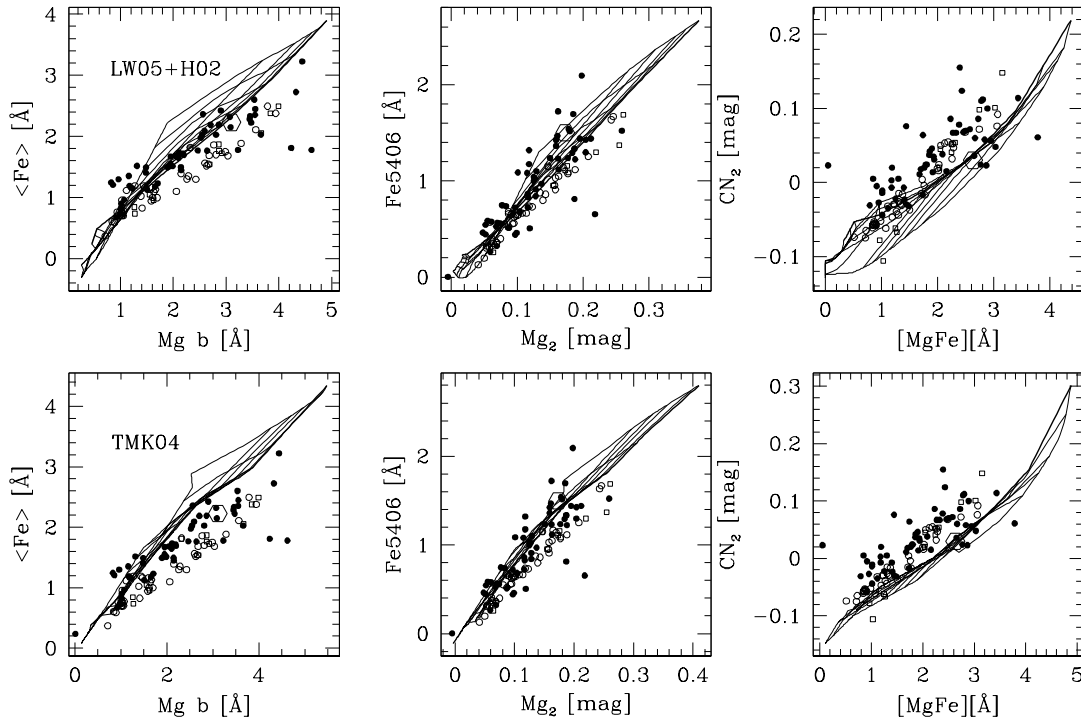


**Figure 10.** NGC 5128 and Milky Way GCs compared to SSP grids of LW05 (top panels) and TMK04 (lower panels) at  $[E/Fe]=0$ . Symbols and SSP grids are the same as for Fig. 9. The NGC 5128 GCs on average exhibit lower Mg/Fe ratios than the MW GCs at a given metallicity.

ally indicated a tendency to underestimate the age of the GCs at low S/N. Informed by our simulations we proceeded to choose a S/N of  $30 \text{ \AA}^{-1}$  as the lower limit for our SSP analysis. This cut in S/N left us with a total of 147 GCs.

The best LW05 and TMK04 model fits for age and metallicity for the two GC samples are shown in Figures 12 and 13. The corresponding (normalised) collapsed age and metallicity distributions are also shown. Error bars for the GCs have been omitted for clarity, but for example the mean errors in age and  $[Z/H]$  for the NGC 5128 GCs are 2 Gy and 0.14 dex respectively (at a mean S/N of 50). For both sets of models, but more obviously for the LW05 SSPs, the NGC 5128 GCs appear to split into two groupings. There is an old ( $> 8$  Gy) population with a wide range of metallicities and an apparently younger, predominantly metal-rich population ( $[Z/H] > -1$ ). The results from using the LW05 models suggest that some 22 out of 147 (15%) of the GCs in our sample may be younger than 8 Gy (henceforth, we will refer to these objects as intermediate age cluster candidates, or IACCs). For the TMK04 models, this fraction drops to 17/147 (12%) of the sample. This disparity between the LW05 and TMK04 models in terms of the number of IACCs is a result of applying a fixed absolute age criteria (i.e. 8 Gy) when there is a difference in the absolute age zero-points between models (c.f. Figures 12 and 13).

Taken at face value, Figures 12 and 13 suggest that a significant proportion of the *metal-rich* GCs are distinctly younger than the classic 12 to 13 Gy characterizing the

metal-poor ones. In fact, the interpretation of the nature of these IACCs is complicated by the fact that a number of Milky Way GCs occupy a similar area of parameter space. Specifically these GCs are NGC 6388, NGC 6441, NGC 6528, NGC 6553 and NGC 5927 (although note in that in Figures 12 and 13, these clusters are over-represented since three of these clusters are in common between the Schiavon *et al.* (2005) and Puzia *et al.* (2002) samples). NGC 6388 and NGC 6441 have been shown to have extended blue horizontal branches despite their high metallicities (Rich *et al.* 1997) which may be affecting their integrated light and thus biasing their age estimates. The other three clusters show no such obvious hot populations but still show enhanced Balmer lines. Understanding the origin of this young signature in the integrated light of ostensibly old GCs is beyond the scope of this paper, but is clearly a priority. Notwithstanding the presence of these “younger” Milky Way clusters, the age distributions of the two GC samples do appear statistically different. Kolmogorov-Smirnov (KS) tests comparing the age distributions of the NGC 5128 and Milky Way GCs find that the age distributions differ at 96% (LW05 models) and 95% confidence (TMK04 models).

We also identify one young cluster which appears to be an outlier in both figures. Cluster HGGH-G279 is younger and more metal-poor than the rest of the IACCs with  $[Z/H], \text{age} = -1.2, 1.7$  Gy ( $-1.2, 2.2$  Gy) LW05 models (TMK04 models). The spectrum of this cluster is shown in Figure 3, which clearly shows the signature of a young stellar

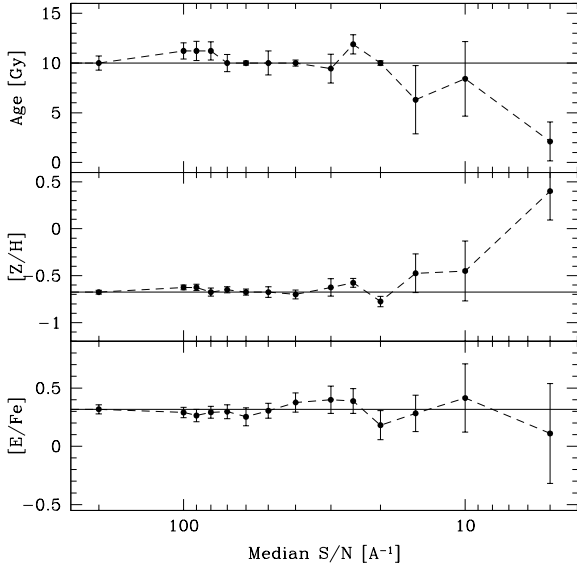


**Figure 11.** Ability of the  $\chi^2$  fitting procedure to recover the input age,  $[Z/H]$  and  $[E/Fe]$  as a function of median S/N for the Milky Way GC NGC 104 (47 Tuc). Symbols with error bars represent the median of 100 Monte Carlo iterations with  $1\sigma$  uncertainties. The solid horizontal lines in each panel show the position of the initial best-fit parameter derived in this case using the LW05 SSP models.

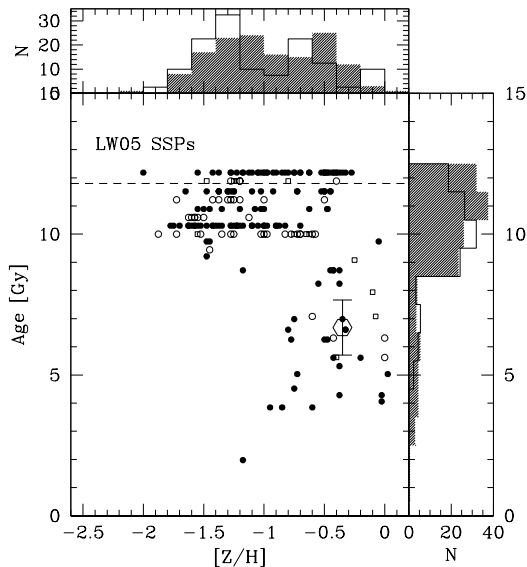


**Figure 12.** Ages and metallicities for all NGC 5128 GCs with  $S/N > 30$  (147 GCs) and Milky Way data (symbols as for Figure 9) using the LW05 models. The shaded and open histograms show the collapsed distributions in age and metallicity for the NGC 5128 and Milky Way GCs respectively. The NGC 5128 datapoints have been offset by +0.3 Gy for display purposes. The horizontal dashed line shows the old age limit of the models.

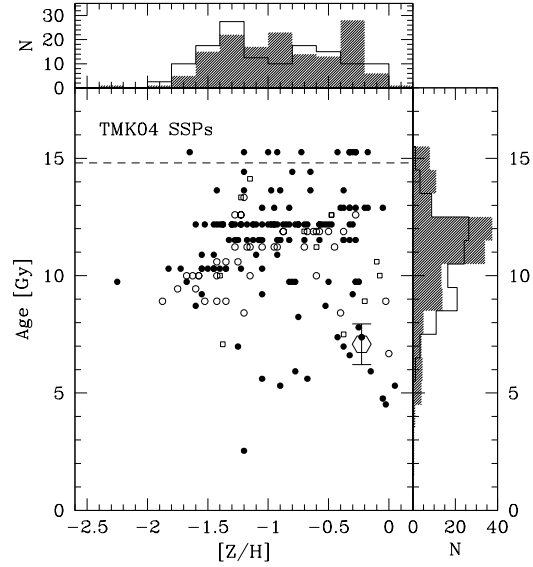


**Figure 13.** Ages and metallicities for NGC 5128 GCs and Milky Way data (symbols as for Figure 9) using TMK04 models.

population. HGHH-G279 was identified as a young cluster candidate spectroscopically by Held *et al.* (2002) and photometrically by PFF04.

In the case of the integrated light of the galaxy itself, the  $r_e/2$  bulge light occupies a position centred somewhere near the middle of the IACC subpopulation ( $\sim 6 - 7$  Gy,  $[Z/H] \sim -0.3$ ). Our spectroscopic metallicity for the NGC 5128 bulge compares favourably with the determination of Harris & Harris (2002) from direct *HST* photometry of red giants. These authors determined an average metallicity  $[Fe/H] = -0.2$  at a projected radius of 8 kpc ( $\sim 1.6 r_e$ ) in NGC 5128. Our age estimates for the bulge are also in good agreement with literature determinations. Based on the AGB bump and red clump locations from *HST/ACS* imaging of a more distant field (38 kpc projected radius), Rejkuba *et al.* 2005 estimated an average age of  $8 \pm 3$  Gy for the halo stars.

The behaviour of our  $[E/Fe]$  estimates versus  $[Z/H]$  derived from the LW05 and TMK04 models for the two GC samples are shown in Figure 14. Confirming the qualitative impressions given in Figure 10, the NGC 5128 GCs appear to be, on average, offset to lower  $[E/Fe]$  than the Milky Way GCs at a given  $[Z/H]$ . This is true for both models and at all metallicities. However, the  $[E/Fe]$  predictions of the two SSPs show significant differences. For the LW05 models, the NGC 5128 and Milky Way sample show quite similar behaviour, although the Milky Way GCs show a smaller scatter in  $[E/Fe]$  at a fixed  $[Z/H]$ .

The  $[E/Fe]$  values derived using the TMK04 models are harder to interpret. As shown by Mendel *et al.* (2007), the Milky Way GCs show a larger scatter in  $[E/Fe]$  at a fixed metallicity than is the case for the LW05 models. In addition, for the Milky Way sample  $[E/Fe]$  increases noticeably at  $[Z/H] \leq -1$ . However, the same behaviour is not seen in the NGC 5128 sample. The NGC 5128 sample shows significant scatter, but the mean  $[E/Fe]$  remains roughly constant with metallicity. This results in a situation where the locii of the

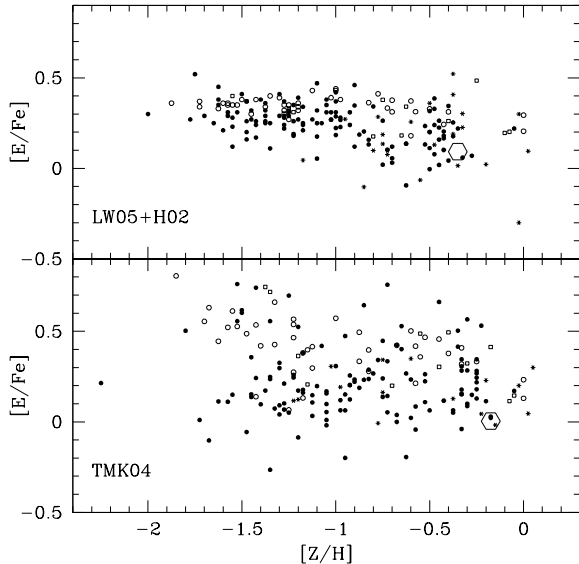


**Figure 14.** The run of  $[E/Fe]$  with metallicity for old NGC 5128 GCs (solid symbols), IACCs (asterisks) and the Milky Way sample (open symbols) from the SSP analysis.

two samples appear to increasingly diverge with decreasing metallicity. The origin of this divergence at low metallicities is unclear, but is possibly related to the relative insensitivity of the TMK04 model indices to  $[E/Fe]$  at low metallicities. Relatively small divergences between the model and data at low metallicities may be amplified and appear as large deviations in  $[E/Fe]$  as the models “pinch” together (see Mendel *et al.* 2007).

In both models, the NGC 5128 GCs generally possess higher  $[E/Fe]$  than the galaxy bulge light ( $[E/Fe] \sim 0.1$ ). Separating by GC age, we find no statistically significant differences in  $[E/Fe]$  between the IACCs and old clusters.

### 3.2.3 Comparison with PFF04

PFF04 compared the Lick  $H\beta$  index and  $[MgFe]'$  index (defined by Thomas *et al.* 2003) to the Thomas *et al.* 2003 SSPs and determined an average age for the metal-rich GCs in NGC 5128 of  $5^{+3}_{-2}$  Gy. Of the 23 GCs in the PFF04 study, 15 are in common with our sample and with sufficient S/N for age/metallicity analysis. Twelve of these we define as metal-rich ( $[Z/H] > -1$ ). We find a mean age of these clusters of  $8.9 \pm 2.7$  Gy (LW05 models), roughly consistent with the PFF04 results. Of the IACCs in common between the samples, the three youngest GCs in PFF04 (HGHH-41, R261 and PFF-100) are also the youngest GCs according to our analysis. Therefore, we find broad agreement between the two studies.

However, we do note an important distinction: PFF04 found that 7 of out 11 of their *metal-rich* sample was younger than 8 Gy. If metal-rich GCs truly reflect field star formation, then this would imply that some 63% of the galaxy field stars were formed at  $z \lesssim 1$ . Our results from the larger sample suggest an IACC fraction of somewhere between 20% (TMK04 models) and 28% (LW05 models). However, this can at least in part be explained by the differences in the

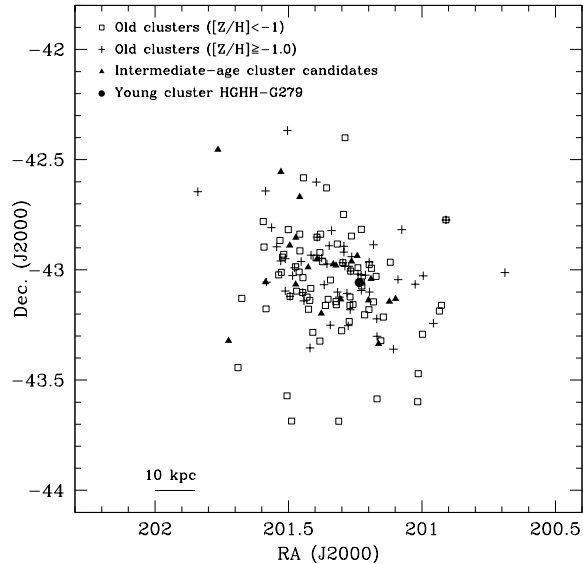


**Figure 15.** Spatial distribution of NGC 5128 GCs.

two samples. The GCs used in the PFF04 analysis were limited to the brightest GCs, all of which had  $V_0 \leq 18.4$ . When we make the same magnitude cut on our larger sample, the IACC fraction rises to 45% of all metal-rich GCs.

### 3.3 Other Properties of the Cluster System

In the following we concentrate on results derived from the LW05 models which in general give lower reduced- $\chi^2$  values than the TMK04 models and do not exhibit an age/metallicity trend for the old *metal-poor* clusters. However, this choice of model does not alter our basic conclusions.

The spatial distribution of the 147 NGC 5128 GCs which have both age and metallicity information is shown in Figure 15. The IACCs show a clear preference towards the inner regions of the galaxy; their spatial clustering properties appear very similar to those of the old metal-rich clusters. In fact we see little difference between the spatial distributions of the IACCs, and the rest of the metal-rich sample. The old blue clusters show a slightly more extended distribution, although the bias along the major axis in our spectroscopic sample and our incompleteness in the very central regions prevents a more quantitative analysis of these distributions (the apparent “ring” feature is a result of this incompleteness in the centre).

In Figure 16, we show the de-reddened  $V$ -band luminosity functions of the old red GCs and IACCs. The IACCs appear on average *fainter* than the old red GCs, with means of  $V_0 = 18.8 \pm 0.2$  and  $18.2 \pm 0.5$  respectively. However, this difference is not statistically significant; a KS test returns a 64% probability that the two distributions are drawn from the same parent distribution.

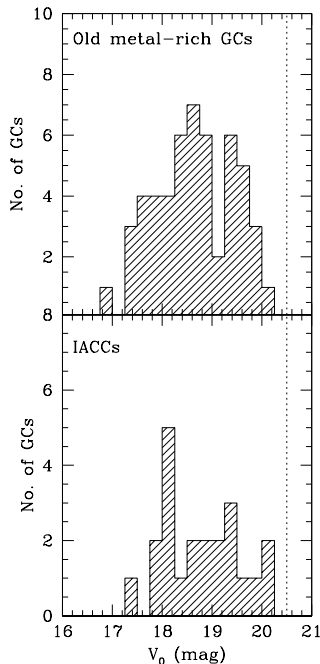


**Figure 16.**  $V$ -band luminosity functions of the old red GCs and the IACCs. The vertical dashed line represents the position of the turnover in the luminosity function at  $V_0 \sim 20.5$  (Harris *et al.* 2004).

#### 4 SUMMARY AND DISCUSSION

We have performed a spectroscopic survey of GCs and GC candidates in the nearby elliptical NGC 5128 using the 2dF instrument on the AAT. We obtained integrated optical spectra ( $\lambda\lambda 3800 - 6100\text{\AA}$ ) of 254 GCs of which 79 are newly confirmed on the basis of their radial velocities and spectra. On higher S/N subsets of these data we derived empirical metallicities for 207 GCs and performed stellar population analyses using two different SSP models for 147 GCs. A parallel analysis was applied to a sample of 42 Milky Way GCs from Schiavon *et al.* (2005) and Puzia *et al.* (2002b), and to an  $r_e/2$  aperture integrated spectrum of the bulge light constructed from 10 dedicated galaxy fibres. Our principal findings are:

- The empirical spectroscopic metallicity distribution function (MDF) of the NGC 5128 GCs is multimodal at high statistical significance, with two clear peaks at  $[M/H] \sim -1.3$  and  $\sim -0.5$ . The mean metallicity of the ngc 5128 GCs is some 0.5 dex more metal-rich than that of the Milky Way GC sample.

- There is evidence for a mild radial metallicity gradient in the NGC 5128 GC system ( $\sim -0.017$  dex/kpc). There is no evidence for gradients in either the metal-poor (blue) or metal-rich (red) subpopulations themselves; the global gradient is attributable to an increasing ratio of blue to red GCs with radius.

- A comparison between the MDFs of the NGC 5128 GCs and the field stars at 20 kpc (Harris & Harris 2000) reveals close coincidence in the locations of the metal-rich ends of the distributions. However, the 8 kpc stellar MDF (Harris

& Harris 2002) possesses a significant fraction of stars ( $\geq 16\%$ ) more metal-rich than the most metal-rich GCs in our sample. The ratio of GCs to field stars sharply increases with decreasing metallicity.

- Comparison with stellar population models suggests that the majority of the NGC 5128 GCs ( $\sim 85 - 90\%$ ) have old ages ( $> 8$  Gy). The remaining fraction of GCs appear younger than this, and all of these objects lie in the red peak of the MDF. However, these GCs lie in a parameter space occupied by a number of Milky Way GCs which have old ages derived from colour-magnitude diagrams, but have younger ages according to the SSP models. The presence of old, hot stellar populations in these GCs mimicking the effects of younger stellar populations cannot be ruled out. The  $r_e/2$  bulge light occupies a location roughly centred amongst the intermediate age cluster candidates (IACCs,  $\sim 6 - 7$  Gy old,  $[Z/H] \sim -0.3$ ).

- SSP model predictions for the abundance ratios ( $[E/Fe]$ ) show significant differences. However, the  $[E/Fe]$  of the NGC 5128 GCs appear, on average, lower than those of the Milky Way GCs at a given metallicity. The IACCs are not differentiated from the old GCs in this regard. The abundance ratio of the bulge light is lower than the bulk of the GCs ( $[E/Fe] \sim 0.1$ ).

We begin by highlighting the principal uncertainty in our analysis. An outstanding, unsolved problem is how to deal with unresolved hot stellar populations (horizontal branch stars, blue stragglers etc.) in the integrated spectra of GCs, which can mimic the effect of young stellar populations (e.g., Burstein *et al.* 1984). This is possibly the origin of the “young” SSP ages for the most metal-rich Milky Way GCs in this study, and remains a key uncertainty in attempts to age-date GCs from integrated spectra (e.g., Beasley *et al.* 2002a; Puzia *et al.* 2005; Cenarro *et al.* 2007). Hot stars in old stellar populations can and are, of course, included in SSPs, but in general follow recipes based on Milky Way GCs (e.g., Vazdekis 1999; Maraston 2000; Lee *et al.* 2000). The behaviour of non-canonical populations cannot be modelled *a priori* and therefore must be estimated by observation. Wider wavelength ranges beyond the optical are urgently required to address this problem. In particular, we look forward to the use of *GALEX* in constraining the near and far UV flux and therefore the hot star populations in unresolved stellar systems. This uncertainty in how to deal with non-canonical populations, and the differences in the age predictions of the TMK04 and LW05 models at high metallicity (see Section 3.2 and Mendel *et al.* (2007)), must be born in mind in the following discussion of GC ages.

One of the main results of this study is that the spectroscopic MDF of the NGC 5128 GCs is clearly bimodal, if not multimodal. The colour distribution of this GC system also appears bimodal (e.g. Harris *et al.* 2004), as do the colour distributions of GC systems for most massive galaxies (e.g., Larsen *et al.* 2001; Harris *et al.* 2004; Strader *et al.* 2004; Peng *et al.* 2006). Yoon *et al.* (2006) have suggested that such bimodal colour distributions might simply be a result of a non-linear colour-metallicity relation, i.e., an intrinsically unimodal metallicity distribution can appear bimodal in broadband colours. However, our results indicate otherwise. The MDFs of extragalactic GCs in massive galaxies are bimodal, and this needs to be accounted for by any models

of GC system (and massive galaxy) formation. Our results for NGC 5128 are in agreement with the results from IR photometry of M87 GCs (Kundu & Zepf 2007) and with the Cohen *et al.* (2003) spectroscopy of M49 GCs as shown by Strader *et al.* (2007).

We are again faced with the problem that the GC systems of massive galaxies are bimodal in colour/metallicity. From a chemical evolution point of view, a unimodal distribution is easier to understand than a bimodal one (e.g., Harris & Harris 2002; Beasley *et al.* 2003; Bekki *et al.* 2003; VanDalsen & Harris 2004; Pipino *et al.* 2007). This would be particularly true if the MDFs of the GCs and field stars were to resemble each other, since the same star formation recipe may reasonably be expected to be applicable to both. However, as shown in Section 3, the GC and stellar MDFs are quite different. The most metal-rich ends of the distributions do show a strong resemblance (c.f. Figure 8), but the radial gradient of the field stars in NGC 5128 suggests that the innermost stars in this galaxy are more metal-rich than the vast majority of the GCs found in this survey (Harris & Harris 2002). Moreover, any resemblance between the MDFs quickly disappears with decreasing metallicity. The inference is that either the ratio of GC formation to field star formation efficiency increases with decreasing metallicity, or that the dynamical destruction efficiency of GCs increases with increasing metallicity (or some combination of the two). This applies equally whether the GCs and field stars are formed *in situ* (e.g., Forbes *et al.* 1997) or come from elsewhere (e.g., Côté, Marzke & West 1998; Beasley *et al.* 2002b). Understanding these differences, and indeed *how* exactly one should compare the field stars to the GCs (e.g., at what radius) remains an important aspect in understanding the galaxy–GC connection.

Our stellar population analysis suggests that there may be a mixture of GC ages in the NGC 5128 system. We find that some 10–15% (SSP model dependent) of the sample may have intermediate ages ( $\sim 4 - 8$  Gy). At least one cluster is younger and more metal-poor than the intermediate-age candidates (HGHH-G279;  $\sim 1 - 2$  Gy,  $[Z/H] \sim -1.2$ ), with Peng *et al.* (2002) finding an even younger cluster ( $< 1$  Gy) in a blue tidal stream in the halo of NGC 5128. A  $\sim 15\%$  fraction of intermediate-age clusters is substantially lower than the  $\sim 67\%$  estimate claimed by PFF04, bringing NGC 5128 more into line with the small contribution of intermediate-age populations found in other nearby ellipticals (Strader *et al.* 2005). The difference between the present study and that of PFF04 can be understood largely in terms of the small sample size of the PFF04 study, which with its brighter magnitude cut harboured an overrepresentative number of young clusters.

Beasley *et al.* (2003) specifically modelled the star formation histories of NGC 5128-like GC systems (i.e., systems of similar mass, morphology and environmental density) with the semianalytical galaxy formation model of Cole *et al.* (2000). Of the eight model systems presented in Beasley *et al.* (2003), the relative fractions of metal-rich GCs formed within the past 8 Gy ( $z \lesssim 1$ ) range from  $\sim 10 - 50\%$ , with a median value of 20%. If we define the fraction of young/old clusters in NGC 5128 as only those GCs in the metal-rich peak ( $[Z/H] > -1$ ), which one might expect are the GCs formed in later star formation episodes, we obtain a young cluster fraction of  $\sim 20 - 30\%$ , in good agreement

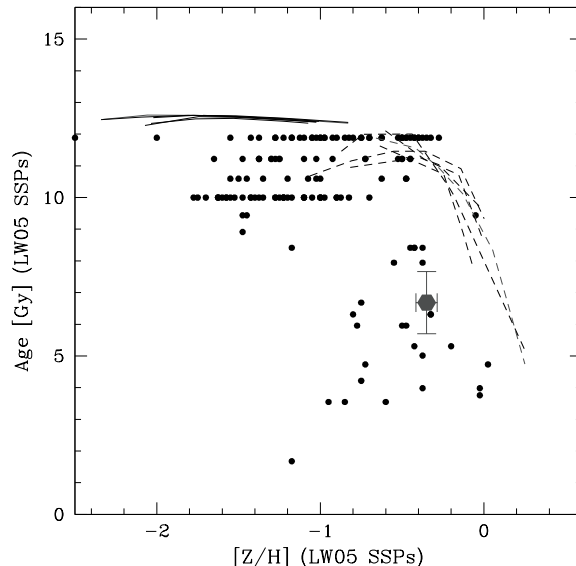


**Figure 17.** Ages and metallicities of 147 NGC 5128 GCs (derived from LW05 SSP models) (solid circles) compared to the predicted age-metallicity relations from Beasley *et al.* (2003). Solid lines are realisations for metal-poor GCs, the dashed lines are for the metal-rich, merger-formed GCs. The hexagon with error bars represents the location of the  $r_e/2$  bulge light.

with the model predictions. Our results are also broadly consistent with the “GC formation history” derived by Kaviraj *et al.* (2005) who, from the  $U - B$  colours of 210 NGC 5128 GCs, estimated that some 25–35% of GC mass was created 2–4 Gy ago.

Beasley *et al.* (2003) also presented a series of age-metallicity relations for GC systems formed using the semi-analytic model. These relations are compared to the ages and metallicities of the GCs in our sample (LW05 models) in Figure 17. At old ages, there is little discriminating power in the SSP models, and in the semianalytic the age of the metal-poor GCs is effectively fixed at  $z = 5$  the “truncation redshift” (corresponding to 12.3 Gy look-back time for the cosmology adopted in Beasley *et al.* 2003). For the metal-rich GCs, the model predicts a clear age-metallicity for the GCs (in fact, such a relation is a generic prediction of semi-analytic models). The model age-metallicity relation reproduces the observations in the broadest sense (in the sense that there do appear to be young and metal-rich GCs in NGC 5128). However, two obvious problems remain. Firstly, it is not clear whether the NGC 5128 sample shows a *relation* as such, but rather a large population of old GCs and a smaller population of younger GCs with similar ages and metallicities. Indeed, the spread in ages in the younger GCs is consistent with our observational errors (although, the metallicities do show a large intrinsic spread). Secondly, it is clear that the model age-metallicity relation is too metal-rich for the observations. A reduction in the effective yield of the model (see Beasley *et al.* 2003) would bring closer agreement with the observations, but this would result in the production of host galaxies which are too metal-poor for their luminosities, affecting the zeropoint of the colour-magnitude relation.

And here lies a generic problem with merger models which attempt to unify GC formation with the formation of the bulk of the host galaxy stars (e.g., Ashman & Zepf 1992; Beasley et al. (2002); Bekki et al. 2002): in a model where metal-rich GCs and the galaxy stars are formed simultaneously through the same mechanism in mergers, the most metal-rich GCs should be as metal-rich as the most metal-rich galaxy stars. Comparison between the GC MDF and the 8 kpc stellar MDF (c.f. Figure 8) suggests that this does not seem to be the case since there is a clear excess of solar and super-solar metallicity stars with respect to GCs. For this “simple” merger model to remain tenable, GC formation and star formation must be decoupled during the merger process such that the stars can enrich to significantly higher levels than the GCs. Otherwise, we are faced with the possibility that the mechanism which produces very metal-rich stars in galaxies is not that which produces metal-rich GCs.

## 5 ACKNOWLEDGEMENTS

MB thanks Trevor Mendel who provided the NSAR model corrections to the LW05 models and useful discussions, Javier Cenarro and Alex Vazdekis for discussions on the stellar population modelling, and Jay Strader for help on the empirical metallicity calibrations. WEH and GLHH thank the Natural Sciences and Engineering Research Council of Canada for financial support.



**Table 1.** Instrumental setup and observing details for 2dF spectroscopy.

Telescope	3.9-m AAT
Detector	Tek 1024×1024 CCD
Image scale	67 $\mu\text{m arcsec}^{-1}$
Pixel size	24 $\mu\text{m}$
CCD inverse gain	2.79 $\text{e}^- \text{ADU}^{-1}$
CCD readout noise	5.2 $\text{e}^-$
Dispersion	2.4 $\text{\AA}^{-1}$ (spectrograph A), 1.8 $\text{\AA}^{-1}$ (spectrograph B)
Resolution <sup>1</sup>	5.3 $\text{\AA}$ (spectrograph A), 4.0 $\text{\AA}$ (spectrograph B)
Integration times	25 hrs (3×3 hrs shallow fields, 2×8 hrs deep fields)
Seeing	1.3–1.6 arcsec

<sup>1</sup> some degradation of resolution with plate position - see text.

**Table 2.** Globular clusters in NGC 5128.

ID	RA (J2000)	Dec. (J2000)	V (mag)	R <sub>V</sub> (km/s)	$\sigma_V$ (km/s)	Median S/N ( $\text{\AA}^{-1}$ )	RV template Sp. type	[M/H] (dex)	$\sigma_{[M/H]}$ (dex)
AAT101906	13 23 58.76	-43 01 35.2	18.9	511	31	55	K	-0.30	0.08
AAT101931	13 23 58.58	-42 57 17.0	19.9	590	144	27	F	-1.93	0.17
AAT102120	13 23 59.61	-42 55 19.4	19.9	293	83	15	F	-2.15	0.48
AAT103195	13 24 05.98	-43 03 54.7	20.1	277	67	32	K	-0.47	0.18
AAT106880	13 24 28.44	-42 57 52.9	20.1	558	98	31	F	-1.66	0.24
AAT107060	13 24 29.23	-43 08 36.6	20.3	600	58	37	K	-0.59	0.13
AAT107145	13 24 29.73	-43 02 06.5	20.1	595	202	16	G	-0.51	0.27
AAT107977	13 24 34.63	-43 12 50.5	20.2	517	123	38	G	-1.02	0.34
AAT109380	13 24 43.58	-43 08 43.2	18.8	465	38	70	G	-1.55	0.11
AAT109711	13 24 45.35	-42 59 33.5	19.3	276	59	56	F	-1.72	0.15
AAT109788	13 24 45.78	-43 02 24.5	19.9	527	30	44	K	-0.04	0.09
AAT110138	13 24 47.61	-43 10 48.5	19.7	358	137	40	G	-1.07	0.25
AAT110410	13 24 49.38	-43 08 17.7	20.3	580	81	16	K	-0.70	0.31
AAT110551	13 24 50.09	-43 07 36.2	20.4	615	76	29	F	-0.87	0.42
AAT111033	13 24 52.98	-43 11 55.8	20.1	302	166	15	K	-0.69	0.31
AAT111185	13 24 54.00	-43 04 24.4	19.9	466	87	38	K	-1.26	0.21
AAT111296	13 24 54.49	-43 05 34.7	20.0	695	45	43	K	-0.10	0.07
AAT111406	13 24 55.29	-43 03 15.6	20.1	669	77	18	G	—	—
AAT111563	13 24 56.08	-43 10 16.4	20.5	649	102	28	F	-0.71	0.13
AAT112158	13 25 00.15	-42 54 09.0	20.4	699	43	11	K	-1.34	0.71
AAT112752	13 25 04.12	-43 00 19.6	19.3	679	82	44	G	-0.80	0.25
AAT112964	13 25 04.61	-43 07 21.7	19.6	456	118	36	K	-1.23	0.19
AAT113428	13 25 07.33	-43 06 20.6	20.0	657	67	34	K	-0.95	0.27
AAT113992	13 25 10.51	-43 03 24.0	20.4	648	58	10	K	—	—
AAT114302	13 25 12.34	-42 58 07.7	20.4	754	143	11	G	-2.41	0.66
AAT114769	13 25 15.12	-42 57 45.7	20.2	650	169	13	G	-2.00	1.22
AAT114913	13 25 15.93	-43 06 03.3	20.4	563	63	43	G	-0.51	0.12
AAT115339	13 25 18.44	-43 04 09.8	20.1	618	108	12	G	—	—
AAT115561	13 25 19.83	-42 58 27.2	20.5	514	46	40	K	-0.10	0.22
AAT115605	13 25 20.44	-42 54 08.5	20.5	713	131	30	G	-1.29	0.40
AAT115679	13 25 20.72	-43 06 35.9	20.4	511	164	9	G	—	—
AAT116025	13 25 23.46	-42 53 26.2	20.0	545	64	42	G	-0.75	0.12
AAT116220	13 25 24.40	-43 07 58.9	19.5	524	41	55	G	-0.90	0.15
AAT116385	13 25 25.39	-42 58 21.5	20.3	550	40	45	K	-0.30	0.06
AAT116531	13 25 26.75	-43 08 53.4	19.8	267	71	13	G	-0.58	0.73
AAT116969	13 25 29.41	-42 53 25.6	20.5	446	61	30	K	-0.55	0.20
AAT117062	13 25 31.04	-42 50 15.0	17.3	412	71	125	G	-0.96	0.06
AAT117287	13 25 31.08	-43 04 17.0	20.4	554	60	29	K	-0.27	0.29
AAT117322	13 25 31.73	-42 55 15.7	20.1	636	133	43	G	-1.13	0.19
AAT117899	13 25 36.05	-42 53 40.3	20.2	609	116	6	G	-3.93	2.76
AAT118198	13 25 37.47	-43 05 44.9	19.6	575	36	29	K	-0.18	0.07
AAT118314	13 25 38.03	-43 16 59.2	19.9	257	59	32	G	-1.28	0.08
AAT118874	13 25 41.36	-42 58 08.9	20.0	570	82	16	G	—	—
AAT119058	13 25 42.53	-43 03 41.5	20.4	385	87	8	G	-1.97	0.75
AAT119596	13 25 46.06	-43 08 24.5	19.7	573	53	37	K	-0.56	0.15
AAT119697	13 25 46.68	-42 53 48.6	20.1	633	108	11	K	—	—
AAT119894	13 25 47.92	-42 55 52.4	20.2	448	90	30	K	-1.63	0.83
AAT120259	13 25 49.73	-43 05 04.7	20.1	477	54	12	K	—	—
AAT120336	13 25 50.22	-43 06 08.5	20.2	452	67	9	K	—	—
AAT120355	13 25 50.37	-43 00 32.6	20.4	548	77	33	G	-0.72	0.31
AAT120515	13 25 51.31	-42 59 29.4	19.9	461	141	17	G	—	—
AAT120976	13 25 54.28	-42 56 20.6	20.4	595	69	28	G	-0.57	0.11
AAT121367	13 25 56.26	-43 01 32.9	20.2	438	80	39	K	-0.86	0.22
AAT121826	13 25 59.49	-42 55 30.8	19.8	448	98	18	G	-0.56	0.33
AAT122146	13 26 01.00	-43 06 55.3	20.1	517	99	15	G	-3.12	1.43
AAT122445	13 26 02.43	-43 00 11.7	20.3	342	98	11	F	-3.75	1.68
AAT122526	13 26 02.90	-43 05 43.0	20.4	506	50	32	K	-0.65	0.19
AAT122794	13 26 04.69	-42 47 35.1	20.0	336	160	13	G	-0.68	0.55
AAT122808	13 26 04.61	-43 09 10.2	20.1	264	131	17	F	-1.05	0.25
AAT123188	13 26 06.94	-43 07 52.6	20.4	364	56	29	K	-0.82	0.18
AAT123453	13 26 08.38	-42 59 18.9	20.1	257	154	26	G	-1.60	0.7
AAT123656	13 26 09.61	-43 07 05.9	20.1	380	93	17	G	-0.88	0.21
AAT125079	13 26 17.29	-43 06 39.3	20.1	513	183	17	G	-1.62	0.71

Table 2 – continued

ID	RA (J2000)	Dec. (J2000)	V (mag)	R <sub>V</sub> (km/s)	σ <sub>V</sub> (km/s)	Median S/N (Å <sup>-1</sup> )	RV Template Sp. type	[M/H] (dex)	σ <sub>[M/H]</sub> (dex)
AAT204119	13 25 25.70	-42 37 40.9	19.8	404	74	33	G	-1.36	0.21
AAT205071	13 25 30.74	-42 30 16.0	18.9	288	61	20	G	-1.57	0.52
AAT208206	13 25 46.49	-42 34 54.1	19.5	293	115	51	F	-1.87	0.19
AAT209412	13 25 53.30	-42 30 52.7	20.2	998	250	10	G	-1.28	1.00
AAT215171	13 26 20.66	-42 38 32.0	19.7	527	48	33	K	-0.57	0.27
AAT222977	13 26 58.91	-42 38 53.4	20.3	655	112	25	F	-1.30	0.45
AAT223403	13 27 00.80	-42 21 39.2	20.5	594	102	11	G	-1.95	1.01
AAT301956	13 23 54.52	-43 20 01.1	20.4	287	162	25	F	-1.58	0.24
AAT305341	13 24 10.97	-43 12 52.8	20.5	440	118	13	G	-0.59	0.25
AAT308432	13 24 25.55	-43 21 35.6	19.4	835	83	45	G	-0.70	0.13
AAT320656	13 25 19.13	-43 12 03.8	19.8	453	232	18	G	-1.65	0.70
AAT321194	13 25 21.32	-43 23 59.3	20.1	254	169	16	G	-1.00	0.37
AAT328533	13 25 54.39	-43 18 40.1	20.3	577	89	11	K	-1.99	0.85
AAT329209	13 25 57.28	-43 41 09.0	19.9	601	66	31	G	-1.72	0.43
AAT329848	13 26 01.29	-43 34 15.5	18.4	558	46	76	F	-1.32	0.14
AAT335187	13 26 23.95	-43 17 44.4	20.5	277	158	14	G	-2.61	1.07
HCH01	13 25 16.22	-42 59 43.4	17.5	629	78	19	K	—	—
HCH02	13 25 16.69	-43 02 08.7	17.9	483	50	18	G	—	—
HCH13	13 25 28.69	-43 02 55.0	19.9	613	37	26	K	-0.57	1.17
HCH16	13 25 30.29	-42 59 34.8	20.0	518	45	26	K	-1.49	1.13
HCH18	13 25 31.60	-43 00 02.8	19.9	550	45	18	G	—	—
HCH21	13 25 34.65	-43 03 27.7	20.0	607	52	29	G	-0.48	0.25
HGHH-01	13 23 44.19	-43 11 11.8	20.0	676	38	62	F	-1.38	0.14
HGHH-04	13 25 01.83	-43 09 25.4	18.0	724	46	64	F	-1.57	0.04
HGHH-06	13 25 22.19	-43 02 45.6	17.2	790	44	43	K	-1.25	0.39
HGHH-07	13 26 05.41	-42 56 32.4	17.2	593	51	92	G	-0.85	0.07
HGHH-11	13 24 54.73	-43 01 21.7	17.9	721	35	60	K	-0.31	0.06
HGHH-17	13 25 39.73	-42 55 59.2	17.6	773	46	108	G	-0.78	0.07
HGHH-19	13 25 43.40	-43 07 22.8	18.1	682	44	41	G	-0.89	0.18
HGHH-20	13 25 49.69	-42 54 49.3	18.0	798	49	50	G	-0.87	0.10
HGHH-21	13 25 52.74	-43 05 46.4	17.9	495	38	50	G	-0.85	0.10
HGHH-22	13 25 53.57	-42 59 07.6	18.2	605	37	66	G	-0.96	0.18
HGHH-23	13 25 54.58	-42 59 25.4	17.2	684	24	62	K	-0.36	0.09
HGHH-25	13 26 02.85	-42 56 57.0	18.5	685	38	53	K	-0.23	0.08
HGHH-29	13 24 40.39	-43 18 05.3	18.1	743	34	65	K	-0.29	0.04
HGHH-31	13 24 57.44	-43 01 08.1	18.4	709	27	37	K	-0.50	0.03
HGHH-34	13 25 40.61	-43 21 13.6	18.1	676	27	57	K	-0.30	0.11
HGHH-36	13 26 07.73	-42 52 00.3	18.4	704	50	56	G	-1.18	0.12
HGHH-37	13 26 10.58	-42 53 42.7	18.4	620	28	71	K	-0.46	0.09
HGHH-40	13 23 42.37	-43 09 37.8	18.1	443	48	48	G	-1.17	0.19
HGHH-41	13 24 38.98	-43 20 06.4	18.6	394	27	59	K	-0.37	0.09
HGHH-42	13 24 50.87	-43 01 22.9	18.9	579	39	42	K	-0.45	0.16
HGHH-43	13 25 04.81	-43 09 38.8	18.6	560	46	55	G	-1.12	0.03
HGHH-44	13 25 31.73	-43 19 22.6	18.7	566	40	51	G	-1.29	0.08
HGHH-45	13 25 34.25	-42 56 59.1	19.0	618	56	39	G	-0.82	0.24
HGHH-46	13 25 25.97	-43 03 25.7	19.1	488	49	28	G	-0.66	0.11
HGHH-48	13 25 49.82	-42 50 15.3	18.7	578	50	47	F	-1.58	0.08
HGHH-G019	13 24 46.46	-43 04 11.6	19.2	735	65	28	G	-1.58	0.15
HGHH-G143	13 25 58.69	-43 07 11.0	19.2	555	78	33	G	-0.93	0.16
HGHH-G170	13 26 06.93	-42 57 35.1	19.2	640	35	36	K	-0.29	0.13
HGHH-G176	13 25 03.13	-42 56 25.1	18.9	567	32	54	K	-0.42	0.14
HGHH-G204	13 25 46.99	-43 02 05.4	18.3	705	36	35	G	-1.82	0.29
HGHH-G219	13 25 17.31	-42 58 46.6	18.8	534	28	51	K	-0.01	0.13
HGHH-G251	13 25 48.54	-42 57 41.2	18.9	570	35	43	K	-0.18	0.12
HGHH-G256	13 25 52.88	-43 02 00.0	19.0	500	46	29	K	-0.43	0.18
HGHH-G271	13 25 13.95	-42 57 42.6	18.7	373	36	29	G	-1.34	0.18
HGHH-G277	13 24 47.37	-42 58 29.8	19.1	738	51	40	G	-1.02	0.10
HGHH-G279	13 24 56.27	-43 03 23.4	19.5	338	54	34	F	-1.73	0.30
HGHH-G284	13 25 46.59	-42 57 03.0	19.9	485	56	22	K	-0.04	0.18
HGHH-G293	13 26 04.20	-42 55 44.7	19.1	633	85	42	G	-1.32	0.11
HGHH-G327	13 25 11.98	-43 04 19.3	19.8	581	50	20	K	-0.10	0.20
HGHH-G329	13 25 10.20	-43 02 06.7	19.7	485	34	29	K	0.13	0.11
HGHH-G331	13 25 19.50	-43 02 28.4	18.9	523	65	19	G	-1.34	1.01

**Table 2** – *continued*

ID	RA (J2000)	Dec. (J2000)	V (mag)	R <sub>V</sub> (km/s)	$\sigma_V$ (km/s)	Median S/N ( $\text{\AA}^{-1}$ )	RV Template Sp. type	[M/H] (dex)	$\sigma_{[M/H]}$ (dex)
HGHH-G342	13 25 05.83	-42 59 00.6	18.2	566	30	41	K	-0.43	0.15
HGHH-G348	13 25 11.10	-42 58 03.0	18.9	330	61	44	G	-0.94	0.10
HGHH-G359	13 25 32.42	-42 58 50.2	18.9	551	53	14	K	-2.41	1.76
HGHH-G369	13 24 57.52	-42 59 23.3	18.7	558	41	59	G	-1.33	0.07
HGHH-G370	13 25 42.25	-42 59 17.0	18.4	557	57	56	G	-0.81	0.13
HGHH-G378	13 25 46.13	-43 01 22.9	19.5	515	43	29	K	-0.01	0.13
HHH86-10	13 24 48.06	-43 08 14.2	18.5	836	41	38	K	-0.75	0.09
HHH86-13	13 25 06.25	-43 15 11.6	18.7	658	37	56	G	-0.81	0.12
HHH86-14	13 25 10.49	-42 44 52.6	17.9	723	41	63	G	-0.84	0.08
HHH86-15	13 25 30.41	-43 11 49.6	18.6	656	28	35	K	-0.44	0.08
HHH86-16	13 25 35.00	-42 36 05.0	18.6	552	37	45	K	-0.71	0.14
HHH86-18	13 25 39.88	-43 05 01.9	17.5	509	49	76	G	-0.78	0.06
HHH86-26	13 26 15.27	-42 48 29.4	18.1	405	24	41	K	-0.10	0.07
HHH86-28	13 24 18.06	-42 49 01.1	18.5	499	48	47	F	-1.82	0.13
HHH86-30	13 24 54.35	-42 53 24.8	17.3	811	32	69	K	-0.48	0.06
HHH86-32	13 25 03.37	-42 50 46.2	18.4	735	30	35	K	-0.12	0.07
HHH86-33	13 25 16.26	-42 50 53.3	18.5	522	39	69	G	-1.26	0.10
HHH86-39	13 26 42.03	-43 07 44.8	17.4	249	59	79	G	-0.53	0.17
HH-024	13 24 40.62	-43 13 17.9	18.4	689	31	52	K	-0.28	0.11
HH-044	13 23 42.33	-43 09 37.4	18.7	337	50	22	G	-0.86	0.13
HH-080	13 23 38.33	-42 46 22.8	17.8	497	33	71	F	-1.68	0.09
HH-090	13 25 21.30	-42 49 18.1	18.6	423	45	21	G	-0.40	0.17
HH-096	13 24 21.42	-43 02 36.9	17.5	541	54	65	K	-1.38	0.10
K-029	13 25 09.19	-42 58 59.2	17.7	677	44	91	G	-0.53	0.06
K-033	13 25 10.25	-42 55 09.5	19.5	582	33	54	G	-0.49	0.10
K-034	13 25 10.27	-42 53 33.1	17.8	464	42	108	K	-0.41	0.04
K-051	13 25 14.25	-43 07 23.6	19.6	590	35	41	K	-0.14	0.16
K-102	13 25 27.98	-43 04 02.2	19.2	613	59	56	K	-0.27	0.08
K-131	13 25 32.88	-43 04 29.2	19.4	639	44	27	K	-0.04	0.12
K-144	13 25 35.16	-42 53 01.0	20.2	593	43	21	K	-0.03	0.07
K-147	13 25 35.50	-42 59 35.2	19.4	538	55	29	K	-0.38	0.09
K-163	13 25 39.88	-43 05 01.9	17.5	487	51	106	G	-0.81	0.10
K-217	13 26 00.81	-43 09 40.1	20.1	314	157	17	G	-1.27	1.02
K-233	13 26 19.66	-43 03 18.6	18.7	622	76	47	G	-0.88	0.15
MAGJM-01	13 25 39.33	-43 00 48.8	18.6	603	48	18	G	-0.19	0.10
MAGJM-06	13 25 36.69	-42 59 59.2	20.0	487	37	10	G	-0.18	0.39
MAGJM-11	13 25 33.94	-42 59 39.4	18.9	508	51	17	K	-0.48	0.11
R105	13 26 33.55	-42 51 00.9	19.9	563	120	26	K	-0.77	0.40
R107	13 26 21.11	-42 48 41.1	19.8	475	61	18	G	-0.33	0.23
R111	13 26 09.71	-42 50 29.5	20.6	640	129	22	K	-0.50	0.13
R117	13 26 21.99	-42 53 45.5	19.7	553	40	43	G	-1.64	0.10
R124	13 26 28.87	-42 52 36.4	19.4	599	103	27	F	-1.23	0.16
R202	13 25 42.00	-43 10 42.2	19.3	279	60	54	F	-1.17	0.16
R203	13 25 40.90	-43 08 16.0	19.8	559	62	43	G	-1.47	0.15
R209	13 25 38.13	-43 13 02.2	20.6	558	100	20	F	-0.43	0.25
R215	13 25 35.64	-43 08 36.8	20.8	529	81	19	G	-1.66	0.56
R223	13 25 32.80	-43 07 02.2	18.8	735	47	25	K	-0.73	0.17
R235	13 25 26.82	-43 09 40.5	19.5	489	49	31	G	-1.03	0.20
R253	13 25 17.33	-43 08 39.0	19.7	622	98	44	F	-1.07	0.09
R254	13 25 16.96	-43 09 28.0	19.4	563	45	36	G	-1.01	0.07
R261	13 25 12.90	-43 07 59.1	18.2	622	29	52	K	-0.49	0.08
PFF-gc001	13 23 49.62	-43 14 32.0	18.9	702	47	60	G	-0.66	0.06
PFF-gc002	13 23 59.51	-43 17 29.1	19.5	685	54	44	F	-1.40	0.11
PFF-gc003	13 24 03.23	-43 28 13.9	19.3	771	69	44	F	-1.70	0.30
PFF-gc004	13 24 03.74	-43 35 53.4	20.0	634	71	34	F	-1.74	0.21
PFF-gc005	13 24 18.92	-43 14 30.1	20.3	664	128	21	G	-0.52	0.24
PFF-gc006	13 24 23.72	-43 07 52.1	19.2	646	39	52	F	-1.56	0.07
PFF-gc007	13 24 24.15	-42 54 20.6	20.1	637	58	16	G	-0.40	0.23
PFF-gc008	13 24 29.20	-43 21 56.5	19.9	520	80	18	K	-0.88	0.25
PFF-gc009	13 24 31.35	-43 11 26.7	19.8	740	68	29	F	-0.99	0.13
PFF-gc011	13 24 36.87	-43 19 16.2	19.0	756	164	38	F	-1.85	0.21
PFF-gc013	13 24 40.42	-43 35 04.9	19.0	839	63	49	F	-1.41	0.11

Table 2 – *continued*

ID	RA (J2000)	Dec. (J2000)	V (mag)	R <sub>V</sub> (km/s)	$\sigma_V$ (km/s)	Median S/N ( $\text{\AA}^{-1}$ )	RV Template Sp. type	[M/H] (dex)	$\sigma_{[M/H]}$ (dex)
PFF-gc014	13 24 41.05	-42 59 48.4	20.2	718	59	19	K	-1.27	0.22
PFF-gc015	13 24 41.20	-43 01 45.6	19.2	571	44	45	G	-1.06	0.12
PFF-gc016	13 24 43.60	-42 53 07.3	19.9	521	46	32	K	-0.32	0.10
PFF-gc018	13 24 47.10	-43 06 01.7	18.9	531	29	66	K	-0.09	0.05
PFF-gc022	13 24 54.33	-43 03 15.5	19.8	601	75	32	G	-1.42	0.45
PFF-gc023	13 24 54.55	-42 48 58.7	19.4	504	53	46	G	-1.19	0.25
PFF-gc024	13 24 55.71	-43 20 39.1	19.8	543	208	18	F	-1.35	0.24
PFF-gc026	13 24 58.45	-42 42 53.3	19.5	580	114	27	F	-1.97	0.20
PFF-gc027	13 25 00.64	-43 05 30.3	19.7	555	67	13	K	-0.47	0.49
PFF-gc032	13 25 03.24	-42 57 40.5	19.7	639	62	45	G	-0.85	0.26
PFF-gc035	13 25 04.48	-43 10 48.4	19.7	636	48	32	K	-0.45	0.15
PFF-gc036	13 25 05.46	-43 14 02.6	19.0	665	42	56	G	-1.25	0.06
PFF-gc039	13 25 09.10	-42 24 00.9	19.0	456	52	46	K	-1.44	0.14
PFF-gc042	13 25 12.21	-43 16 33.9	19.0	659	41	49	F	-1.46	0.09
PFF-gc043	13 25 12.45	-43 14 07.4	19.4	564	55	25	F	-0.95	0.09
PFF-gc046	13 25 14.83	-43 41 10.6	18.9	502	53	59	G	-1.44	0.08
PFF-gc048	13 25 15.79	-42 49 15.1	19.8	483	116	26	G	-0.85	0.32
PFF-gc051	13 25 22.35	-43 15 00.1	19.8	480	60	38	K	-0.63	0.09
PFF-gc055	13 25 30.72	-42 48 13.4	19.9	524	123	27	F	-1.76	0.35
PFF-gc058	13 25 35.12	-42 56 45.3	18.7	473	52	47	G	-1.31	0.14
PFF-gc059	13 25 39.65	-43 04 01.4	20.0	557	49	28	G	0.00	0.16
PFF-gc061	13 25 42.62	-42 45 10.9	20.2	508	71	20	K	-0.93	0.29
PFF-gc064	13 25 43.90	-42 50 42.7	19.7	572	50	29	G	-0.42	0.15
PFF-gc066	13 25 47.14	-43 06 08.8	19.9	601	82	40	K	-1.07	0.13
PFF-gc067	13 25 48.77	-43 11 38.7	19.6	592	104	24	G	-1.29	0.10
PFF-gc068	13 25 49.27	-43 02 20.4	19.6	420	51	26	G	-0.61	0.33
PFF-gc069	13 25 49.93	-42 40 08.2	19.9	510	71	36	K	-0.36	0.16
PFF-gc073	13 25 52.78	-42 58 41.7	20.0	434	46	23	K	-0.26	0.18
PFF-gc074	13 25 53.37	-42 51 12.4	20.0	482	49	40	G	-0.88	0.10
PFF-gc075	13 25 53.50	-43 03 56.6	19.5	710	49	41	G	-0.36	0.08
PFF-gc076	13 25 53.75	-43 19 48.6	19.1	375	29	27	K	-0.44	0.18
PFF-gc078	13 25 58.47	-43 08 06.3	19.3	546	42	29	K	-0.39	0.11
PFF-gc079	13 25 58.91	-42 53 18.9	19.6	463	68	47	F	-0.64	0.11
PFF-gc080	13 25 59.55	-42 32 39.4	20.0	616	123	16	G	-0.69	0.29
PFF-gc081	13 26 00.15	-42 49 00.7	19.3	308	61	37	G	-1.38	0.29
PFF-gc082	13 26 00.98	-42 22 03.4	19.2	593	42	47	K	-0.49	0.12
PFF-gc083	13 26 01.83	-42 58 15.0	19.9	455	46	27	K	-0.41	0.19
PFF-gc084	13 26 02.25	-43 08 55.6	19.8	452	83	26	K	-0.71	0.31
PFF-gc085	13 26 06.42	-43 00 38.1	19.4	572	59	47	G	-1.40	0.18
PFF-gc086	13 26 06.55	-43 06 14.5	20.0	479	52	19	K	-1.01	0.42
PFF-gc087	13 26 06.87	-42 33 17.3	19.1	856	50	44	G	-1.20	0.10
PFF-gc088	13 26 08.86	-43 01 21.4	19.0	546	50	58	F	-1.50	0.18
PFF-gc089	13 26 20.21	-43 10 35.6	18.9	548	36	42	F	-1.72	0.08
PFF-gc090	13 26 20.53	-43 03 18.5	19.3	519	56	47	K	-0.32	0.10
PFF-gc091	13 26 21.14	-43 42 24.6	19.3	669	57	28	F	-1.24	0.13
PFF-gc092	13 26 21.31	-42 57 19.1	19.9	472	127	20	G	-1.04	0.49
PFF-gc093	13 26 22.65	-42 46 49.8	19.6	593	139	34	F	-1.39	0.10
PFF-gc094	13 26 23.66	-43 00 45.6	20.0	372	144	22	G	-1.63	0.32
PFF-gc095	13 26 25.50	-42 57 06.2	19.6	446	39	26	G	-0.30	0.10
PFF-gc096	13 26 30.29	-42 34 41.7	19.7	483	122	24	K	-0.80	0.10
PFF-gc097	13 26 45.40	-43 26 34.1	18.7	642	47	44	F	-1.53	0.11
PFF-gc098	13 26 53.94	-43 19 17.7	18.3	650	37	41	G	-0.75	0.15
PFF-gc099	13 26 59.82	-42 32 40.5	19.9	538	80	28	F	-1.52	0.12
PFF-gc100	13 27 03.41	-42 27 17.2	18.4	527	31	64	K	-0.41	0.08
PFF-gc101	13 27 21.56	-42 38 41.4	18.7	252	71	67	G	-0.54	0.14
PFF-gc102	13 28 18.45	-42 33 12.5	19.3	576	119	24	G	-1.40	0.20
VHH81-02	13 24 51.49	-43 12 11.1	18.5	646	37	55	G	-1.14	0.13
VHH81-03	13 24 58.21	-42 56 10.0	17.7	591	37	48	K	-0.22	0.08
VHH81-05	13 25 16.12	-42 52 58.2	17.7	563	41	70	G	-1.44	0.15
WHH-03	13 24 32.19	-43 10 56.8	19.5	775	74	20	G	-1.52	0.50
WHH-06	13 24 47.38	-42 57 51.2	19.7	666	56	35	K	-0.31	0.15
WHH-14	13 25 25.50	-42 56 31.3	20.1	654	223	10	G	-1.22	1.79
WHH-15	13 25 26.78	-42 52 39.9	19.8	565	151	15	G	-1.07	0.33
WHH-17	13 25 29.26	-42 57 47.2	18.6	623	48	71	G	-0.90	0.05

**Table 2** – *continued*

ID	RA (J2000)	Dec. (J2000)	V (mag)	$R_V$ (km/s)	$\sigma_V$ (km/s)	Median S/N ( $\text{\AA}^{-1}$ )	RV template Sp. type	[M/H] (dex)	$\sigma_{[M/H]}$ (dex)
WHH-18	13 25 30.08	-42 56 47.0	18.4	721	40	66	K	-0.47	0.12
WHH-20	13 25 34.36	-42 51 06.0	19.0	269	42	51	G	-0.93	0.04
WHH-25	13 25 50.37	-43 04 08.3	20.0	515	58	25	K	-0.73	0.23

GC nomenclature: AAT= this study; HCH=Holland, Côté & Hesser (1999); HGHH=Harris *et al.* (1992); HHH86=Hesser, Harris & Harris (1986); HH=Harris & Harris (2004); K=Kraft *et al.* (2001); MAGJM=Minniti *et al.* (1996); R=Rejkuba (2001); PFF=Peng *et al.* (2004); WHH=Woodley *et al.* (2005)

**Table 3.** Objects classified as foreground stars.

ID	RA (J2000)	Dec. (J2000)	V (mag)	R <sub>V</sub> (km/s)	σ <sub>V</sub> (km/s)	ID	RA (J2000)	Dec. (J2000)	V (mag)	R <sub>V</sub> (km/s)	σ <sub>V</sub> (km/s)
AAT101585	13 23 57.23	-42 53 28.0	17.9	244	58	AAT230032	13 27 32.58	-42 34 12.3	19.3	35	57
AAT102095	13 24 00.48	-42 44 55.0	18.1	158	65	AAT230068	13 27 32.81	-42 27 50.9	18.3	232	76
AAT102515	13 24 02.59	-42 46 44.1	19.7	126	127	AAT230095	13 27 32.91	-42 24 05.0	18.5	-8	37
AAT103919	13 24 10.23	-43 16 54.0	20.3	57	78	AAT233409	13 27 49.47	-42 37 44.1	18.4	-53	40
AAT104121	13 24 12.74	-42 44 51.3	19.5	140	138	AAT233795	13 27 49.53	-42 16 11.4	20.0	83	81
AAT105234	13 24 19.31	-42 49 03.1	20.1	177	133	AAT241043	13 28 10.08	-42 44 52.9	20.1	-60	87
AAT105988	13 24 23.31	-42 59 48.4	19.8	-27	136	AAT302285	13 23 56.39	-43 15 58.5	19.0	7	32
AAT106539	13 24 26.04	-43 09 48.5	20.1	-216	12	AAT303463	13 24 02.04	-43 16 51.3	19.4	43	55
AAT107133	13 24 29.56	-43 05 28.2	19.7	36	74	AAT303554	13 24 02.06	-43 25 40.7	20.2	229	119
AAT107289	13 24 31.24	-42 47 02.2	19.7	131	166	AAT304867	13 24 08.62	-43 16 27.1	19.9	305	56
AAT108131	13 24 36.48	-42 48 41.1	19.4	76	125	AAT305415	13 24 10.76	-43 27 57.4	20.0	26	238
AAT108156	13 24 36.43	-42 50 03.4	20.2	108	113	AAT306381	13 24 15.13	-43 37 11.9	19.1	-89	141
AAT108430	13 24 38.10	-42 56 04.5	19.6	129	101	AAT307040	13 24 18.89	-43 25 51.7	18.3	182	43
AAT109282	13 24 42.77	-43 00 56.1	19.9	190	106	AAT307315	13 24 19.30	-43 40 33.7	20.1	72	65
AAT110286	13 24 48.43	-43 14 33.7	19.8	161	196	AAT307343	13 24 20.08	-43 34 09.1	19.8	68	58
AAT110819	13 24 52.29	-42 54 50.2	19.8	180	295	AAT308734	13 24 26.28	-43 27 04.7	19.2	41	94
AAT110922	13 24 53.03	-42 54 00.8	19.9	9	324	AAT308921	13 24 27.31	-43 22 41.6	19.6	22	56
AAT111727	13 24 57.17	-43 16 55.8	20.2	122	127	AAT310053	13 24 32.05	-43 26 53.4	19.4	55	58
AAT112157	13 25 00.87	-42 45 46.7	19.1	84	58	AAT310884	13 24 35.39	-43 35 30.4	20.1	102	162
AAT112222	13 25 00.72	-43 06 14.8	19.5	187	85	AAT312895	13 24 44.83	-43 25 22.4	19.9	147	268
AAT114993	13 25 16.44	-43 03 33.1	20.4	352	136	AAT315922	13 24 57.52	-43 41 00.3	20.0	-34	59
AAT118418	13 25 39.36	-42 44 30.6	18.4	-130	6	AAT317105	13 25 02.94	-43 38 03.5	20.2	-84	70
AAT118872	13 25 41.26	-43 14 56.8	20.1	21	71	AAT317156	13 25 03.25	-43 34 15.1	19.9	170	145
AAT122115	13 26 00.92	-43 02 46.3	19.7	149	110	AAT319460	13 25 13.48	-43 32 53.2	20.2	-35	101
AAT122338	13 26 02.62	-42 58 06.5	18.8	48	86	AAT321171	13 25 20.93	-43 27 08.4	20.4	-127	15
AAT123757	13 26 10.14	-42 50 52.6	19.2	-150	21	AAT321782	13 25 23.76	-43 35 15.7	19.3	-154	23
AAT123875	13 26 10.55	-43 01 05.9	20.2	231	143	AAT322337	13 25 26.12	-43 25 19.6	20.4	-76	122
AAT124070	13 26 12.12	-42 49 03.6	19.1	117	80	AAT322437	13 25 26.67	-43 37 12.3	18.4	-51	43
AAT124257	13 26 14.02	-43 02 45.8	19.6	1	144	AAT323035	13 25 29.46	-43 38 41.5	20.0	14	49
AAT124456	13 26 13.97	-43 13 57.8	19.5	48	76	AAT323231	13 25 30.32	-43 18 24.7	19.5	-150	6
AAT124828	13 26 16.28	-43 12 01.1	18.2	137	73	AAT325083	13 25 38.62	-43 28 35.4	19.9	-50	75
AAT125504	13 26 19.44	-43 01 05.4	20.2	-42	80	AAT325900	13 25 42.29	-43 11 28.2	20.4	39	77
AAT126525	13 26 25.45	-42 58 21.2	19.7	131	70	AAT326353	13 25 44.11	-43 43 23.3	20.4	1	72
AAT129830	13 26 44.65	-43 07 19.5	19.6	10	81	AAT326526	13 25 45.24	-43 41 03.9	18.8	117	56
AAT130804	13 26 51.53	-42 58 27.3	17.8	18	54	AAT327430	13 25 49.33	-43 34 49.9	19.1	109	71
AAT133435	13 26 53.05	-43 00 17.4	20.2	-67	98	AAT328174	13 25 52.90	-43 39 36.7	19.7	-81	146
AAT133627	13 26 51.09	-43 13 07.0	19.7	85	63	AAT329038	13 25 56.63	-43 28 28.3	20.0	102	155
AAT201526	13 25 12.86	-42 38 23.2	18.8	45	40	AAT333843	13 26 18.22	-43 26 17.7	20.2	-3	80
AAT201574	13 25 13.74	-42 21 01.5	20.4	80	61	AAT333871	13 26 18.07	-43 41 08.8	20.4	-199	14
AAT201953	13 25 15.09	-42 27 40.2	19.8	146	163	AAT335854	13 26 27.32	-43 34 34.7	18.7	-44	40
AAT202985	13 25 20.32	-42 28 21.1	19.9	181	146	AAT337751	13 26 35.38	-43 14 40.5	20.4	-107	13
AAT203071	13 25 20.63	-42 37 42.0	19.9	-22	71	AAT338104	13 26 38.01	-43 39 06.0	19.1	-24	96
AAT203409	13 25 22.15	-42 35 34.5	20.3	-100	5	AAT338620	13 26 39.36	-43 18 25.1	20.1	-69	140
AAT203425	13 25 23.02	-42 19 42.8	18.4	-6	30	AAT339070	13 26 41.45	-43 22 12.1	19.3	69	114
AAT204913	13 25 29.49	-42 39 54.9	20.4	-105	8	AAT339496	13 26 43.68	-43 27 04.2	19.5	-186	26
AAT205531	13 25 32.71	-42 25 19.1	19.9	-203	19	AAT340112	13 26 53.58	-43 16 42.9	19.9	-59	45
AAT205707	13 25 33.96	-42 21 31.4	20.0	-14	91	AAT340154	13 26 56.70	-43 33 52.8	19.2	72	55
AAT205855	13 25 34.44	-42 19 08.3	20.2	-26	81	AAT340410	13 26 49.46	-43 09 57.7	18.4	224	94
AAT206594	13 25 37.72	-42 45 16.1	19.7	-2	52	AAT341090	13 26 49.98	-43 23 05.6	19.8	131	88
AAT208829	13 25 49.60	-42 18 04.3	19.8	103	264	AAT341578	13 26 45.79	-43 32 49.5	20.2	-12	80
AAT211222	13 26 01.04	-42 41 50.3	20.2	-80	112	AAT343715	13 26 59.87	-43 25 01.5	20.2	147	139
AAT212102	13 26 05.28	-42 37 11.1	20.4	-28	84	AAT344437	13 26 59.14	-43 35 17.2	17.8	-16	52
AAT213437	13 26 12.07	-42 19 06.6	20.1	182	226	HH-018	13 26 41.08	-43 16 23.6	18.0	0	53
AAT215414	13 26 21.51	-42 37 53.2	19.6	168	116	HH-039	13 28 06.35	-43 03 47.2	18.7	-80	230
AAT216699	13 26 27.80	-42 24 09.8	20.5	86	89	HH-043	13 27 44.52	-42 58 35.9	19.7	-18	99
AAT220215	13 26 45.54	-42 39 43.2	19.2	169	139	HH-046	13 22 35.93	-43 04 37.2	18.3	3	33
AAT220565	13 26 47.03	-42 21 15.8	18.5	-68	70	HH-051	13 25 31.09	-43 27 15.6	19.8	-126	14
AAT221287	13 26 50.55	-42 37 11.3	19.3	-104	10	HH-069	13 26 47.12	-43 18 57.2	19.9	7	133
AAT221465	13 26 51.51	-42 37 50.3	20.2	-59	53	HH-071	13 27 42.71	-43 19 36.5	21.0	-189	16
AAT222438	13 26 56.13	-42 29 03.0	20.1	-16	77	HH-081	13 23 55.97	-42 36 45.8	17.9	81	66

**Table 3** – *continued*

ID	RA (J2000)	Dec. (J2000)	V (mag)	R <sub>V</sub> (km/s)	σ <sub>V</sub> (km/s)	ID	RA (J2000)	Dec. (J2000)	V (mag)	R <sub>V</sub> (km/s)	σ <sub>V</sub> (km/s)
AAT223804	13 27 03.92	-42 31 38.0	20.0	34	102	K-122	13 25 32.16	-43 10 41.0	19.2	23	57
AAT224771	13 27 08.24	-42 16 20.0	19.8	-30	68	K-192	13 25 48.71	-43 03 23.4	18.7	27	45
AAT227692	13 27 21.49	-42 25 59.4	20.3	15	208	K-200	13 25 53.63	-43 01 33.0	19.0	197	201
AAT228436	13 27 25.03	-42 36 53.2	20.3	-73	159	K-209	13 25 57.42	-42 53 41.6	19.1	133	176
AAT230032	13 27 32.58	-42 34 12.3	19.3	35	57	PPF-gc054	13 25 30.28	-43 41 53.6	20.0	169	108

**Table 4.** Objects classified as background galaxies.

ID	RA (J2000)	Dec. (J2000)	R <sub>V</sub> (10 <sup>4</sup> km/s)	ID	RA (J2000)	Dec. (J2000)	R <sub>V</sub> (10 <sup>4</sup> km/s)
AAT102536	13 24 02.23	-42 59 48.3	5.9	AAT335231	13 26 25.17	-43 25 35.1	5.3
AAT103264	13 24 06.92	-43 03 45.8	6.3	AAT337834	13 26 36.38	-43 22 21.2	3.5
AAT103993	13 24 11.42	-43 14 25.2	3.4	AAT344178	13 26 56.27	-43 31 30.4	4.9
AAT104679	13 24 16.00	-43 04 32.7	3.8	HGHH-27	13 26 37.99	-42 45 49.9	0.2
AAT105959	13 24 23.99	-42 54 10.8	4.6	HH-001	13 24 02.67	-42 48 32.2	0.5
AAT106695	13 24 28.18	-42 53 04.3	1.3	HH-004	13 24 30.88	-42 52 40.9	3.5
AAT107035	13 24 29.04	-43 06 45.2	5.7	HH-005	13 24 35.59	-42 50 59.5	3.3
AAT109567	13 24 45.08	-42 55 22.0	6.4	HH-007	13 24 47.49	-42 46 40.2	3.4
AAT110351	13 24 48.82	-43 16 17.3	4.2	HH-009	13 26 49.28	-42 55 16.6	6.3
AAT111252	13 24 55.58	-42 44 40.1	4.8	HH-013	13 26 18.30	-42 45 26.4	4.4
AAT112141	13 25 00.76	-42 47 35.2	3.7	HH-015	13 26 02.23	-43 17 35.2	4.7
AAT112692	13 25 03.29	-43 08 14.4	3.1	HH-016	13 26 43.29	-43 05 47.6	7.5
AAT114369	13 25 13.25	-42 45 09.5	3.6	HH-017	13 26 49.31	-43 04 57.7	1.5
AAT118869	13 25 43.43	-42 50 03.4	4.8	HH-025	13 24 28.49	-43 14 56.1	4.6
AAT123412	13 26 08.89	-42 53 42.6	4.4	HH-026	13 24 25.33	-43 18 32.9	3.6
AAT125104	13 26 17.77	-42 46 14.2	6.4	HH-033	13 25 44.42	-42 38 25.6	4.8
AAT125921	13 26 22.12	-43 09 10.8	2.1	HH-035	13 26 12.28	-42 35 06.8	6.5
AAT204988	13 25 31.75	-42 15 12.5	3.6	HH-036	13 25 33.44	-42 35 42.8	6.3
AAT207376	13 25 42.19	-42 37 37.8	3.5	HH-040	13 28 21.73	-42 54 17.4	3.6
AAT208065	13 25 45.77	-42 34 18.0	1.5	HH-041	13 27 47.92	-42 54 48.1	3.6
AAT210524	13 25 57.88	-42 38 58.3	3.0	HH-045	13 23 49.66	-43 07 36.3	2.9
AAT219426	13 26 44.05	-42 35 49.1	4.8	HH-048	13 22 45.36	-43 00 42.9	1.6
AAT220871	13 26 49.17	-42 35 31.4	3.5	HH-052	13 24 55.71	-43 22 48.4	0.9
AAT230104	13 27 33.04	-42 20 33.8	4.6	HH-054	13 24 45.22	-43 23 19.2	1.7
AAT231696	13 27 40.36	-42 31 00.1	5.8	HH-060	13 26 59.78	-42 55 26.5	1.3
AAT236547	13 28 13.45	-42 36 53.7	4.5	HH-062	13 27 27.53	-43 01 07.6	2.0
AAT237431	13 28 09.64	-42 42 19.1	5.7	HH-064	13 27 46.38	-43 02 17.7	4.4
AAT238378	13 28 03.22	-42 31 45.2	5.2	HH-065	13 27 53.39	-43 04 48.7	5.7
AAT303828	13 24 03.29	-43 37 07.7	2.0	HH-067	13 27 05.60	-43 15 18.0	3.6
AAT309050	13 24 27.18	-43 40 27.7	3.6	HH-087	13 25 36.42	-42 39 29.7	6.6
AAT310057	13 24 34.26	-43 38 51.5	3.2	HH-094	13 24 00.94	-43 04 55.0	5.9
AAT310433	13 24 34.16	-43 18 31.8	3.0	HH-097	13 24 07.77	-43 02 01.7	6.4
AAT312010	13 24 43.03	-43 28 02.6	3.2	HH-098	13 23 46.32	-42 57 38.7	5.9
AAT329828	13 25 59.99	-43 42 03.7	6.1	HH-099	13 23 56.70	-42 59 59.8	1.3
AAT333607	13 26 18.30	-43 28 40.0	3.6	HH-101	13 23 32.61	-42 58 22.6	2.6



## REFERENCES

- Ashman, K. M., & Zepf, S. E. 1992, *ApJ*, 384, 50
- Ashman, K. M., Bird, C. M., & Zepf, S. E. 1994, *AJ*, 108, 2348
- Beasley, M. A., Sharples, R. M., Bridges, T. J., Hanes, D. A., Zepf, S. E., Ashman, K. M., & Geisler, D. 2000, *MNRAS*, 318, 1249
- Beasley, M. A., Hoyle, F., & Sharples, R. M. 2002a, *MNRAS*, 336, 168
- Beasley, M. A., Baugh, C. M., Forbes, D. A., Sharples, R. M., & Frenk, C. S. 2002b, *MNRAS*, 333, 383
- Beasley, M. A., Harris, W. E., Harris, G. L. H., & Forbes, D. A. 2003, *MNRAS*, 340, 341
- Bekki, K., Forbes, D. A., Beasley, M. A., & Couch, W. J. 2002, *MNRAS*, 335, 1176
- Bekki, K., Harris, W. E., & Harris, G. L. H. 2003, *MNRAS*, 338, 587
- Bekki, K., & Peng, E. W. 2006, *MNRAS*, 370, 1737
- Brodie, J. P., & Strader, J. 2006, *ARA&A*, 44, 193
- Burstein, D., Faber, S. M., Gaskell, C. M., & Krumm, N. 1984, *ApJ*, 287, 586
- Cenarro, A. J., Beasley, M. A., Strader, J., Brodie, J. P., & Forbes, D. A. 2007, *AJ*, 134, 391
- Clark, G. W. 1975, *ApJL*, 199, L143
- Cohen, J. G., Blakeslee, J. P., & Ryzhov, A. 1998, *ApJ*, 496, 808
- Cohen, J. G., Blakeslee, J. P., & Côté, P. 2003, *ApJ*, 592, 866
- Cole, S., Lacey, C. G., Baugh, C. M., & Frenk, C. S. 2000, *MNRAS*, 319, 168
- Colless, M., et al. 2001, *MNRAS*, 328, 1039
- Côté, P., Marzke, R. O., & West, M. J. 1998, *ApJ*, 501, 554
- De Angeli, F., Piotto, G., Cassisi, S., Busso, G., Recio-Blanco, A., Salaris, M., Aparicio, A., & Rosenberg, A. 2005, *AJ*, 130, 116
- Dufour, R. J., Harvel, C. A., Martins, D. M., Schiffer, F. H., III, Talent, D. L., Wells, D. C., van den Bergh, S., & Talbot, R. J., Jr. 1979, *AJ*, 84, 284
- Forbes, D. A., Brodie, J. P., & Grillmair, C. J. 1997, *AJ*, 113, 1652
- Harris, W. E. 1996, *AJ*, 112, 1487
- Harris, W. E., Whitmore, B. C., Karakla, D., Okoń, W., Baum, W. A., Hanes, D. A., & Kavelaars, J. J. 2006a, *ApJ*, 636, 90
- Harris, W. E., Harris, G. L. H., Barmby, P., McLaughlin, D. E., & Forbes, D. A. 2006b, *AJ*, 132, 2187
- Harris, G. L. H., et al. 2004, *AJ*, 128, 712
- Harris, W. E., & Harris, G. L. H. 2002, *AJ*, 123, 3108
- Harris, G. L. H., & Harris, W. E. 2000, *AJ*, 120, 2423
- Held, E. V., Federici, L., Cacciari, C., & Testa, V. 2002, *Extragalactic Star Clusters*, IAU symposium 207, p269
- Hempel, M., Kissler-Patig, M., Puzia, T. H., & Hilker, M. 2007, *A&A*, 463, 493
- Hesser, J. E., Harris, H. C., & Harris, G. L. H. 1986, *ApJL*, 303, L51
- Houdashelt, M. L., Trager, S. C., Worthey, G., & Bell, R. A. 2002, *BAAS*, 34, 1118 (H02)
- Jordán, A., Côté, P., West, M. J., & Marzke, R. O. 2002, *ApJL*, 576, L113
- Kaviraj, S., Ferreras, I., Yoon, S.-J., & Yi, S. K. 2005, *A&A*, 439, 913
- Kundu, A., et al. 2005, *ApJL*, 634, L41
- Kundu, A., & Zepf, S. E. 2007, *ApJL*, 660, L109
- Larsen, S. S., Brodie, J. P., Huchra, J. P., Forbes, D. A., & Grillmair, C. J. 2001, *AJ*, 121, 2974
- Larsen, S. S., Brodie, J. P., & Strader, J. 2005, *A&A*, 443, 413
- Lee, H.-c., Yoon, S.-J., & Lee, Y.-W. 2000, *AJ*, 120, 998
- Lee, H.-c., & Worthey, G. 2005, *ApJS*, 160, 176 (LW05)
- Lee, H.-c., Worthey, G., Trager, S. C., & Faber, S. M. 2006, (astro-ph/0605425)
- Lewis, I. J., et al. 2002, *MNRAS*, 333, 279
- Malin, D. F. 1978, *Nature*, 276, 591
- Maraston, C. 1998, *MNRAS*, 300, 872
- Mendel, J. T., Proctor, R. N., & Forbes, D. A. 2007, *MNRAS*, 379, 1618
- Mould, J., & Aaronson, M. 1980, *ApJ*, 240, 464
- Peng, E. W., Ford, H. C., Freeman, K. C., & White, R. L. 2002, *AJ*, 124, 3144
- Peng, E. W., Ford, H. C., & Freeman, K. C. 2004, *ApJ*, 602, 705 (PFF04)
- Peng, E. W., Ford, H. C., & Freeman, K. C. 2004b, *ApJS*, 150, 367
- Peng, E. W., Ford, H. C., & Freeman, K. C. 2004c, *ApJ*, 602, 685
- Peng, E. W., et al. 2006, *ApJ*, 639, 95
- Perrett, K. M., Bridges, T. J., Hanes, D. A., Irwin, M. J., Brodie, J. P., Carter, D., Huchra, J. P., & Watson, F. G. 2002, *AJ*, 123, 2490
- Pierce, M., et al. 2006, *MNRAS*, 366, 1253
- Pipino, A., Puzia, T. H., & Matteucci, F. 2007, *ApJ*, 665, 295
- Pritzl, B. J., Venn, K. A., & Irwin, M. 2005, *AJ*, 130, 2140
- Proctor, R. N., Forbes, D. A., & Beasley, M. A. 2004, *MNRAS*, 355, 1327
- Puzia, T. H., Kissler-Patig, M., Brodie, J. P., & Huchra, J. P. 1999, *AJ*, 118, 2734
- Puzia, T. H., Zepf, S. E., Kissler-Patig, M., Hilker, M., Minniti, D., & Goudfrooij, P. 2002a, *A&A*, 391, 453
- Puzia, T. H., Saglia, R. P., Kissler-Patig, M., Maraston, C., Greggio, L., Renzini, A., & Ortolani, S. 2002b, *A&A*, 395, 45
- Puzia, T. H., Kissler-Patig, M., Thomas, D., Maraston, C., Saglia, R. P., Bender, R., Goudfrooij, P., & Hempel, M. 2005, *A&A*, 439, 997
- Rejkuba, M. 2004, *A&A*, 413, 903
- Rejkuba, M., Greggio, L., Harris, W. E., Harris, G. L. H., & Peng, E. W. 2005, *APJ*, 631, 262
- Richardson, S., & Green, P.G., 1997, *JR Stat. Soc. B*, 59, 731
- Salaris, M., & Cassisi, S. 2007, *A&A*, 461, 493
- Schiavon, R. P., Rose, J. A., Courteau, S., & MacArthur, L. A. 2005, *ApJS*, 160, 163
- Sharples, R. 1988, *The Harlow-Shapley Symposium on Globular Cluster Systems in Galaxies*, IAU symposium 126, p. 545
- Sheather, S.J., & Jones, M.C. 1991, *J R Stat. Soc. B*, 53, 683
- Silverman, B. W. 1986, *Monographs on Statistics and Applied Probability*, London: Chapman and Hall, 1986
- Strader, J., Brodie, J. P., & Forbes, D. A. 2004, *AJ*, 127, 3431
- Strader, J., Brodie, J. P., Cenarro, A. J., Beasley, M. A., & Forbes, D. A. 2005, *AJ*, 130, 1315
- Strader, J., Brodie, J. P., Spitler, L., & Beasley, M. A. 2006, *AJ*, 132, 2333
- Strader, J., Beasley, M. A., & Brodie, J. P. 2007, *AJ*, 133, 2015
- Taylor, K., Bailey, J., Wilkins, T., Shortridge, K., & Glazebrook, K. 1996, *Astronomical Data Analysis Software and Systems V*, George H. Jacoby and Jeannette Barnes, eds. Vol 101, p 195

**Table 5.** Lick indices measured for NGC 5128 globular clusters.

ID	H $\delta_A$ (Å)	H $\delta_F$ (Å)	CN <sub>1</sub> (mag)	CN <sub>2</sub> (mag)	Ca4227 (Å)	G4300 (Å)	H $\gamma_A$ (Å)	H $\gamma_F$ (Å)	Fe4383 (Å)	Ca4455 (Å)	Fe4531 (Å)
AAT101906	0.785	1.218	0.042	0.060	0.743	4.451	-3.595	-0.671	3.707	1.164	3.499
AAT103195	-2.774	-0.416	-0.100	-0.073	1.537	5.786	-5.228	-3.009	1.893	0.595	1.030
AAT106880	0.805	0.355	-0.052	-0.071	0.663	2.125	0.915	1.622	0.326	1.625	0.185
AAT107060	1.139	1.038	-0.022	0.023	1.163	4.021	-2.474	0.164	2.078	0.153	1.218
AAT107977	1.725	1.445	-0.072	-0.035	0.681	2.304	0.116	0.394	-0.307	0.231	1.624
AAT109380	-0.404	0.520	-0.045	-0.031	0.231	3.770	-2.003	-0.174	1.777	0.469	1.221
AAT109711	3.198	2.383	-0.078	-0.059	-0.088	0.206	2.551	2.038	-0.159	-0.026	0.709
AAT109788	-1.711	0.325	0.034	0.065	1.363	-1.010	-4.346	-0.305	5.633	1.532	3.400
AAT110138	2.527	1.523	-0.033	-0.017	0.382	2.340	0.655	0.989	0.246	0.787	2.331
AAT111185	-0.312	0.883	-0.009	0.004	0.216	1.895	-0.768	-0.271	0.648	0.572	0.820
AAT111296	-7.341	-0.066	0.235	0.252	0.468	5.225	-5.120	-1.366	4.425	0.755	2.186
AAT112752	0.594	0.296	0.036	0.030	0.003	3.011	-4.898	0.086	5.609	0.063	3.770
AAT112964	-9.590	-3.274	0.089	0.103	-0.056	3.108	-0.306	1.201	1.811	0.779	0.257
AAT113428	1.979	1.855	-0.005	0.037	-0.128	4.513	-1.470	-0.131	0.759	0.259	2.590
AAT114913	-2.001	0.230	0.023	0.035	0.792	5.821	-3.972	-0.010	4.474	1.592	1.489
AAT115561	-0.047	0.666	0.023	0.040	0.068	4.571	-3.693	-0.389	2.392	0.824	3.320
AAT115605	-3.203	1.552	0.026	0.131	-1.219	1.454	2.615	2.608	3.207	1.897	2.149
AAT116025	1.177	3.597	0.008	0.008	0.237	5.168	-2.808	-0.047	3.913	0.628	0.572
AAT116220	0.100	1.145	-0.013	0.020	0.516	3.516	-1.599	0.190	1.678	0.582	1.576
AAT116385	-1.210	0.674	-0.020	-0.010	1.819	6.214	-6.161	-2.086	3.877	0.283	3.356
AAT116969	0.310	1.282	0.040	0.034	1.351	3.256	-2.737	1.185	5.742	1.512	2.007
AAT117062	0.709	1.302	-0.006	0.011	0.482	3.516	-1.422	0.289	2.044	0.547	1.795
AAT117322	-1.139	-0.030	0.028	0.021	0.098	2.758	0.678	1.584	1.348	0.108	2.886
AAT118314	0.787	0.990	-0.052	-0.025	0.675	2.688	-1.730	-0.065	2.038	0.168	1.890
AAT119596	-2.483	0.542	0.001	0.039	0.168	2.405	-2.842	-0.518	3.646	0.670	1.568
AAT119894	-0.933	2.197	-0.005	0.044	1.080	4.526	-4.247	-1.533	-3.720	-0.418	3.208
AAT120355	3.151	3.925	-0.064	-0.032	0.091	2.056	-1.294	0.546	5.947	0.222	-0.397
AAT121367	1.971	2.115	-0.101	-0.098	1.359	3.293	-1.181	0.190	1.013	1.214	2.675
AAT122526	1.628	2.217	-0.073	-0.024	0.761	2.754	-1.186	-0.101	2.045	0.978	0.492
AAT204119	0.350	1.576	-0.070	-0.080	0.798	4.344	-3.135	0.043	3.059	-0.957	2.531
AAT208206	0.631	1.088	-0.013	0.023	0.487	-0.490	3.316	2.969	1.403	0.169	0.792
AAT215171	-2.662	0.696	0.010	0.053	0.864	4.675	-3.211	-0.246	4.888	1.641	2.916
AAT308432	-0.785	0.835	0.016	0.028	0.345	3.602	-3.427	-0.324	4.119	1.561	1.978
AAT329209	-6.467	-4.908	-0.081	-0.115	1.495	3.684	-0.066	1.173	1.131	-0.166	1.276
AAT329848	2.171	1.895	-0.045	-0.022	0.069	1.957	1.566	2.007	0.762	0.860	1.135
HGHH-01	2.879	2.399	-0.067	-0.035	0.280	2.237	1.041	1.554	0.718	0.768	1.106
HGHH-04	2.706	2.571	-0.033	-0.005	-0.049	2.162	1.679	1.963	1.102	0.285	1.167
HGHH-06	-5.013	0.735	0.224	0.284	4.543	6.791	-4.001	0.528	5.483	0.500	6.502
HGHH-07	0.818	1.534	0.012	0.042	0.542	3.192	-0.686	0.837	2.015	0.622	1.874
HGHH-11	-1.217	0.228	0.064	0.100	0.661	4.620	-3.617	-0.443	3.593	1.132	2.502
HGHH-17	1.096	1.665	0.008	0.037	0.291	3.207	-0.946	0.871	2.667	0.833	2.300
HGHH-19	0.107	1.539	0.013	0.068	0.801	3.059	-1.102	0.615	2.817	1.024	2.200
HGHH-20	0.311	1.248	-0.010	0.024	0.704	3.346	-1.741	0.428	3.296	0.815	2.065
HGHH-21	0.261	1.643	0.029	0.064	0.503	3.401	-1.053	0.978	2.758	0.821	2.070
HGHH-22	1.383	1.606	-0.015	0.024	0.562	3.240	-0.993	0.219	0.877	0.875	2.258
HGHH-23	-1.971	0.235	0.079	0.124	0.918	4.636	-4.001	-1.019	4.004	1.237	2.644
HGHH-25	0.084	1.091	0.025	0.048	0.525	3.888	-3.473	-0.808	3.896	1.057	2.342
HGHH-29	-0.845	1.084	0.039	0.058	1.065	4.333	-3.581	-0.875	3.646	1.236	2.775
HGHH-31	-3.626	0.209	0.145	0.165	1.450	5.492	-5.453	-1.473	2.954	0.408	3.493
HGHH-34	-1.423	0.499	0.009	0.036	1.156	4.443	-4.128	-0.532	3.959	0.883	2.648
HGHH-36	0.276	1.457	0.043	0.076	0.151	2.128	0.338	1.224	0.936	0.622	0.837
HGHH-37	-0.176	0.588	0.042	0.067	0.610	3.487	-3.244	-0.441	3.636	0.941	1.837
HGHH-40	-0.747	1.336	-0.001	0.049	-0.593	2.784	-1.183	1.410	3.628	0.570	0.158
HGHH-41	-2.512	0.426	0.080	0.112	0.669	4.031	-2.895	-0.317	2.938	1.081	3.148
HGHH-42	-2.525	-1.351	0.058	0.076	0.830	4.243	-2.447	0.008	2.667	1.054	2.779
HGHH-43	1.886	1.615	-0.051	-0.030	0.472	2.277	0.190	1.418	1.957	0.397	1.055
HGHH-44	1.091	1.526	-0.016	0.020	0.248	2.181	0.535	1.792	1.250	0.410	1.378
HGHH-45	1.920	2.012	-0.042	-0.013	0.308	2.615	1.316	1.939	2.747	0.505	1.579
HGHH-48	2.886	2.716	-0.023	0.016	0.151	2.076	1.582	1.542	0.644	0.464	0.510
HGHH-G143	0.048	0.514	0.019	-0.045	-0.780	2.655	-1.183	0.499	2.608	0.902	2.277
HGHH-G170	-1.208	0.219	0.119	0.175	1.246	5.477	-6.308	-1.047	5.839	1.356	2.802
HGHH-G176	-4.152	-0.467	0.109	0.155	1.518	5.567	-5.095	-1.336	4.644	1.412	3.045
HGHH-G204	4.541	3.891	-0.078	-0.004	0.936	2.934	0.822	1.757	0.478	0.926	1.433

Table 5 – continued

ID	H $\delta_A$ (Å)	H $\delta_F$ (Å)	CN <sub>1</sub> (mag)	CN <sub>2</sub> (mag)	Ca4227 (Å)	G4300 (Å)	H $\gamma_A$ (Å)	H $\gamma_F$ (Å)	Fe4383 (Å)	Ca4455 (Å)	Fe4531 (Å)
HGHH-G219	-1.482	0.351	0.043	0.061	0.799	4.262	-3.775	-0.479	4.009	0.993	3.880
HGHH-G251	0.232	1.300	0.016	0.044	0.351	4.420	-5.186	-1.253	3.939	0.768	3.363
HGHH-G277	1.782	2.040	-0.017	0.008	0.535	2.661	0.126	0.617	1.914	0.857	1.242
HGHH-G279	5.133	3.901	-0.142	-0.173	-0.274	-2.198	6.235	4.374	-0.477	0.368	0.852
HGHH-G293	3.825	2.239	-0.061	-0.035	0.625	2.675	0.391	0.839	1.150	0.620	1.041
HGHH-G342	-1.172	1.116	0.071	0.123	0.980	4.837	-3.556	-0.316	5.000	1.177	3.977
HGHH-G348	-1.034	0.044	-0.050	-0.052	0.281	2.587	-0.921	-0.017	1.612	0.297	2.999
HGHH-G369	1.728	2.013	-0.022	0.005	0.499	2.521	0.475	1.248	1.075	0.583	1.676
HGHH-G370	-0.131	0.811	0.009	0.031	0.887	4.449	-2.388	0.441	1.860	1.102	2.402
HHH86-10	-0.657	0.705	0.006	0.055	0.599	3.302	-1.853	0.227	2.794	1.359	2.533
HHH86-13	0.154	0.821	0.017	0.038	0.206	4.406	-2.243	-0.373	1.487	0.617	2.629
HHH86-14	0.917	1.442	0.013	0.046	0.542	3.125	-0.947	0.601	2.283	0.658	2.357
HHH86-15	-1.499	-0.977	0.080	0.077	0.222	4.447	-4.442	-1.185	4.483	0.611	2.872
HHH86-16	0.178	0.680	0.024	0.059	0.579	3.559	-1.683	0.015	1.882	1.214	2.264
HHH86-18	1.093	1.428	0.009	0.035	0.420	2.839	-0.951	0.763	2.525	0.578	2.175
HHH86-26	-2.401	-0.443	0.088	0.113	1.008	5.602	-6.845	-1.693	5.701	1.504	3.871
HHH86-28	1.190	1.337	-0.045	-0.021	-0.263	1.571	1.287	1.529	-0.424	0.271	0.880
HHH86-30	-0.370	0.580	0.031	0.067	0.778	3.750	-2.435	0.037	3.361	1.071	2.625
HHH86-32	-3.066	-1.056	0.121	0.199	1.597	5.905	-4.689	-0.954	4.110	1.973	2.283
HHH86-33	1.808	1.719	-0.027	0.003	0.130	2.648	0.188	1.488	1.687	0.858	1.784
HHH86-39	-1.559	0.274	-0.011	0.023	1.196	4.865	-4.832	-1.767	3.179	0.542	1.750
HH-024	-2.988	0.457	0.068	0.110	0.672	5.582	-6.667	-1.061	7.578	1.142	3.513
HH-080	0.792	1.229	-0.015	0.005	0.046	1.691	1.225	1.582	0.424	0.162	0.644
HH-096	1.853	1.537	-0.023	-0.007	0.137	2.539	0.250	1.010	0.921	0.475	1.204
K-029	-0.226	0.847	0.045	0.078	0.559	3.513	-2.193	-0.114	2.784	0.870	2.135
K-033	-0.260	0.753	0.057	0.086	0.507	4.306	-3.374	-0.684	2.206	0.810	3.071
K-034	-0.623	0.627	0.046	0.072	0.808	4.445	-3.576	-0.301	3.386	1.073	2.547
K-051	-0.997	0.981	-0.001	0.030	0.025	5.130	-4.176	-0.346	4.201	1.029	2.585
K-102	-0.193	1.384	0.030	0.056	0.654	4.872	-4.017	-0.675	3.272	0.912	2.531
K-163	1.134	1.541	-0.013	0.014	0.562	2.924	-0.859	0.545	1.844	0.892	2.136
K-217	-2.834	-0.596	0.060	0.127	0.745	5.021	-4.255	0.232	4.813	0.142	2.305
K-233	2.224	0.879	-0.027	-0.017	0.238	3.263	-0.669	0.540	1.642	1.021	2.802
R117	2.933	2.433	-0.045	-0.010	0.230	1.634	1.921	2.292	0.625	0.138	1.372
R202	2.399	1.957	-0.043	-0.023	0.053	2.393	0.302	1.036	0.921	0.927	1.326
R203	3.264	2.682	-0.052	-0.014	0.355	1.354	1.944	1.731	0.206	0.863	0.000
R235	2.374	2.830	-0.055	-0.016	0.055	1.202	0.710	1.675	2.765	0.976	1.321
R253	-0.313	1.656	0.030	0.040	-0.130	4.850	-1.403	0.782	2.154	0.101	3.059
R254	1.684	1.376	-0.055	-0.032	0.432	2.174	0.356	1.355	1.897	1.225	1.948
R261	-0.316	0.613	0.049	0.086	0.393	3.625	-2.332	0.099	3.819	1.169	2.665
VHH81-02	1.995	1.658	-0.059	-0.032	0.296	3.095	-0.411	0.937	1.289	0.802	1.389
VHH81-03	-0.506	0.666	0.034	0.072	0.688	4.376	-3.748	-0.520	4.388	0.766	3.000
VHH81-05	2.621	2.141	-0.038	-0.014	0.182	2.247	0.903	1.584	0.693	0.288	1.113
PFF-gc001	0.295	0.818	-0.013	0.015	0.555	3.669	-2.069	-0.188	2.564	0.850	1.853
PFF-gc002	2.825	2.113	-0.082	-0.056	0.303	1.859	0.311	1.217	1.322	0.766	1.661
PFF-gc003	3.111	2.233	-0.103	-0.087	0.033	2.194	1.543	1.306	-0.891	1.400	1.686
PFF-gc004	4.176	3.175	-0.117	-0.091	0.531	2.477	0.527	1.116	-0.250	0.645	1.471
PFF-gc006	2.139	2.163	-0.064	-0.044	0.618	2.151	1.300	1.546	1.032	0.274	0.946
PFF-gc011	4.033	2.308	-0.052	-0.033	-0.207	2.583	2.570	2.436	0.423	-0.369	-1.827
PFF-gc013	2.261	1.353	-0.093	-0.068	-0.045	2.113	1.829	1.867	1.073	0.767	1.740
PFF-gc015	2.195	1.900	-0.043	0.008	0.212	3.602	0.043	1.179	1.613	0.165	1.724
PFF-gc016	1.467	2.797	-0.026	-0.029	0.165	5.723	-6.227	-1.113	4.166	2.730	4.120
PFF-gc018	-1.547	0.733	0.087	0.114	0.653	4.304	-4.972	-1.554	4.228	1.289	3.314
PFF-gc022	4.482	3.406	-0.101	-0.083	0.051	0.080	2.793	1.745	-0.782	0.693	0.205
PFF-gc023	1.839	2.627	-0.032	0.007	0.485	2.319	1.517	1.793	0.017	0.289	0.440
PFF-gc032	2.104	1.973	-0.014	0.012	0.468	3.112	0.073	1.006	0.489	0.699	3.204
PFF-gc035	-0.982	-0.070	0.014	0.021	1.075	4.358	-3.109	-1.005	2.080	0.912	1.901
PFF-gc036	2.314	2.104	-0.034	-0.007	-0.076	2.625	0.206	1.350	1.413	0.532	1.357
PFF-gc039	-0.469	-0.165	-0.024	-0.018	0.065	6.707	-5.332	-1.894	2.224	-0.297	1.053
PFF-gc042	4.016	2.621	-0.077	-0.047	0.405	1.964	0.954	1.594	1.298	0.149	0.470
PFF-gc046	0.357	0.528	-0.045	-0.027	0.148	4.003	-3.032	-0.661	1.702	0.185	0.978
PFF-gc051	-1.876	0.753	0.082	0.121	0.503	4.693	-2.586	-0.213	3.272	0.736	2.784
PFF-gc058	2.481	2.817	-0.043	-0.003	0.878	1.369	1.189	2.138	1.746	1.015	1.863
PFF-gc066	0.265	-0.250	-0.046	-0.017	0.848	4.878	-1.734	0.052	0.907	0.726	2.582

**Table 5** – *continued*

ID	H $\delta$ <sub>A</sub> (Å)	H $\delta$ <sub>F</sub> (Å)	CN <sub>1</sub> (mag)	CN <sub>2</sub> (mag)	Ca4227 (Å)	G4300 (Å)	H $\gamma$ <sub>A</sub> (Å)	H $\gamma$ <sub>F</sub> (Å)	Fe4383 (Å)	Ca4455 (Å)	Fe4531 (Å)
PFF-gc069	0.477	2.232	0.096	0.124	0.976	6.490	-3.030	-0.070	2.919	1.236	2.047
PFF-gc074	2.453	2.922	-0.036	-0.011	0.666	3.721	-0.638	1.465	2.777	0.798	2.139
PFF-gc075	-0.230	0.968	0.000	0.028	0.844	4.833	-3.362	-0.273	4.638	0.597	4.044
PFF-gc079	1.696	2.474	-0.045	-0.038	0.409	3.931	-2.148	-0.290	2.459	0.851	2.495
PFF-gc081	2.289	2.222	-0.009	0.015	0.519	2.418	0.724	1.199	-0.246	0.762	1.004
PFF-gc082	-3.192	-1.235	0.097	0.093	0.857	3.323	-2.707	-0.592	2.536	1.306	3.842
PFF-gc085	1.947	1.863	-0.093	-0.066	0.074	1.513	1.079	1.381	1.726	0.726	0.810
PFF-gc087	1.513	1.418	-0.025	-0.005	0.311	2.053	1.862	2.105	1.238	0.883	1.060
PFF-gc088	2.146	1.931	-0.039	-0.011	0.320	2.356	1.342	1.474	0.239	0.845	2.099
PFF-gc089	1.657	1.693	-0.052	-0.041	0.185	1.780	2.459	2.350	1.038	0.873	1.160
PFF-gc090	-0.035	0.226	0.077	0.094	0.511	4.176	-3.464	0.076	5.333	0.538	3.099
PFF-gc093	3.035	1.695	-0.089	-0.080	-0.234	1.043	1.671	1.684	0.843	0.312	1.412
PFF-gc097	1.813	1.955	-0.029	-0.003	0.275	1.346	1.464	1.710	1.599	1.002	1.441
PFF-gc098	1.064	1.415	-0.024	-0.009	0.488	2.866	-0.592	0.739	2.408	0.883	1.676
PFF-gc100	-1.194	0.636	0.044	0.070	0.471	3.679	-2.443	0.280	3.662	0.908	3.033
PFF-gc101	-1.894	-0.274	-0.002	0.024	1.082	5.496	-4.563	-1.757	3.212	0.980	2.331
WHH-06	-0.610	-0.927	0.098	0.125	0.562	7.417	-7.741	-1.720	5.375	1.142	2.454
WHH-17	1.751	2.104	-0.042	-0.017	0.629	2.991	-0.773	0.728	2.112	0.474	1.477
WHH-18	-1.257	0.059	0.046	0.068	0.615	4.460	-3.220	-0.365	3.007	1.067	1.920
WHH-20	0.775	1.498	-0.012	0.018	0.532	3.585	-0.873	1.038	2.080	1.107	2.378

Thomas, D., Maraston, C., & Bender, R. 2003, MNRAS, 339, 897

Thomas, D., Maraston, C., & Korn, A. 2004, MNRAS, 351, L19  
(TMK04)

Tonry, J., & Davis, M. 1979, AJ, 84, 1511

Trager, S. C., Worthey, G., Faber, S. M., Burstein, D., & Gonzalez, J. J. 1998, ApJS, 116, 1

van den Bergh, S., Hesser, J. E., & Harris, G. L. H. 1981, AJ, 86, 24

VanDalsen, M. L., & Harris, W. E. 2004, AJ, 127, 368

Vazdekis, A. 1999, ApJ, 513, 224

Woodley, K. A., Harris, W. E., & Harris, G. L. H. 2005, AJ, 129, 2654

Woodley, K. A., Harris, W. E., Beasley, M. A., Peng, E. W., Bridges, T. J., Forbes, D. A., & Harris, G. L. H. 2007, AJ, 134, 494

Worthey, G., & Ottaviani, D. L. 1997, ApJS, 111, 377

Yoon, S.-J., Yi, S. K., & Lee, Y.-W. 2006, Science, 311, 1129

Zinn, R., & West, M. J. 1984, ApJS, 55, 45

Table 5 – continued

ID	C <sub>2</sub> 4668 (Å)	H $\beta$ (Å)	Fe5015 (Å)	Mg <sub>1</sub> (mag)	Mg <sub>2</sub> (mag)	Mg <i>b</i> (Å)	Fe5270 (Å)	Fe5335 (Å)	Fe5406 (Å)	Fe5709 (Å)	Fe5782 (Å)	Na D (Å)
AAT101906	2.396	1.538	4.222	0.061	0.185	3.070	2.484	2.150	1.695	0.667	0.572	1.124
AAT103195	-1.130	0.258	2.546	0.085	0.263	4.235	2.227	1.355	1.385	0.319	-0.206	0.539
AAT106880	-0.617	2.715	1.815	0.041	0.080	0.958	0.434	0.298	1.011	0.314	-0.068	-0.694
AAT107060	1.921	1.881	4.190	0.069	0.168	3.445	2.222	1.318	1.395	0.911	0.105	6.539
AAT107977	-0.119	2.040	1.913	0.053	0.127	1.968	1.615	1.813	1.308	0.441	0.447	2.768
AAT109380	-0.980	1.614	2.339	0.017	0.052	0.929	0.825	0.531	0.545	0.270	-0.039	-0.081
AAT109711	0.400	2.553	1.189	-0.001	0.052	1.017	0.945	0.679	0.444	0.271	-0.011	-0.015
AAT109788	4.759	0.860	4.727	0.086	0.238	3.691	2.671	2.909	1.794	0.867	0.307	2.532
AAT110138	-6.743	2.574	3.781	0.022	0.103	1.842	1.640	1.386	1.288	0.562	0.176	3.778
AAT111185	2.014	1.740	1.833	-0.007	0.093	2.027	0.630	1.407	0.905	0.692	-0.110	2.197
AAT111296	1.500	1.539	3.864	0.084	0.218	4.003	2.572	2.728	1.786	0.670	0.527	3.598
AAT112752	-1.077	1.468	5.216	-0.003	0.087	2.808	1.867	0.775	0.954	1.060	0.254	1.999
AAT112964	1.572	1.244	1.048	0.009	0.063	1.146	0.848	1.370	1.074	0.214	-0.188	-0.926
AAT113428	3.291	1.830	3.457	0.029	0.136	2.586	2.137	1.976	0.347	0.839	-0.369	6.735
AAT114913	1.255	1.886	5.178	0.056	0.165	2.230	2.134	1.512	1.422	0.842	0.277	3.842
AAT115561	4.477	1.579	4.253	0.061	0.198	3.770	3.428	3.451	2.151	0.931	0.497	4.081
AAT115605	4.229	1.041	0.896	0.025	0.041	0.780	2.277	1.524	-0.125	-0.744	-0.078	0.934
AAT116025	2.259	1.636	3.424	0.076	0.150	2.023	1.752	1.585	0.722	-0.013	0.218	-0.674
AAT116220	0.475	2.020	3.382	0.025	0.118	2.150	1.895	1.001	1.319	0.502	-0.013	7.085
AAT116385	2.045	2.315	5.478	0.070	0.203	3.299	2.430	2.327	1.278	0.689	0.763	1.553
AAT116969	2.824	2.617	2.460	0.030	0.100	2.137	2.172	1.822	1.312	0.381	-0.316	1.864
AAT117062	0.959	1.883	2.913	0.031	0.117	1.890	1.770	1.212	0.828	0.530	0.227	1.426
AAT117322	2.343	1.457	3.694	0.021	0.083	1.092	1.231	1.568	1.131	0.333	0.098	1.403
AAT118314	1.635	2.564	2.263	0.009	0.083	1.203	1.317	0.839	0.609	-0.011	0.540	0.176
AAT119596	2.158	2.231	3.331	0.100	0.207	3.208	2.298	1.507	0.636	1.164	0.324	1.237
AAT119894	1.623	1.012	1.776	0.009	0.049	0.865	0.639	1.999	0.845	0.758	0.705	0.827
AAT120355	-1.175	2.331	5.310	0.072	0.114	2.211	0.597	1.969	1.451	-0.220	-0.034	-1.831
AAT121367	0.852	0.463	2.220	0.061	0.158	3.264	2.056	1.605	0.527	0.816	0.286	9.285
AAT122526	0.604	1.639	2.510	0.050	0.145	3.393	2.589	1.932	0.614	0.943	1.042	2.969
AAT204119	0.127	1.828	0.662	0.037	0.083	0.963	0.618	0.673	0.724	-0.427	-0.597	-2.301
AAT208206	6.001	2.530	-1.063	-0.014	-0.005	0.011	0.277	0.197	0.003	0.028	-0.327	0.743
AAT215171	1.325	1.810	1.770	0.026	0.139	3.104	3.182	1.615	0.390	0.866	0.279	0.011
AAT308432	1.419	2.225	-1.069	-0.026	0.107	2.346	1.724	1.668	0.999	0.777	0.094	-2.504
AAT329209	0.866	1.938	0.163	-0.007	0.055	1.924	0.282	-0.844	-0.030	0.909	-0.389	-2.669
AAT329848	0.026	2.382	1.845	0.025	0.087	1.159	1.449	1.257	0.514	0.367	0.018	0.939
HGHH-01	0.024	2.419	2.362	0.022	0.074	0.963	1.429	1.170	0.559	0.451	0.141	2.121
HGHH-04	0.101	2.311	1.512	0.015	0.069	1.012	0.870	0.788	0.323	0.223	-0.107	2.464
HGHH-06	1.494	2.614	3.847	0.033	0.092	1.142	1.100	1.443	-0.161	0.768	0.053	2.995
HGHH-07	0.653	1.926	2.752	0.039	0.125	2.101	1.788	1.504	0.999	0.552	0.151	1.424
HGHH-11	2.408	1.640	4.707	0.055	0.187	3.550	2.396	2.306	1.338	0.850	0.554	3.126
HGHH-17	1.048	2.152	3.311	0.038	0.125	2.042	1.775	1.592	1.041	0.561	0.291	1.231
HGHH-19	0.225	1.930	3.247	0.045	0.124	1.240	1.323	1.388	1.392	0.190	0.256	1.454
HGHH-20	0.510	1.796	3.647	0.027	0.116	2.145	1.715	1.275	0.725	0.547	0.267	1.623
HGHH-21	0.791	1.908	2.644	0.025	0.101	1.948	1.568	1.538	1.087	0.643	0.045	4.148
HGHH-22	1.405	1.919	3.088	0.031	0.115	1.953	1.842	1.502	1.082	0.467	0.270	3.090
HGHH-23	3.525	1.555	4.459	0.069	0.180	2.706	2.149	2.227	1.517	0.865	0.482	5.525
HGHH-25	2.287	1.407	4.178	0.061	0.195	3.535	3.011	2.190	1.439	0.791	0.476	2.619
HGHH-29	2.434	1.755	4.786	0.074	0.204	3.455	2.541	2.123	1.426	0.695	0.495	2.287
HGHH-31	1.003	1.660	3.453	0.060	0.199	3.089	2.073	1.764	1.168	0.860	0.721	1.854
HGHH-34	2.498	2.002	5.211	0.051	0.162	2.901	2.592	2.258	1.722	0.905	0.272	1.328
HGHH-36	0.115	2.418	2.780	0.041	0.104	1.480	1.560	1.248	0.684	0.312	0.096	0.037
HGHH-37	2.637	1.770	4.303	0.047	0.161	2.546	2.119	1.935	1.467	0.755	0.394	1.112
HGHH-40	0.353	1.707	3.098	0.045	0.093	1.301	0.978	0.823	0.751	0.200	0.152	-1.816
HGHH-41	3.252	1.666	4.813	0.064	0.187	3.445	2.203	2.365	1.331	0.593	0.538	2.021
HGHH-42	0.573	1.473	5.107	0.037	0.153	2.670	2.419	2.719	1.165	0.363	0.352	1.432
HGHH-43	-0.824	2.136	2.737	0.032	0.097	1.706	1.334	1.127	0.723	0.464	0.168	1.759
HGHH-44	0.761	2.753	1.286	0.018	0.083	1.232	1.302	0.991	0.740	0.417	0.170	0.683
HGHH-45	2.321	2.253	2.115	0.016	0.070	1.510	1.654	2.363	1.177	-2.673	0.615	2.070
HGHH-48	0.164	2.313	2.174	0.010	0.059	0.927	1.051	0.911	0.364	-0.407	-0.122	0.324
HGHH-G143	-3.087	2.130	2.132	0.051	0.155	2.933	1.658	0.780	0.581	0.383	-0.007	-0.014
HGHH-G170	1.524	1.235	4.314	0.038	0.163	3.414	2.496	2.361	1.111	0.760	0.522	3.181
HGHH-G176	0.143	1.297	3.842	0.053	0.178	3.227	2.335	1.222	1.539	0.886	0.522	3.752

Table 5 – *continued*

ID	C <sub>2</sub> 4668 (Å)	H $\beta$ (Å)	Fe5015 (Å)	Mg <sub>1</sub> (mag)	Mg <sub>2</sub> (mag)	Mg <i>b</i> (Å)	Fe5270 (Å)	Fe5335 (Å)	Fe5406 (Å)	Fe5709 (Å)	Fe5782 (Å)	Na D (Å)
HGHH-G204	-0.313	2.614	0.608	0.019	-0.003	-0.634	-0.377	0.657	0.275	0.036	-0.242	1.809
HGHH-G219	4.053	1.225	5.544	0.045	0.198	4.441	3.148	3.300	2.093	1.212	0.839	3.859
HGHH-G251	3.921	2.377	4.896	0.045	0.186	4.088	2.162	2.752	1.902	0.900	0.632	2.405
HGHH-G277	0.930	2.332	3.273	0.025	0.115	1.422	1.789	1.223	0.839	0.168	0.190	-0.373
HGHH-G279	0.695	4.323	2.194	0.013	0.050	0.226	1.183	0.491	1.002	0.164	0.089	2.842
HGHH-G293	1.015	1.333	3.772	0.006	0.065	1.281	1.273	1.295	0.560	0.433	0.291	-1.578
HGHH-G342	2.236	1.931	4.868	0.010	0.122	2.761	2.247	2.188	1.260	0.902	0.282	5.158
HGHH-G348	1.873	1.231	2.367	0.008	0.129	2.862	1.459	1.151	0.889	0.282	0.166	2.151
HGHH-G369	0.153	2.324	2.498	0.033	0.097	1.507	1.325	0.928	0.442	0.069	0.177	0.770
HGHH-G370	2.206	2.089	4.663	0.030	0.118	2.186	1.574	1.864	1.176	0.523	0.163	1.890
HHH86-10	1.746	1.542	4.449	0.045	0.138	2.314	2.022	1.670	0.738	0.735	0.388	1.887
HHH86-13	1.264	1.910	3.280	0.039	0.137	2.465	1.966	1.568	0.969	0.438	0.151	0.578
HHH86-14	0.947	2.051	3.530	0.030	0.116	2.102	1.785	1.652	0.865	0.665	0.164	1.677
HHH86-15	1.305	1.869	3.936	0.069	0.178	2.774	2.346	1.686	1.188	0.833	0.631	3.881
HHH86-16	1.766	1.741	3.212	0.036	0.134	2.633	2.218	1.951	0.831	0.387	0.399	1.864
HHH86-18	1.709	2.047	3.187	0.038	0.127	2.198	1.850	1.535	1.022	0.600	0.290	3.021
HHH86-26	3.715	1.342	3.250	0.083	0.212	3.759	2.685	2.391	1.862	0.921	0.858	5.213
HHH86-28	-0.684	2.383	0.586	-0.001	0.027	0.400	0.733	0.474	0.228	0.412	-0.154	2.218
HHH86-30	1.979	2.007	3.982	0.068	0.177	2.592	2.382	1.802	1.236	0.958	0.600	1.569
HHH86-32	2.250	1.627	5.466	0.071	0.217	3.905	2.985	2.475	1.619	0.858	0.780	1.925
HHH86-33	0.004	2.153	2.785	0.011	0.077	1.193	1.459	0.876	0.747	0.499	0.021	0.809
HHH86-39	-1.366	0.986	2.176	0.058	0.218	4.620	1.930	1.629	0.655	0.410	0.062	2.811
HH-024	4.960	1.644	5.255	0.079	0.204	3.475	2.807	1.641	1.297	0.714	0.415	1.097
HH-080	0.291	2.354	1.378	0.004	0.048	0.992	0.679	0.783	0.463	0.331	0.056	-0.311
HH-096	0.441	2.135	2.801	0.011	0.070	1.172	1.398	0.984	0.564	0.398	0.178	0.306
K-029	1.802	2.043	3.703	0.057	0.162	2.811	2.163	1.888	1.232	0.773	0.356	1.419
K-033	3.994	1.596	4.644	0.053	0.188	3.659	2.130	1.928	1.224	0.802	0.544	2.997
K-034	2.527	1.763	4.288	0.056	0.184	3.088	2.333	1.965	1.293	0.881	0.507	2.700
K-051	2.084	2.102	4.023	0.065	0.168	3.004	3.541	2.583	2.019	0.922	1.077	5.990
K-102	2.826	1.789	4.492	0.059	0.212	3.554	2.469	2.428	1.440	0.802	0.491	3.647
K-163	1.170	2.104	3.157	0.044	0.129	2.115	1.948	1.518	1.101	0.545	0.303	2.014
K-217	2.340	1.649	4.557	0.040	0.135	2.352	2.176	1.349	1.302	0.764	-0.038	1.271
K-233	0.715	1.671	3.920	0.048	0.112	1.929	2.259	1.257	1.080	0.644	0.434	2.112
R117	0.133	3.277	1.782	0.007	0.043	0.785	1.078	0.752	0.432	0.478	0.182	-1.003
R202	-0.390	2.562	2.007	0.033	0.104	1.313	1.395	1.638	0.673	0.290	0.341	2.538
R203	-0.504	2.308	1.379	0.030	0.074	1.203	1.207	0.928	0.612	0.224	0.245	2.117
R235	0.359	2.853	1.922	0.033	0.094	0.887	1.809	1.596	0.627	0.430	0.233	5.575
R253	-0.585	3.248	3.204	0.003	0.090	1.958	1.497	1.371	0.538	0.918	-0.005	0.693
R254	0.137	2.164	2.046	0.018	0.106	1.865	1.331	1.362	0.925	0.298	0.224	3.219
R261	2.830	1.790	4.214	0.048	0.159	2.520	2.091	1.858	1.362	0.839	0.343	2.650
VHH81-02	0.406	2.057	2.243	0.047	0.119	1.486	1.460	1.524	0.506	0.518	0.199	0.986
VHH81-03	3.764	1.837	4.652	0.064	0.193	3.130	2.578	2.331	1.723	0.955	0.610	2.159
VHH81-05	-0.332	2.462	1.389	0.012	0.061	0.825	1.431	1.057	0.577	0.217	-0.117	1.324
PFF-gc001	1.566	1.750	3.697	0.052	0.163	2.641	2.134	1.394	1.118	0.358	0.449	1.655
PFF-gc002	-0.110	1.922	3.000	-0.009	0.051	1.081	1.197	1.164	0.516	0.480	0.140	4.143
PFF-gc003	0.211	1.675	3.043	0.015	0.062	1.256	0.638	1.376	0.415	0.105	0.287	-1.592
PFF-gc004	-0.851	2.116	1.282	0.029	0.068	0.741	0.984	0.278	0.706	0.696	0.594	3.032
PFF-gc006	0.180	2.640	1.732	0.000	0.059	1.069	1.057	0.867	0.263	0.257	-0.111	2.823
PFF-gc011	-1.516	2.323	2.089	0.022	0.066	0.842	0.340	-0.159	-0.204	0.491	-0.530	-1.936
PFF-gc013	0.274	2.454	2.147	-0.004	0.051	1.807	0.921	1.092	0.487	0.375	-0.134	0.783
PFF-gc015	1.866	2.386	3.161	0.038	0.080	1.672	1.754	1.292	0.902	0.448	-0.073	-0.053
PFF-gc016	1.883	1.825	4.365	0.053	0.190	2.737	2.338	2.418	1.347	0.952	0.644	0.626
PFF-gc018	4.273	1.540	5.907	0.100	0.259	4.325	3.058	2.394	1.522	0.885	0.799	4.256
PFF-gc022	0.110	2.702	3.035	0.019	0.041	0.385	2.067	1.394	1.310	0.299	0.245	3.299
PFF-gc023	0.965	2.210	2.950	0.027	0.093	1.682	1.717	1.217	1.031	0.139	0.170	1.151
PFF-gc032	1.174	1.760	3.088	0.045	0.133	2.296	1.866	2.172	1.044	0.608	0.125	0.630
PFF-gc035	1.821	2.028	3.408	0.045	0.166	3.094	2.790	1.999	1.450	1.071	0.064	4.692
PFF-gc036	0.677	2.403	2.638	0.023	0.099	1.657	1.304	1.054	0.460	0.466	-0.024	2.468
PFF-gc039	-0.209	0.991	2.125	0.005	0.052	0.931	1.159	0.834	0.402	0.324	0.092	-1.518
PFF-gc042	0.296	2.841	0.674	0.022	0.069	1.071	1.191	0.559	0.601	0.459	-0.101	-1.139
PFF-gc046	-0.931	1.404	1.396	0.009	0.068	1.014	1.071	0.722	0.526	0.114	0.172	3.582
PFF-gc051	0.156	1.359	3.779	0.029	0.138	2.547	2.295	1.581	0.964	0.641	0.291	3.557
PFF-gc058	2.059	2.697	2.053	0.012	0.055	0.910	1.258	1.243	0.664	0.409	0.180	1.231
PFF-gc066	0.393	2.282	3.220	0.052	0.132	2.058	1.270	1.326	0.884	0.737	-0.271	2.953

Table 5 – *continued*

ID	C <sub>2</sub> 4668 (Å)	H $\beta$ (Å)	Fe5015 (Å)	Mg <sub>1</sub> (mag)	Mg <sub>2</sub> (mag)	Mg <i>b</i> (Å)	Fe5270 (Å)	Fe5335 (Å)	Fe5406 (Å)	Fe5709 (Å)	Fe5782 (Å)	Na D (Å)
PFF-gc069	3.492	1.254	5.470	0.043	0.190	3.116	2.796	2.698	0.962	0.805	0.438	3.435
PFF-gc074	1.795	1.879	3.691	0.018	0.105	2.015	1.998	1.236	0.835	0.681	0.127	1.238
PFF-gc075	1.803	1.566	4.477	0.098	0.213	3.037	2.367	1.930	1.080	0.483	0.273	1.307
PFF-gc079	1.477	2.431	3.056	0.094	0.202	1.978	1.926	1.823	1.102	0.395	0.138	5.134
PFF-gc081	-0.334	2.255	1.857	0.021	0.084	1.420	2.015	1.330	0.303	0.505	0.169	0.217
PFF-gc082	0.805	1.851	4.602	0.037	0.150	2.936	2.159	1.861	1.734	0.634	0.644	1.479
PFF-gc085	-0.495	2.321	2.189	0.034	0.069	0.896	0.592	0.932	0.944	-0.084	0.081	-0.071
PFF-gc087	1.074	2.634	3.385	0.023	0.077	1.922	1.096	1.245	0.797	0.446	0.269	0.080
PFF-gc088	-1.042	2.380	2.311	0.010	0.055	0.858	1.224	1.186	0.586	0.396	0.204	3.979
PFF-gc089	-0.064	2.850	0.790	0.001	0.053	0.932	0.477	0.515	0.445	0.326	-0.209	1.711
PFF-gc090	2.798	1.584	4.072	0.073	0.201	3.233	2.625	1.955	1.046	0.914	0.302	1.984
PFF-gc093	1.565	2.013	1.226	0.046	0.084	1.140	1.136	0.827	0.744	0.421	0.324	4.556
PFF-gc097	-0.649	2.260	1.713	0.010	0.057	1.145	1.197	0.500	0.343	0.263	-0.297	1.590
PFF-gc098	1.030	2.117	4.164	0.036	0.114	1.774	1.821	1.719	1.427	0.559	0.255	1.877
PFF-gc100	1.209	2.119	4.141	0.051	0.159	2.861	2.337	2.043	1.425	0.838	0.414	2.288
PFF-gc101	0.656	1.330	2.334	0.026	0.187	4.235	2.234	1.382	0.812	0.766	0.216	1.075
WHH-06	4.375	1.601	3.111	0.077	0.178	2.296	2.494	2.276	1.535	0.992	0.746	1.449
WHH-17	0.521	2.175	3.243	0.051	0.128	1.989	1.779	1.246	0.911	0.476	0.260	1.595
WHH-18	2.175	1.937	3.151	0.035	0.150	2.562	2.504	2.220	1.236	0.686	0.362	2.146
WHH-20	1.020	1.745	3.138	0.039	0.128	1.922	1.694	1.324	0.841	0.486	0.374	1.639

**Table 6.** Lick index errors measured for NGC 5128 globular clusters.

ID	H $\delta_{\Lambda}$ (Å)	H $\delta_{\text{F}}$ (Å)	CN <sub>1</sub> (mag)	CN <sub>2</sub> (mag)	Ca4227 (Å)	G4300 (Å)	H $\gamma_{\Lambda}$ (Å)	H $\gamma_{\text{F}}$ (Å)	Fe4383 (Å)	Ca4455 (Å)	Fe4531 (Å)
AAT101906	0.966	0.563	0.032	0.033	0.536	0.873	1.021	0.461	1.213	0.505	0.686
AAT103195	1.492	0.956	0.042	0.045	0.713	1.172	1.429	0.833	1.771	0.807	1.172
AAT106880	1.305	0.856	0.041	0.044	0.723	1.252	1.304	0.674	1.814	0.816	1.280
AAT107060	1.170	0.736	0.037	0.039	0.626	1.045	1.173	0.582	1.462	0.663	0.930
AAT107977	1.015	0.612	0.034	0.035	0.583	0.988	1.078	0.520	1.425	0.633	0.882
AAT109380	0.842	0.462	0.029	0.029	0.484	0.780	0.916	0.368	1.099	0.437	0.590
AAT109711	0.846	0.467	0.030	0.030	0.506	0.846	0.926	0.373	1.180	0.489	0.679
AAT109788	1.118	0.666	0.035	0.037	0.575	1.083	1.128	0.534	1.316	0.579	0.804
AAT110138	0.985	0.592	0.034	0.035	0.583	0.983	1.067	0.504	1.404	0.609	0.854
AAT111185	1.065	0.629	0.035	0.036	0.605	1.015	1.102	0.548	1.432	0.628	0.915
AAT111296	1.524	0.860	0.039	0.041	0.647	1.017	1.194	0.604	1.393	0.615	0.847
AAT112752	1.035	0.638	0.033	0.035	0.581	0.949	1.109	0.500	1.301	0.603	0.811
AAT112964	1.480	0.922	0.037	0.039	0.638	1.039	1.136	0.548	1.464	0.656	0.964
AAT113428	1.098	0.665	0.036	0.038	0.655	1.036	1.186	0.606	1.551	0.705	0.971
AAT114913	1.092	0.647	0.034	0.035	0.572	0.924	1.114	0.520	1.327	0.581	0.837
AAT115561	1.068	0.647	0.035	0.036	0.598	0.952	1.117	0.532	1.374	0.606	0.817
AAT115605	1.868	1.088	0.049	0.054	0.974	1.583	1.500	0.803	2.032	0.930	1.489
AAT116025	1.107	0.613	0.035	0.037	0.603	0.954	1.116	0.534	1.349	0.602	0.867
AAT116220	0.923	0.525	0.031	0.031	0.517	0.842	0.970	0.417	1.189	0.494	0.669
AAT116385	1.032	0.603	0.033	0.035	0.538	0.897	1.112	0.544	1.312	0.590	0.779
AAT116969	1.308	0.810	0.041	0.045	0.697	1.202	1.337	0.660	1.612	0.754	1.125
AAT117062	0.724	0.354	0.027	0.025	0.432	0.694	0.832	0.276	0.965	0.347	0.435
AAT117322	1.031	0.617	0.033	0.035	0.581	0.957	1.053	0.480	1.359	0.597	0.820
AAT118314	1.215	0.767	0.038	0.041	0.657	1.116	1.238	0.635	1.607	0.754	1.090
AAT119596	1.220	0.726	0.036	0.038	0.635	1.042	1.165	0.576	1.441	0.649	0.922
AAT119894	1.414	0.815	0.042	0.046	0.726	1.192	1.401	0.769	1.958	0.866	1.121
AAT120355	1.021	0.570	0.035	0.037	0.631	1.064	1.178	0.577	1.447	0.691	1.035
AAT121367	1.002	0.584	0.034	0.035	0.570	0.986	1.097	0.533	1.400	0.602	0.842
AAT122526	1.206	0.731	0.039	0.041	0.683	1.187	1.281	0.679	1.673	0.769	1.117
AAT204119	1.333	0.826	0.040	0.044	0.697	1.164	1.342	0.693	1.681	0.853	1.155
AAT208206	0.928	0.535	0.031	0.032	0.524	0.894	0.951	0.388	1.226	0.529	0.740
AAT215171	1.600	0.966	0.044	0.049	0.762	1.289	1.494	0.811	1.816	0.852	1.253
AAT308432	1.139	0.684	0.035	0.037	0.596	0.972	1.106	0.528	1.323	0.569	0.811
AAT329209	1.892	1.382	0.048	0.053	0.786	1.379	1.447	0.792	1.935	0.918	1.295
AAT329848	0.779	0.407	0.028	0.027	0.461	0.749	0.867	0.312	1.047	0.400	0.537
HGHH-01	0.836	0.456	0.030	0.029	0.493	0.809	0.918	0.366	1.139	0.457	0.629
HGHH-04	0.826	0.443	0.029	0.029	0.490	0.798	0.908	0.354	1.124	0.454	0.617
HGHH-06	1.390	0.802	0.038	0.041	0.536	0.965	1.188	0.567	1.413	0.669	0.866
HGHH-07	0.760	0.386	0.028	0.027	0.448	0.724	0.856	0.302	1.009	0.379	0.489
HGHH-11	0.912	0.517	0.030	0.030	0.503	0.811	0.961	0.405	1.137	0.463	0.623
HGHH-17	0.747	0.375	0.027	0.026	0.443	0.711	0.846	0.290	0.989	0.364	0.464
HGHH-19	1.183	0.713	0.037	0.038	0.616	1.033	1.138	0.554	1.430	0.632	0.887
HGHH-20	0.970	0.559	0.032	0.033	0.544	0.902	1.031	0.462	1.261	0.542	0.750
HGHH-21	0.945	0.531	0.031	0.032	0.534	0.873	1.000	0.433	1.234	0.526	0.732
HGHH-22	0.837	0.455	0.029	0.029	0.487	0.795	0.921	0.374	1.124	0.447	0.602
HGHH-23	0.970	0.556	0.031	0.032	0.514	0.832	0.984	0.431	1.157	0.472	0.639
HGHH-25	0.988	0.575	0.033	0.033	0.548	0.884	1.028	0.470	1.225	0.517	0.710
HGHH-29	0.899	0.496	0.030	0.030	0.495	0.808	0.953	0.403	1.123	0.451	0.607
HGHH-31	1.378	0.822	0.039	0.041	0.634	1.037	1.250	0.645	1.515	0.698	0.936
HGHH-34	0.929	0.524	0.030	0.030	0.498	0.819	0.971	0.411	1.142	0.472	0.640
HGHH-36	0.918	0.515	0.031	0.031	0.516	0.839	0.944	0.390	1.173	0.481	0.667
HGHH-37	0.861	0.478	0.030	0.029	0.486	0.790	0.929	0.375	1.095	0.437	0.584
HGHH-40	1.055	0.611	0.033	0.035	0.589	0.939	1.047	0.465	1.281	0.552	0.791
HGHH-41	0.989	0.560	0.031	0.032	0.522	0.842	0.983	0.428	1.180	0.485	0.648
HGHH-42	1.185	0.754	0.035	0.037	0.599	0.979	1.120	0.540	1.385	0.614	0.847
HGHH-43	0.890	0.505	0.031	0.031	0.514	0.853	0.961	0.401	1.192	0.500	0.696
HGHH-44	0.899	0.506	0.031	0.031	0.516	0.854	0.958	0.396	1.202	0.506	0.697
HGHH-45	0.994	0.584	0.033	0.035	0.569	0.952	1.046	0.472	1.339	0.594	0.849
HGHH-48	0.921	0.520	0.032	0.032	0.546	0.903	0.995	0.439	1.287	0.548	0.785
HGHH-G143	1.303	0.833	0.040	0.042	0.724	1.153	1.244	0.634	1.597	0.737	1.057
HGHH-G170	1.284	0.796	0.039	0.041	0.663	1.078	1.311	0.664	1.506	0.705	0.986
HGHH-G176	1.071	0.621	0.033	0.034	0.531	0.876	1.057	0.490	1.237	0.524	0.713
HGHH-G204	1.053	0.614	0.036	0.038	0.599	1.023	1.122	0.535	1.507	0.675	0.990



Table 6 – continued

ID	H $\delta_A$ (Å)	H $\delta_F$ (Å)	CN <sub>1</sub> (mag)	CN <sub>2</sub> (mag)	Ca4227 (Å)	G4300 (Å)	H $\gamma_A$ (Å)	H $\gamma_F$ (Å)	Fe4383 (Å)	Ca4455 (Å)	Fe4531 (Å)
HGHH-G219	1.023	0.599	0.033	0.033	0.546	0.883	1.033	0.466	1.232	0.532	0.714
HGHH-G251	1.098	0.655	0.035	0.037	0.610	0.966	1.143	0.558	1.358	0.607	0.825
HGHH-G277	1.000	0.581	0.034	0.035	0.579	0.974	1.076	0.514	1.384	0.606	0.881
HGHH-G279	0.998	0.584	0.035	0.036	0.607	1.091	1.035	0.457	1.473	0.660	0.956
HGHH-G293	0.970	0.582	0.033	0.035	0.568	0.950	1.053	0.493	1.365	0.593	0.845
HGHH-G342	1.095	0.638	0.035	0.037	0.592	0.978	1.156	0.562	1.390	0.637	0.882
HGHH-G348	1.024	0.614	0.033	0.034	0.564	0.944	1.050	0.496	1.325	0.576	0.778
HGHH-G369	0.859	0.471	0.030	0.030	0.499	0.823	0.936	0.383	1.163	0.477	0.654
HGHH-G370	0.919	0.525	0.031	0.031	0.510	0.829	0.974	0.412	1.187	0.488	0.669
HHH86-10	1.193	0.733	0.037	0.038	0.623	1.040	1.162	0.574	1.457	0.642	0.911
HHH86-13	0.918	0.526	0.031	0.031	0.518	0.833	0.977	0.427	1.195	0.494	0.667
HHH86-14	0.871	0.485	0.030	0.030	0.496	0.810	0.934	0.382	1.133	0.459	0.613
HHH86-15	1.251	0.815	0.037	0.040	0.656	1.056	1.236	0.636	1.475	0.687	0.952
HHH86-16	1.047	0.635	0.034	0.035	0.566	0.938	1.060	0.498	1.320	0.561	0.789
HHH86-18	0.800	0.424	0.028	0.028	0.467	0.758	0.888	0.333	1.059	0.414	0.545
HHH86-26	1.208	0.749	0.036	0.038	0.607	0.983	1.200	0.594	1.365	0.613	0.845
HHH86-28	0.955	0.559	0.032	0.032	0.553	0.911	0.993	0.437	1.295	0.552	0.775
HHH86-30	0.848	0.465	0.029	0.029	0.480	0.783	0.919	0.366	1.089	0.433	0.575
HHH86-32	1.418	0.911	0.040	0.043	0.661	1.094	1.314	0.685	1.569	0.703	1.011
HHH86-33	0.831	0.453	0.029	0.029	0.488	0.791	0.909	0.353	1.107	0.440	0.598
HHH86-39	0.829	0.446	0.029	0.028	0.466	0.755	0.906	0.360	1.053	0.408	0.535
HH-024	1.112	0.647	0.033	0.035	0.561	0.891	1.090	0.496	1.215	0.531	0.724
HH-080	0.830	0.452	0.029	0.029	0.483	0.789	0.897	0.345	1.105	0.442	0.596
HH-096	0.819	0.444	0.029	0.029	0.486	0.793	0.910	0.360	1.116	0.449	0.608
K-029	0.782	0.406	0.028	0.027	0.455	0.735	0.871	0.319	1.022	0.388	0.504
K-033	0.941	0.539	0.031	0.032	0.527	0.850	0.998	0.444	1.207	0.503	0.675
K-034	0.755	0.382	0.027	0.026	0.440	0.708	0.851	0.295	0.984	0.360	0.455
K-051	1.085	0.636	0.035	0.036	0.608	0.947	1.130	0.536	1.356	0.607	0.837
K-102	0.913	0.506	0.031	0.031	0.513	0.829	0.987	0.427	1.172	0.488	0.661
K-163	0.744	0.373	0.027	0.026	0.441	0.711	0.845	0.290	0.989	0.363	0.463
K-217	1.408	0.885	0.040	0.043	0.696	1.128	1.337	0.674	1.608	0.785	1.088
K-233	0.886	0.517	0.031	0.031	0.530	0.870	0.989	0.435	1.232	0.516	0.710
R117	0.971	0.567	0.033	0.034	0.569	0.955	1.029	0.459	1.356	0.595	0.835
R202	0.874	0.490	0.030	0.030	0.516	0.844	0.953	0.401	1.193	0.488	0.683
R203	0.950	0.547	0.033	0.033	0.554	0.939	1.009	0.451	1.322	0.561	0.823
R235	1.133	0.672	0.037	0.040	0.663	1.128	1.182	0.576	1.554	0.712	1.054
R253	1.120	0.657	0.035	0.036	0.589	0.924	1.071	0.496	1.338	0.587	0.795
R254	1.084	0.668	0.035	0.038	0.612	1.042	1.120	0.537	1.457	0.645	0.936
R261	0.957	0.555	0.031	0.032	0.532	0.865	1.001	0.439	1.205	0.508	0.703
VHH81-02	0.888	0.504	0.031	0.030	0.516	0.844	0.962	0.406	1.195	0.493	0.688
VHH81-03	0.977	0.569	0.032	0.032	0.538	0.877	1.031	0.465	1.223	0.528	0.715
VHH81-05	0.797	0.424	0.029	0.028	0.474	0.772	0.890	0.335	1.086	0.431	0.579
PFF-gc001	0.903	0.516	0.031	0.030	0.512	0.834	0.963	0.414	1.159	0.473	0.641
PFF-gc002	0.976	0.578	0.033	0.034	0.568	0.948	1.038	0.472	1.335	0.579	0.820
PFF-gc003	0.961	0.568	0.033	0.033	0.561	0.924	1.011	0.459	1.336	0.555	0.801
PFF-gc004	1.057	0.638	0.036	0.038	0.619	1.038	1.125	0.548	1.514	0.678	0.959
PFF-gc006	0.890	0.500	0.031	0.031	0.511	0.853	0.955	0.401	1.207	0.505	0.706
PFF-gc011	1.021	0.626	0.035	0.036	0.607	0.986	1.065	0.492	1.433	0.650	0.981
PFF-gc013	0.940	0.558	0.032	0.032	0.541	0.891	0.981	0.424	1.258	0.528	0.735
PFF-gc015	0.989	0.588	0.033	0.034	0.565	0.922	1.034	0.471	1.309	0.571	0.797
PFF-gc016	1.258	0.742	0.040	0.042	0.694	1.090	1.342	0.687	1.588	0.693	1.013
PFF-gc018	0.916	0.508	0.030	0.030	0.502	0.809	0.961	0.410	1.118	0.449	0.595
PFF-gc022	1.128	0.688	0.038	0.041	0.677	1.176	1.157	0.584	1.632	0.730	1.063
PFF-gc023	0.964	0.544	0.033	0.033	0.550	0.916	1.007	0.446	1.316	0.565	0.792
PFF-gc032	0.965	0.562	0.033	0.033	0.551	0.908	1.017	0.458	1.306	0.560	0.758
PFF-gc035	1.254	0.796	0.038	0.041	0.650	1.095	1.258	0.666	1.588	0.723	1.016
PFF-gc036	0.866	0.481	0.030	0.030	0.509	0.827	0.944	0.387	1.172	0.484	0.669
PFF-gc039	1.032	0.635	0.033	0.035	0.571	0.894	1.099	0.537	1.318	0.585	0.801
PFF-gc042	0.886	0.506	0.031	0.031	0.523	0.873	0.971	0.413	1.230	0.525	0.741
PFF-gc046	0.869	0.492	0.030	0.030	0.501	0.807	0.951	0.402	1.149	0.473	0.647
PFF-gc051	1.169	0.689	0.035	0.038	0.611	0.982	1.141	0.559	1.406	0.633	0.888
PFF-gc058	0.902	0.500	0.031	0.032	0.516	0.882	0.970	0.404	1.225	0.518	0.731
PFF-gc066	1.074	0.682	0.035	0.036	0.589	0.963	1.108	0.537	1.407	0.612	0.845

**Table 6** – *continued*

ID	H $\delta$ <sub>A</sub> (Å)	H $\delta$ <sub>F</sub> (Å)	CN <sub>1</sub> (mag)	CN <sub>2</sub> (mag)	Ca4227 (Å)	G4300 (Å)	H $\gamma$ <sub>A</sub> (Å)	H $\gamma$ <sub>F</sub> (Å)	Fe4383 (Å)	Ca4455 (Å)	Fe4531 (Å)
PFF-gc069	1.248	0.734	0.038	0.041	0.635	1.013	1.213	0.615	1.488	0.650	0.924
PFF-gc074	1.078	0.630	0.036	0.038	0.607	1.018	1.138	0.539	1.442	0.644	0.906
PFF-gc075	1.088	0.653	0.035	0.036	0.582	0.957	1.122	0.537	1.339	0.604	0.807
PFF-gc079	0.981	0.559	0.033	0.033	0.549	0.895	1.050	0.487	1.311	0.578	0.803
PFF-gc081	1.086	0.653	0.036	0.038	0.617	1.045	1.118	0.545	1.498	0.664	0.942
PFF-gc082	1.090	0.662	0.034	0.035	0.564	0.939	1.068	0.507	1.309	0.547	0.740
PFF-gc085	0.965	0.564	0.033	0.033	0.563	0.940	1.026	0.464	1.329	0.577	0.814
PFF-gc087	1.010	0.604	0.033	0.035	0.571	0.956	1.034	0.465	1.349	0.577	0.836
PFF-gc088	0.868	0.485	0.030	0.030	0.504	0.821	0.930	0.379	1.171	0.473	0.647
PFF-gc089	1.002	0.594	0.033	0.035	0.568	0.956	1.026	0.459	1.351	0.586	0.843
PFF-gc090	1.056	0.649	0.034	0.035	0.567	0.931	1.086	0.499	1.284	0.575	0.774
PFF-gc093	1.071	0.671	0.036	0.038	0.645	1.084	1.134	0.551	1.542	0.703	1.001
PFF-gc097	1.007	0.594	0.033	0.035	0.569	0.957	1.028	0.463	1.330	0.573	0.819
PFF-gc098	1.063	0.641	0.035	0.036	0.594	0.985	1.093	0.518	1.387	0.612	0.870
PFF-gc100	0.897	0.499	0.030	0.030	0.498	0.808	0.944	0.386	1.122	0.457	0.608
PFF-gc101	0.856	0.473	0.029	0.029	0.479	0.779	0.939	0.395	1.100	0.436	0.583
WHH-06	1.187	0.771	0.037	0.040	0.648	1.011	1.299	0.661	1.472	0.683	0.980
WHH-17	0.827	0.444	0.029	0.029	0.479	0.780	0.907	0.355	1.095	0.436	0.584
WHH-18	0.878	0.492	0.030	0.029	0.491	0.793	0.939	0.385	1.113	0.446	0.606
WHH-20	0.946	0.543	0.031	0.032	0.531	0.872	0.995	0.432	1.232	0.517	0.714

Table 6 – continued

ID	C <sub>2</sub> 4668 (Å)	H $\beta$ (Å)	Fe5015 (Å)	Mg <sub>1</sub> (mag)	Mg <sub>2</sub> (mag)	Mg <i>b</i> (Å)	Fe5270 (Å)	Fe5335 (Å)	Fe5406 (Å)	Fe5709 (Å)	Fe5782 (Å)	Na D (Å)
AAT101906	1.058	0.412	0.731	0.015	0.020	0.398	0.383	0.447	0.325	0.318	0.251	0.382
AAT103195	1.746	0.668	1.329	0.018	0.023	0.627	0.659	0.768	0.556	0.473	0.421	0.573
AAT106880	1.915	0.690	1.479	0.019	0.025	0.722	0.786	0.896	0.643	0.536	0.489	0.685
AAT107060	1.359	0.516	1.020	0.016	0.022	0.512	0.544	0.635	0.459	0.406	0.359	0.460
AAT107977	1.361	0.510	1.043	0.016	0.022	0.531	0.554	0.637	0.465	0.430	0.371	0.510
AAT109380	0.923	0.359	0.614	0.014	0.019	0.361	0.344	0.409	0.299	0.301	0.236	0.362
AAT109711	1.036	0.398	0.741	0.015	0.020	0.403	0.396	0.467	0.342	0.329	0.268	0.400
AAT109788	1.203	0.477	0.873	0.015	0.021	0.453	0.450	0.514	0.380	0.351	0.292	0.419
AAT110138	1.434	0.494	0.974	0.016	0.021	0.511	0.532	0.617	0.452	0.405	0.350	0.473
AAT111185	1.357	0.519	1.051	0.016	0.022	0.531	0.576	0.654	0.485	0.429	0.383	0.524
AAT111296	1.264	0.475	0.906	0.016	0.021	0.456	0.461	0.530	0.387	0.357	0.295	0.411
AAT112752	1.245	0.469	0.853	0.015	0.021	0.453	0.469	0.556	0.399	0.360	0.308	0.438
AAT112964	1.422	0.553	1.101	0.016	0.022	0.544	0.562	0.648	0.464	0.400	0.344	0.487
AAT113428	1.462	0.568	1.151	0.017	0.022	0.575	0.610	0.704	0.536	0.450	0.405	0.486
AAT114913	1.254	0.480	0.898	0.016	0.021	0.479	0.479	0.557	0.403	0.367	0.309	0.423
AAT115561	1.252	0.496	0.940	0.016	0.021	0.479	0.483	0.554	0.411	0.375	0.317	0.427
AAT115605	2.039	0.790	1.590	0.020	0.025	0.747	0.771	0.893	0.671	0.549	0.487	0.610
AAT116025	1.262	0.485	0.936	0.016	0.021	0.484	0.490	0.563	0.415	0.371	0.308	0.460
AAT116220	1.032	0.398	0.731	0.015	0.020	0.408	0.406	0.485	0.352	0.338	0.280	0.375
AAT116385	1.210	0.451	0.840	0.015	0.021	0.451	0.456	0.524	0.388	0.360	0.295	0.436
AAT116969	1.651	0.611	1.275	0.017	0.023	0.608	0.633	0.731	0.547	0.458	0.417	0.557
AAT117062	0.705	0.292	0.413	0.013	0.019	0.291	0.245	0.301	0.221	0.259	0.182	0.302
AAT117322	1.245	0.485	0.905	0.016	0.021	0.481	0.484	0.557	0.405	0.371	0.312	0.437
AAT118314	1.657	0.617	1.323	0.018	0.023	0.667	0.712	0.834	0.616	0.532	0.469	0.668
AAT119596	1.371	0.529	1.051	0.016	0.022	0.520	0.530	0.616	0.457	0.389	0.337	0.468
AAT119894	1.739	0.663	1.269	0.017	0.023	0.627	0.659	0.733	0.544	0.456	0.404	0.558
AAT120355	1.528	0.549	1.118	0.017	0.022	0.552	0.586	0.650	0.472	0.429	0.372	0.551
AAT121367	1.315	0.517	0.998	0.016	0.021	0.507	0.539	0.630	0.471	0.406	0.361	0.439
AAT122526	1.608	0.582	1.176	0.017	0.022	0.568	0.605	0.710	0.543	0.488	0.428	0.589
AAT204119	1.770	0.662	1.381	0.018	0.023	0.669	0.709	0.819	0.593	0.505	0.461	0.636
AAT208206	1.068	0.425	0.818	0.015	0.020	0.431	0.434	0.508	0.374	0.351	0.293	0.421
AAT215171	1.855	0.669	1.392	0.018	0.024	0.646	0.677	0.802	0.602	0.494	0.448	0.622
AAT308432	1.210	0.456	0.919	0.015	0.021	0.459	0.463	0.536	0.397	0.355	0.298	0.464
AAT329209	1.896	0.675	1.465	0.019	0.024	0.678	0.766	0.899	0.648	0.519	0.488	0.695
AAT329848	0.851	0.340	0.579	0.014	0.019	0.350	0.325	0.389	0.289	0.297	0.230	0.353
HGHH-01	0.972	0.377	0.678	0.014	0.019	0.387	0.371	0.440	0.324	0.317	0.253	0.374
HGHH-04	0.959	0.373	0.668	0.014	0.019	0.379	0.367	0.433	0.319	0.315	0.251	0.368
HGHH-06	1.360	0.483	0.910	0.016	0.021	0.473	0.469	0.537	0.398	0.341	0.279	0.389
HGHH-07	0.780	0.316	0.495	0.013	0.019	0.317	0.282	0.340	0.250	0.275	0.202	0.322
HGHH-11	0.961	0.382	0.667	0.014	0.019	0.376	0.364	0.427	0.316	0.314	0.248	0.370
HGHH-17	0.744	0.303	0.448	0.013	0.019	0.303	0.260	0.316	0.232	0.264	0.189	0.309
HGHH-19	1.330	0.492	0.944	0.016	0.021	0.494	0.493	0.565	0.404	0.369	0.308	0.439
HGHH-20	1.140	0.433	0.791	0.015	0.020	0.424	0.421	0.493	0.363	0.341	0.279	0.405
HGHH-21	1.117	0.430	0.804	0.015	0.020	0.432	0.434	0.508	0.375	0.356	0.301	0.417
HGHH-22	0.934	0.366	0.630	0.014	0.019	0.364	0.342	0.406	0.297	0.302	0.236	0.353
HGHH-23	0.963	0.380	0.649	0.014	0.019	0.370	0.347	0.405	0.297	0.302	0.236	0.348
HGHH-25	1.075	0.421	0.748	0.015	0.020	0.402	0.390	0.458	0.337	0.322	0.256	0.378
HGHH-29	0.938	0.370	0.636	0.014	0.019	0.366	0.347	0.410	0.301	0.304	0.237	0.360
HGHH-31	1.426	0.531	1.044	0.016	0.022	0.521	0.533	0.614	0.452	0.393	0.330	0.471
HGHH-34	0.993	0.393	0.700	0.015	0.020	0.394	0.383	0.450	0.330	0.325	0.265	0.391
HGHH-36	1.039	0.401	0.733	0.015	0.020	0.399	0.382	0.447	0.327	0.317	0.253	0.385
HGHH-37	0.893	0.355	0.590	0.014	0.019	0.351	0.324	0.384	0.282	0.293	0.224	0.348
HGHH-40	1.154	0.442	0.820	0.015	0.020	0.438	0.436	0.506	0.367	0.339	0.276	0.417
HGHH-41	0.994	0.393	0.686	0.014	0.019	0.382	0.371	0.431	0.319	0.315	0.248	0.370
HGHH-42	1.297	0.491	0.910	0.016	0.021	0.479	0.482	0.551	0.412	0.374	0.311	0.441
HGHH-43	1.069	0.407	0.744	0.015	0.020	0.409	0.405	0.476	0.350	0.327	0.265	0.385
HGHH-44	1.075	0.416	0.804	0.015	0.020	0.435	0.437	0.514	0.379	0.353	0.294	0.426
HGHH-45	1.299	0.505	1.022	0.016	0.022	0.530	0.556	0.635	0.475	0.496	0.372	0.528
HGHH-48	1.171	0.445	0.855	0.015	0.020	0.458	0.464	0.542	0.401	0.377	0.311	0.448
HGHH-G143	1.622	0.574	1.160	0.017	0.022	0.547	0.570	0.661	0.482	0.408	0.348	0.489
HGHH-G170	1.457	0.558	1.042	0.016	0.022	0.511	0.526	0.605	0.448	0.395	0.337	0.466
HGHH-G176	1.101	0.422	0.745	0.015	0.020	0.399	0.388	0.459	0.329	0.320	0.257	0.377

Table 6 – *continued*

ID	C <sub>2</sub> 4668 (Å)	H $\beta$ (Å)	Fe5015 (Å)	Mg <sub>1</sub> (mag)	Mg <sub>2</sub> (mag)	Mg <i>b</i> (Å)	Fe5270 (Å)	Fe5335 (Å)	Fe5406 (Å)	Fe5709 (Å)	Fe5782 (Å)	Na D (Å)
HGHH-G204	1.488	0.546	1.133	0.017	0.022	0.575	0.606	0.686	0.501	0.432	0.381	0.518
HGHH-G219	1.105	0.434	0.759	0.015	0.020	0.406	0.401	0.464	0.346	0.337	0.274	0.391
HGHH-G251	1.225	0.475	0.893	0.016	0.021	0.455	0.472	0.534	0.392	0.360	0.298	0.421
HGHH-G277	1.330	0.498	0.962	0.016	0.021	0.506	0.508	0.594	0.437	0.391	0.333	0.501
HGHH-G279	1.451	0.536	1.140	0.017	0.022	0.596	0.623	0.732	0.528	0.473	0.421	0.551
HGHH-G293	1.262	0.487	0.909	0.016	0.021	0.479	0.487	0.564	0.417	0.374	0.311	0.471
HGHH-G342	1.346	0.498	0.925	0.016	0.021	0.476	0.485	0.559	0.416	0.388	0.337	0.459
HGHH-G348	1.208	0.475	0.897	0.016	0.021	0.462	0.480	0.562	0.412	0.379	0.321	0.445
HGHH-G369	1.012	0.389	0.702	0.014	0.019	0.391	0.378	0.446	0.329	0.319	0.253	0.381
HGHH-G370	1.026	0.402	0.706	0.015	0.020	0.393	0.381	0.444	0.324	0.313	0.248	0.365
HHH86-10	1.378	0.526	1.000	0.016	0.021	0.511	0.522	0.603	0.447	0.386	0.328	0.454
HHH86-13	1.040	0.403	0.730	0.015	0.020	0.402	0.393	0.464	0.343	0.327	0.265	0.394
HHH86-14	0.953	0.373	0.650	0.014	0.019	0.374	0.357	0.421	0.312	0.308	0.243	0.364
HHH86-15	1.456	0.555	1.091	0.017	0.022	0.549	0.563	0.654	0.477	0.413	0.352	0.476
HHH86-16	1.198	0.464	0.879	0.015	0.021	0.456	0.460	0.537	0.400	0.366	0.302	0.432
HHH86-18	0.854	0.341	0.567	0.014	0.019	0.342	0.315	0.376	0.276	0.289	0.219	0.336
HHH86-26	1.277	0.497	0.929	0.016	0.021	0.470	0.477	0.548	0.399	0.370	0.310	0.426
HHH86-28	1.184	0.442	0.871	0.015	0.020	0.457	0.463	0.543	0.399	0.363	0.308	0.429
HHH86-30	0.900	0.359	0.611	0.014	0.019	0.358	0.333	0.395	0.291	0.300	0.233	0.363
HHH86-32	1.474	0.549	1.048	0.016	0.022	0.522	0.533	0.617	0.456	0.413	0.357	0.510
HHH86-33	0.928	0.360	0.615	0.014	0.019	0.361	0.337	0.402	0.293	0.296	0.229	0.349
HHH86-39	0.852	0.339	0.558	0.014	0.019	0.330	0.308	0.370	0.275	0.288	0.219	0.335
HH-024	1.080	0.423	0.750	0.015	0.020	0.407	0.397	0.467	0.341	0.322	0.256	0.383
HH-080	0.910	0.352	0.606	0.014	0.019	0.354	0.333	0.393	0.289	0.294	0.225	0.351
HH-096	0.944	0.369	0.649	0.014	0.019	0.375	0.359	0.428	0.315	0.311	0.246	0.375
K-029	0.796	0.319	0.496	0.013	0.019	0.316	0.280	0.337	0.248	0.273	0.201	0.321
K-033	1.032	0.411	0.733	0.015	0.020	0.399	0.397	0.462	0.343	0.328	0.263	0.382
K-034	0.733	0.302	0.441	0.013	0.019	0.299	0.256	0.311	0.229	0.264	0.187	0.306
K-051	1.274	0.486	0.935	0.016	0.021	0.480	0.477	0.559	0.411	0.377	0.314	0.423
K-102	1.024	0.403	0.713	0.015	0.020	0.394	0.383	0.445	0.329	0.318	0.253	0.367
K-163	0.744	0.303	0.452	0.013	0.019	0.304	0.261	0.318	0.234	0.266	0.191	0.309
K-217	1.622	0.619	1.228	0.017	0.023	0.613	0.639	0.745	0.539	0.460	0.412	0.561
K-233	1.122	0.439	0.839	0.015	0.020	0.444	0.440	0.522	0.379	0.362	0.306	0.448
R117	1.257	0.463	0.921	0.016	0.021	0.479	0.486	0.568	0.417	0.370	0.313	0.458
R202	1.059	0.404	0.760	0.015	0.020	0.417	0.409	0.476	0.354	0.339	0.275	0.400
R203	1.240	0.467	0.928	0.016	0.021	0.478	0.484	0.567	0.419	0.381	0.321	0.447
R235	1.591	0.585	1.241	0.017	0.023	0.628	0.648	0.752	0.558	0.477	0.425	0.532
R253	1.245	0.455	0.886	0.015	0.021	0.463	0.473	0.548	0.407	0.354	0.301	0.423
R254	1.431	0.540	1.096	0.017	0.022	0.552	0.583	0.673	0.495	0.438	0.382	0.515
R261	1.070	0.421	0.766	0.015	0.020	0.419	0.413	0.480	0.353	0.336	0.274	0.397
VHH81-02	1.050	0.403	0.749	0.015	0.020	0.417	0.412	0.481	0.358	0.328	0.264	0.391
VHH81-03	1.102	0.436	0.808	0.015	0.020	0.437	0.436	0.506	0.372	0.351	0.290	0.424
VHH81-05	0.906	0.354	0.621	0.014	0.019	0.363	0.341	0.406	0.300	0.303	0.237	0.358
PFF-gc001	0.979	0.385	0.679	0.014	0.019	0.382	0.366	0.434	0.319	0.313	0.246	0.372
PFF-gc002	1.239	0.464	0.886	0.016	0.021	0.473	0.482	0.567	0.421	0.383	0.329	0.445
PFF-gc003	1.230	0.466	0.886	0.016	0.021	0.473	0.491	0.567	0.422	0.377	0.314	0.479
PFF-gc004	1.478	0.551	1.145	0.017	0.022	0.585	0.616	0.722	0.523	0.459	0.406	0.559
PFF-gc006	1.083	0.414	0.790	0.015	0.020	0.428	0.430	0.505	0.375	0.351	0.292	0.408
PFF-gc011	1.416	0.515	1.032	0.016	0.021	0.531	0.560	0.658	0.478	0.394	0.349	0.501
PFF-gc013	1.136	0.432	0.820	0.015	0.020	0.433	0.445	0.522	0.387	0.354	0.296	0.421
PFF-gc015	1.198	0.454	0.867	0.015	0.021	0.455	0.458	0.537	0.393	0.357	0.301	0.440
PFF-gc016	1.564	0.605	1.165	0.017	0.022	0.582	0.596	0.676	0.496	0.420	0.358	0.516
PFF-gc018	0.920	0.369	0.619	0.014	0.019	0.358	0.336	0.399	0.294	0.299	0.228	0.344
PFF-gc022	1.576	0.576	1.197	0.017	0.023	0.629	0.653	0.764	0.562	0.491	0.439	0.560
PFF-gc023	1.184	0.448	0.856	0.015	0.020	0.451	0.453	0.530	0.387	0.366	0.307	0.447
PFF-gc032	1.189	0.460	0.871	0.015	0.021	0.458	0.464	0.530	0.395	0.363	0.306	0.443
PFF-gc035	1.524	0.580	1.191	0.017	0.022	0.580	0.601	0.706	0.523	0.454	0.410	0.526
PFF-gc036	1.026	0.399	0.736	0.015	0.020	0.408	0.404	0.477	0.352	0.336	0.277	0.398
PFF-gc039	1.213	0.464	0.871	0.015	0.020	0.457	0.459	0.540	0.395	0.360	0.304	0.452
PFF-gc042	1.132	0.428	0.847	0.015	0.020	0.449	0.454	0.537	0.392	0.358	0.303	0.448
PFF-gc046	1.007	0.393	0.713	0.015	0.020	0.401	0.394	0.467	0.345	0.336	0.275	0.391
PFF-gc051	1.363	0.522	1.003	0.016	0.021	0.514	0.528	0.620	0.456	0.403	0.350	0.474
PFF-gc058	1.134	0.437	0.830	0.015	0.020	0.434	0.425	0.494	0.362	0.334	0.275	0.400
PFF-gc066	1.308	0.489	0.963	0.016	0.021	0.495	0.508	0.586	0.433	0.391	0.344	0.461

Table 6 – continued

ID	C <sub>2</sub> 4668 (Å)	Hβ (Å)	Fe5015 (Å)	Mg <sub>1</sub> (mag)	Mg <sub>2</sub> (mag)	Mg <i>b</i> (Å)	Fe5270 (Å)	Fe5335 (Å)	Fe5406 (Å)	Fe5709 (Å)	Fe5782 (Å)	Na D (Å)
PFF-gc069	1.370	0.541	1.007	0.016	0.022	0.516	0.524	0.598	0.453	0.390	0.332	0.452
PFF-gc074	1.335	0.504	0.960	0.016	0.021	0.495	0.503	0.589	0.433	0.383	0.327	0.464
PFF-gc075	1.268	0.488	0.922	0.016	0.021	0.478	0.480	0.555	0.405	0.369	0.308	0.444
PFF-gc079	1.184	0.436	0.842	0.015	0.020	0.463	0.460	0.534	0.389	0.358	0.302	0.417
PFF-gc081	1.407	0.524	1.054	0.016	0.022	0.533	0.546	0.639	0.475	0.410	0.353	0.502
PFF-gc082	1.148	0.448	0.824	0.015	0.020	0.431	0.426	0.496	0.361	0.348	0.284	0.413
PFF-gc085	1.209	0.445	0.849	0.015	0.020	0.449	0.451	0.522	0.380	0.364	0.302	0.441
PFF-gc087	1.227	0.460	0.882	0.015	0.021	0.460	0.475	0.549	0.401	0.368	0.309	0.454
PFF-gc088	1.016	0.389	0.701	0.014	0.019	0.395	0.381	0.450	0.333	0.320	0.257	0.366
PFF-gc089	1.277	0.475	0.959	0.016	0.021	0.491	0.510	0.593	0.433	0.386	0.335	0.463
PFF-gc090	1.160	0.454	0.833	0.015	0.020	0.438	0.431	0.505	0.372	0.343	0.284	0.408
PFF-gc093	1.508	0.565	1.168	0.017	0.022	0.580	0.610	0.705	0.513	0.445	0.392	0.511
PFF-gc097	1.257	0.470	0.928	0.016	0.021	0.483	0.498	0.586	0.430	0.386	0.335	0.461
PFF-gc098	1.295	0.489	0.934	0.016	0.021	0.494	0.502	0.582	0.424	0.386	0.329	0.463
PFF-gc100	0.955	0.372	0.647	0.014	0.019	0.369	0.351	0.413	0.304	0.304	0.238	0.357
PFF-gc101	0.917	0.365	0.631	0.014	0.019	0.357	0.345	0.414	0.308	0.307	0.242	0.366
WHH-06	1.437	0.553	1.086	0.016	0.022	0.542	0.541	0.625	0.457	0.400	0.344	0.505
WHH-17	0.908	0.355	0.602	0.014	0.019	0.355	0.331	0.394	0.288	0.295	0.227	0.347
WHH-18	0.924	0.365	0.632	0.014	0.019	0.363	0.340	0.401	0.297	0.299	0.231	0.351
WHH-20	1.105	0.428	0.789	0.015	0.020	0.427	0.422	0.494	0.363	0.341	0.277	0.402

 Table 7. Polynomial coefficients for Lick index–metallicity relations of the Schiavon *et al.* (2005) Milky Way GCs from least-squares fitting. For a given index *I*,  $[M/H]_I = a_0 + a_1 \times I + a_2 \times I^2$ . *r* is the correlation coefficient of the fit and the rms is  $\sqrt{\chi^2/n}$ .

Index	<i>a</i> 0	<i>a</i> 1	<i>a</i> 2	<i>r</i>	rms
HdA	-0.6686	-0.2740	-0.0085	0.951	0.154
HdF	-0.1620	-0.5950	0.0185	0.936	0.177
CN <sub>1</sub>	-0.9923	10.4795	-25.9525	0.939	0.173
CN <sub>2</sub>	-0.9397	9.9741	-26.3867	0.945	0.164
Ca4227	-3.1711	4.5438	-1.5422	0.956	0.147
G4300	-2.5675	0.6073	-0.0365	0.935	0.178
Hγ <sub>A</sub>	-0.6686	-0.2740	-0.0085	0.951	0.154
Hγ <sub>F</sub>	-0.1620	-0.5950	0.0185	0.936	0.177
Fe4383	-2.2373	0.7071	-0.0539	0.959	0.142
Ca4455	-6.8786	6.0187	-1.2593	0.929	0.185
Fe4531	-3.4927	1.6508	-0.2138	0.908	0.210
C <sub>2</sub> 4668	-1.1142	0.5493	-0.0749	0.927	0.188
Hβ	-0.4124	0.4997	-0.3862	0.878	0.240
Fe5015	—	—	—	—	—
Mg <sub>1</sub>	-2.2199	33.2872	-26.1750	0.917	0.199
Mg <sub>2</sub>	-2.4490	14.5595	-21.0308	0.954	0.150
Mg <i>b</i>	-2.4214	0.8438	-0.0713	0.952	0.153
Fe5270	-2.6124	1.3299	-0.1449	0.955	0.149
Fe5335	-2.5049	1.4480	-0.1690	0.946	0.162
Fe5406	-2.2713	1.9360	-0.3772	0.946	0.162
Fe5709	-2.2739	2.2509	0.0105	0.921	0.195
Fe5782	-2.1993	2.5623	-0.5959	0.821	0.286
Na D	—	—	—	—	—